UNIVERSITÀ DEGLI STUDI DI MILANO

PhD Course in Veterinary and Animal Science – Class XXXVIII
Department of Veterinary Medicine and Animal Sciences

TESI DI DOTTORATO DI RICERCA

Use of near-infrared fluorescence with indocyanine green in small animal surgical oncology and in cadaveric anatomical study

MVET-05/A

PhD Candidate: Dr. Elisa Maria Gariboldi
R13704
ORCID n: 0000-0002-6705-6653

Tutor: Prof. Damiano Stefanello
Co-tutor: Prof.ssa Roberta Ferrari
Coordinator: Prof. Fabrizio Ceciliani

Academic Year 2024-2025

Summary

1. Introduction

1.1 Background:

In the recent 15 years, small animal surgery has observed significant technological advancements, largely driven by the integration of tools and techniques translating from human medicine. As a result, the connection between human and veterinary surgical approaches, particularly in dogs and cats, are increasing, opening new frontiers in precision and personalized care also for companion animals (Buote, 2024; Favril et al., 2018; Gibson, 2024; Holt et al., 2020; Mattoon and Bryan, 2013).
A rising number of veterinary institutions are investing in advanced technologies, and growing scientific research is focused on technological innovations that improve diagnostic accuracy and therapeutic outcomes in pet healthcare (Dobson, 2019; Mattoon and Bryan, 2013). This trend is particularly evident in the management of spontaneous oncologic diseases in dogs and cats, where technology is reshaping both clinical practice and research priorities.

One of the most promising technologies contributing to the transformation in real-time guided surgery is near-infrared fluorescence (NIRF) imaging (Favril et al., 2018). This technique consists in the administration of fluorescent dyes that emit light in the near-infrared spectrum, allowing for real-time intraoperative visualization of structures of interest (Favril et al., 2018).
NIRF technology involves an imaging system that emits light at specific wavelengths to excite fluorescent agents. The fluorescence emitted in response is then detected and recorded using a specific camera. Fluorophores are activated when illuminated with light in the near-infrared spectrum (typically with a wavelength between 650 and 900 nm). The fluorescence of dyes can highlight target anatomical structures (e.g., lymphatic vessels, lymph nodes, blood vessels).

The most used dye in both veterinary and human applications is indocyanine green (ICG), a water-soluble fluorophore with favorable optical properties, including excitation in the near-infrared spectrum and fluorescence emission peaking at approximately 830 nm (Alander et al., 2012; Alius et al., 2018; Dai et al., 2023). According to the clinical application, ICG can be administered intradermally/subcutaneously or intravenously: ICG binds to plasma proteins (such as albumin and lipoproteins), has low toxicity, and offers a high signal-to-noise ratio with minimal autofluorescence from surrounding tissues (Alander et al., 2012; Dai et al., 2023). NIR fluorescence can penetrate soft tissues up to 10–15 mm, enabling the effective visualization of superficial fluorescent structures

located up to about 1 cm beneath the surface with NIRF imaging technology (Dai et al., 2023). (Figure 1).

Figure 1. Example of a NIRF imaging system and ICG for clinical use

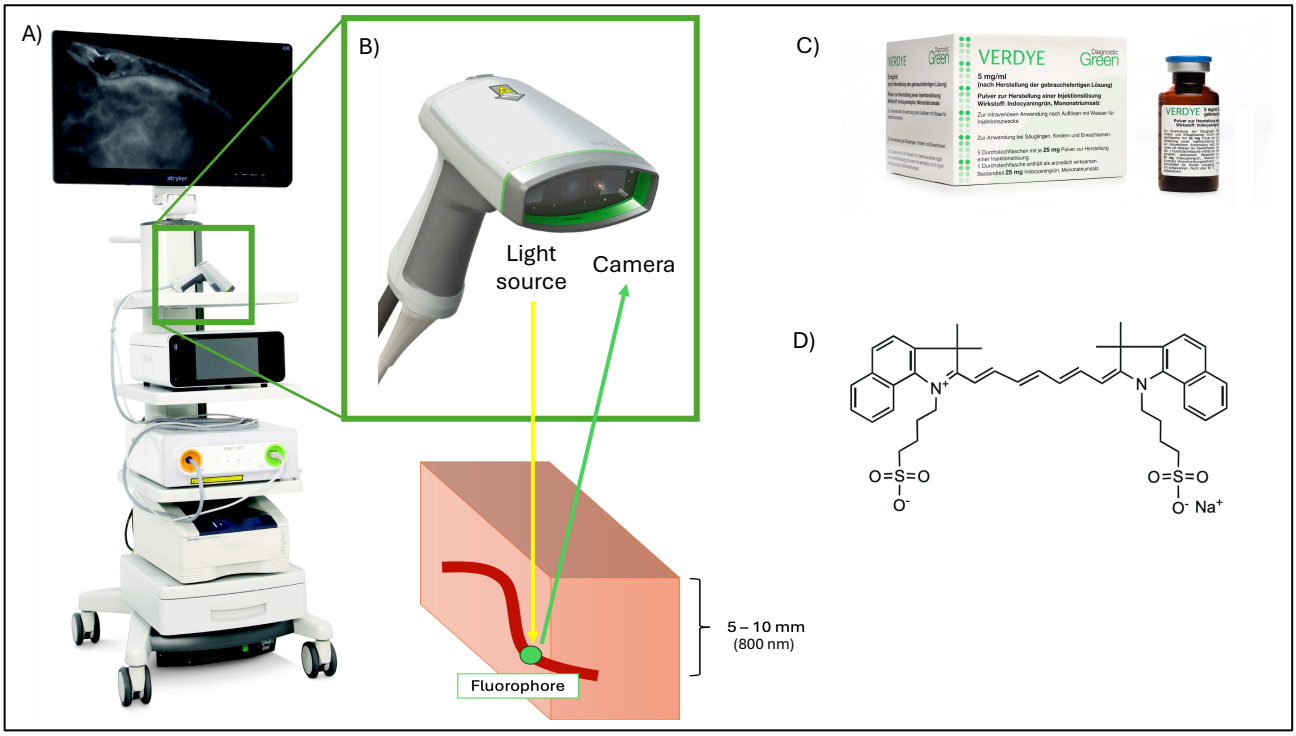

Note: **A)** example of a NIRF system for clinical practice use in humans or small animal medicine (SPY-PHI QP System Stryker). The Veterinary Teaching Hospital of the University of Milan currently uses this technology in clinical practice with **B)** the Portable Handheld Imager camera SPY-PHI and a schematic representation of the near-infrared light emission and recording by the camera. **C)** Example of ICG for clinical use and **D)** molecular representation of the ICG.

The clinical applications of NIRF-ICG in human medicine span various surgical specialties, including general surgery and surgical oncology. These applications involve SLN mapping and removal, angiography and vascular surgery, liver surgery and cholecystectomy, as well as plastic and reconstructive surgery, neurosurgery, and intraoperative tumor visualization and guided removal (Alander et al., 2012; Morales-Conde et al., 2022; Preziosi et al., 2024; Rosenthal et al., 2015).

While the use of NIRF imaging is well-established in various fields of human surgery, its clinical application in canine and feline medicine remains in the early stages. The number of published veterinary studies is still limited, however it has grown exponentially over the past ten years (Alvarez-Sanchez et al., 2023; Arz et al., 2022; Beer et al., 2022; Eiger et al., 2024; Favril et al., 2020, 2018;

Holt et al., 2020; Korpita et al., 2022; Larose et al., 2024; Morris et al., 2019; Mullen et al., 2024; Quinlan et al., 2021; Steffey and Mayhew, 2018; Wan et al., 2021).

Figure 2. Examples of NIRF-ICG surgical application in the Veterinary Teaching Hospital of the University of Milan clinical practice

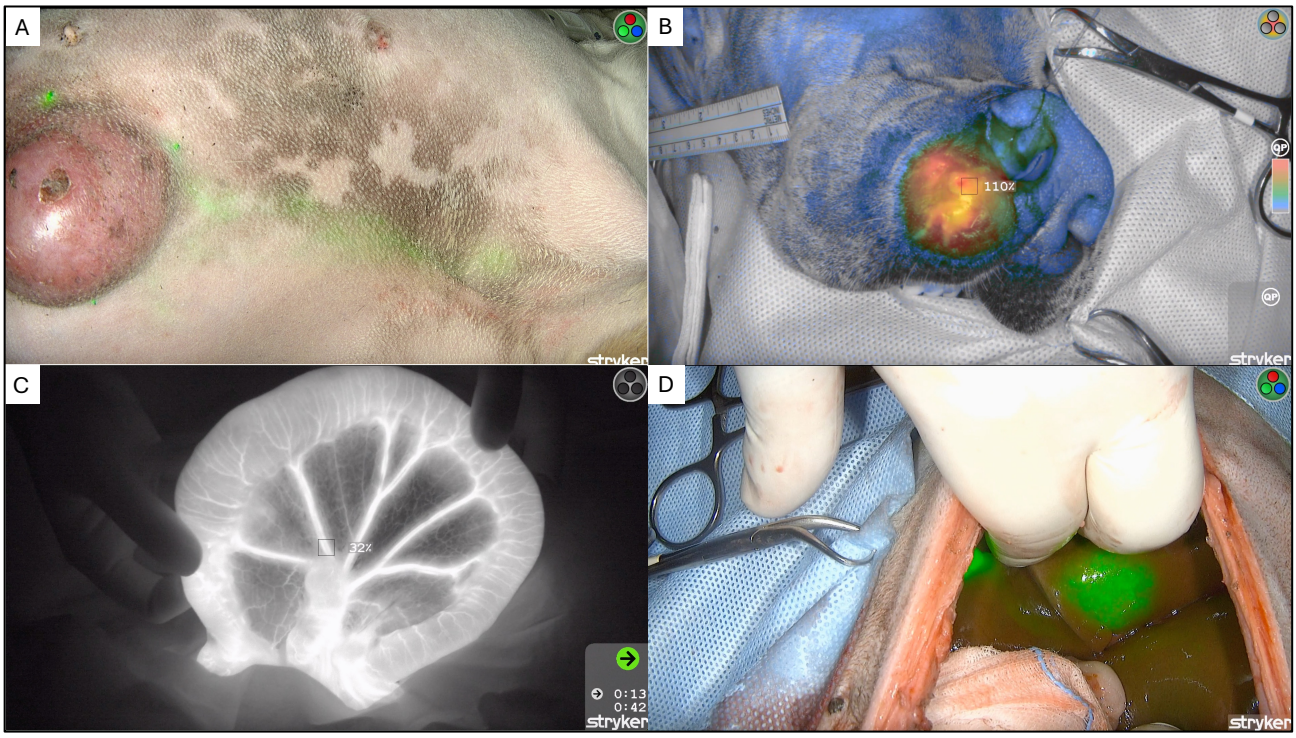

Note: Some of the daily surgical uses of NIRF technology (SPY-PHI QP System Stryker) in the Veterinary Teaching Hospital of the University of Milan. A: sentinel lymph node mapping and removal; B: fluorescence-guided surgery for tumor removal; C: assessment of bowel perfusion in an intestinal tumor removal; D: fluorescence-guided hepatic surgery for liver mass removal.

According to these preliminary data, the implementation of NIRF-ICG in small animal surgical oncology may offer a range of benefits, as already reported in human medicine (Favril et al., 2018). Besides, studying this technology in the context of spontaneous tumors in dogs and cats offers an additional incentive through translational medicine (Favril et al., 2020; Holt et al., 2020, 2014), as both species serve as valuable models not only for human oncology but also for the development and application of surgical techniques. This growing integration between veterinary and human medicine reflects that the advanced surgical technologies in canine and feline patients elevate standards of care for animals while simultaneously providing valuable insights to human medicine through a truly translational approach.

As small animals' surgical oncology continues to evolve, technologies like NIRF imaging exemplify the potential for interdisciplinary innovation. The upcoming chapters will delve into the state of the art in veterinary literature concerning the clinical application of NIRF-ICG, which provided the basis for the conception of the PhD project. The project is structured into three main branches, each focusing on the use of NIRF-ICG:

1) Enhance the knowledge in SLN mapping and extirpation in canine and feline surgical oncology
2) Explore the use of free-ICG in guided surgery to improve the probability of completing excision in two challenge cutaneous cancers in dogs, such as mast cell tumors and soft tissue sarcomas
3) Apply the updates in NIRF technology to enhance the knowledge of the lymphatic anatomy in the feline species using a cadaveric study

These branches address concepts whose background and theoretical foundations will be discussed in the following chapters.

1.2. The use of NIRF-ICG for sentinel lymph node removal:

The sentinel lymph node (SLN) is the first lymph node that may receive metastases from a malignant tumor (Morton et al., 1992.). Drawing from experience in human medicine, for years, the veterinary literature has focused on mapping the SLN. The importance of SLN extirpation has been widely described in various solid malignant tumors in dogs and cats, leading to more accurate staging, improved prognostic information, and therapeutic planning (Chiti et al., 2022, 2021; Marconato et al., 2020; Stefanello et al., 2024).

A tumor may be associated with a single or multiple SLNs, which may be located within one or several distinct sentinel lymphocentrums (SLCs) (Gariboldi et al., 2023; Stefanello et al., 2024). It is important to underline that although a SLC may contain one or more lymph nodes, not all of them are necessarily SLNs—that is, not all are directly connected to the tumor's drainage (Figure 3) (Gariboldi et al., 2023). Therefore, it is essential to use appropriate techniques to accurately identify both the SLCs and the SLNs associated with the tumor and to ensure the correct detection and removal of all SLNs.

Figure 3. Schematic representation of a tumor associated with a sentinel lymphocentrum (SLC) containing more than one lymph node: one sentinel lymph node (SLN) and one non-SLN.

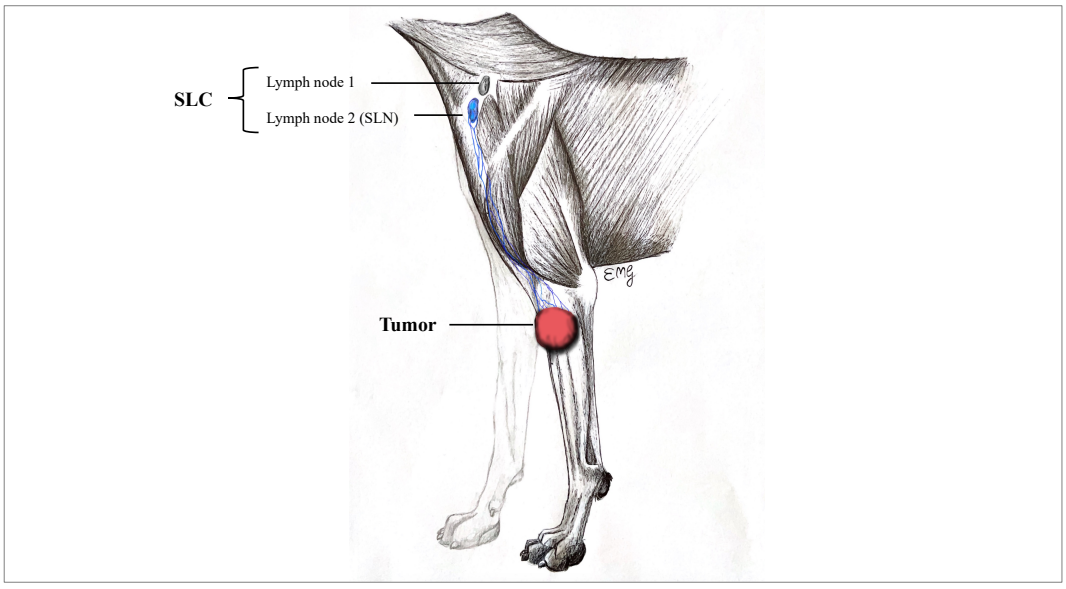

Building on this concept, it is appropriate to define two phases for SLC and SLN detection:

1. **Mapping**, a lymphography that leads to the identification of the SLC(s).
2. **Surgical exploration** of the SLC, which results in the identification of the individual SLN(s) within the lymphocentrum.

The combination of both phases leads to an improvement in the detection rate (Manfredi et al., 2021; Wan et al., 2021). The mapping is a process mostly represented by an imaging system for lymphography. The mapping results in the indication for the surgeon of the SLC to be explored. Then, during the surgical exploration of the SLC, the intraoperative guidance is essential for the complete extirpation of all SLNs within the SLC (e.g., dyes that can enhance the surgeon's visualization of lymph nodes during tissue dissection).

In veterinary literature, various techniques using different tracers or their combination are described in identifying the SLN (Alvarez-Sanchez et al., 2023; Chiti et al., 2025, 2022, 2021; Ferrari et al., 2020; Lapsley et al., 2021; Wan et al., 2021; Worley, 2014). The principle of the use of tracers is conserved across applications: the tracers are peritumoral and once injected, the tracer is drained through the lymphatic vessels originating from the peritumoral tissue, thereby following the same anatomical and functional pathways that would be used by metastatic tumor cells to reach the sentinel lymph node. The injection is eventually followed by the application of an imaging modality that enables tracer visualization.

Considering the differences between tracers and the imaging technologies, the tracers can be divided into three main categories:

- **Tracers exclusively for mapping**: tracers (e.g., iohexol or Lipiodol) that can be identified only through preoperative imaging (such as X-ray or CT) and therefore need to be combined with a tracer for the intraoperative guidance.
- **Tracers exclusively for surgical exploration use**: these tracers do not allow preoperative mapping of SLCs and must be combined with a technique that can identify them before surgery (e.g., methylene blue).
- **Tracers for both mapping and surgical exploration**: tracers that can be identified both in the preoperative mapping and at the same time can be visible/used by the surgeons for the intraoperative guidance (e.g., Technetium-99m or ICG)

Consequently, according to the ability to detect the SLC and SLN, the techniques can be classified as:

- **Multiple tracer techniques**: techniques that need to combine more than one tracer to ensure both mapping and surgical exploration (e.g., contrast-enhanced ultrasound, radiographic indirect lymphography, indirect computed tomography lymphography combined with methylene blue or NIRF for surgical exploration)

- **Single tracer techniques:** techniques that can use a single tracer for both mapping and surgical exploration (e.g., lymphoscintigraphy and NIRF)

The current knowledge is that combining different SLN mapping methods is desirable to improve detection rates in oncologic patients (Alvarez-Sanchez et al., 2023; Gariboldi et al., 2023; Manfredi et al., 2021; Wan et al., 2021).

In this context, the use of NIRF-ICG has recently attracted research interest (Alvarez-Sanchez et al., 2023; Arz et al., 2022; Beer et al., 2022; Wan et al., 2021). The technique involves the peritumoral injection of ICG (Alvarez-Sanchez et al., 2023; Arz et al., 2022; Beer et al., 2022; Wan et al., 2021), NIRF imaging is then used to perform lymphography, allowing the visualization of fluorescent drainage pathways and the identification of the SLC (Figure 4).

Figure 4. Example of NIRF-ICG in SLN detection

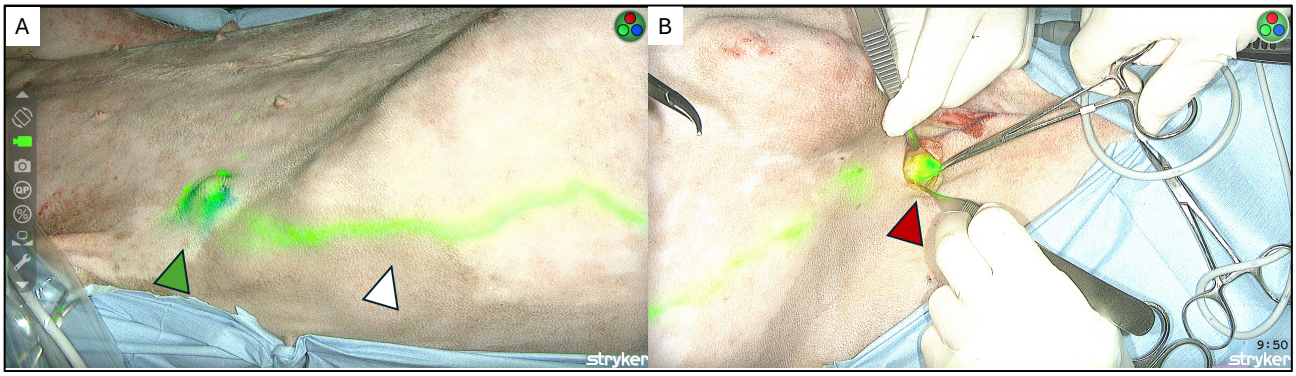

Note: A: mapping for SLC detection. The tumor and site of injection of ICG in the abdominal region (green arrow); lymphatic drainage goes to axillary SLC (white arrow); B surgical exploration guided by NIRF-ICG with axillary SLN detection (red arrow).

As previously discussed, a key feature of NIRF is its ability to detect fluorescence up to 10 mm deep (Dai et al., 2023). This makes superficial cutaneous drainage pathways visible through the NIRF camera, enabling effective lymphographic mapping.

Once the SLC is identified, it is surgically explored to remove the fluorescent SLNs. The detection and excision process is guided by the fluorescence of ICG, which remains visible through the tissues. Very small nodes embedded in fat can be easily located in this way.

This concept of intraoperative guidance, typical of techniques such as NIRF-ICG (or, for example, lymphoscintigraphy with technetium-99m), is absent in the case of methylene blue, which becomes visible only when the node is directly exposed, thus preventing real-time tissue-guided detection.

An additional advantage of these guided techniques is the ability to detect and remove all SLNs within the lymphocenter (Gariboldi et al., 2023). After each node is excised, a check is performed to assess

for residual fluorescence. Although perinodal ICG fluorescence leakage may occur after SLN removal, potentially complicating the interpretation of residual fluorescence during lymphocenter exploration, this system (similarly to residual radioactivity checks in lymphoscintigraphy) still allows for a precise and complete removal of all sentinel nodes associated with the tumor. These techniques are especially valuable in cases of non-palpable or normal-sized lymph nodes, where identification within the lymphocenter may otherwise be challenging.
Moreover, the intraoperative guidance reduces the need for extensive dissection and minimizes the risk of intra- and postoperative complications (Chiti et al., 2023; Mattioli et al., 2025).

Studies on fluorescence-guided SLN detection in dogs and cats have emerged over the past ten years, with a marked increase in the last five, during which NIRF-ICG has been applied either alone or in combination with other methods (Alvarez-Sanchez et al., 2023; Favril et al., 2019; Wan et al., 2021). Table 1 summarizes the main studies in the veterinary literature concerning the use of NIRF-ICG for SLN mapping and removal in recent years. It is noteworthy that research in this area has significantly intensified from 2022 to the present, corresponding to the period of the current doctoral thesis project, highlighting a growing interest and an increasing number of applications in veterinary practice.

Table 1. State of the art on the use of NIRF-ICG for SLN detection and removal in dogs and cats

Study	Animals	Included tumors	Technique for lymphography
Before the PhD project period			
Souza et al 2016 http://dx.doi.org/10.1590/0103-8478cr20151144	15 Dogs (healthy)	15 Healthy mammary glands	6 dogs NIRF-ICG 6 dogs MB 3 dogs control group
Townsend et al 2018 https://doi.org/10.2460/ajvr.79.9.995	6 Dogs (healthy)	6 Healthy oral mucosae	NIRF-ICG
Favril et al 2018 https://doi.org/10.1111/vco.12449	6 Dogs (healthy)	6 Inguinal, axillary, and popliteal skin regions	NIRF-ICG + CEUS
Wan et al 2021 https://doi.org/10.1111/vco.12675	14 Dogs	14 Oral tumors	NIRF-ICG + CTL + MB
Arz et al 2022 https://doi.org/10.1177/20551169221074961	1 Cat	3 MCT	NIRF-ICG
Beer et al 2022 https://doi.org/10.1111/jsap.13529	35 dogs	35 MCT	NIRF-ICG
During the PhD project period (October 2022 - October 2025)			
Chiti et al 2022 https://doi.org/10.3390/ani12223116	12 cats	14 Solid malignant tumors	9 NIRF-ICG 5 LPS

Gariboldi et al 2022 https://doi.org/10.3390/ani12172195	33 dogs	34 Scars from solid malignant tumors	22 LPS + MB 10 NIRF-ICG 2 NIRF-ICG + LPS + MB
Alvarez-Sanchez et al 2023 https://doi.org/10.1111/vsu.13929	20 dogs	20 MCT	NIRF-ICG + CTL
Griffin et al 2024 https://doi.org/10.1186/s44356-024-00005-0	8 dogs	8 AGASACA	NIRF-ICG + CTL
Nolff et al 2023 https://doi.org/10.3389/fvets.2023.1178454	1 dog	Malignant insulinoma	NIRF-ICG
Kim et al 2025 https://doi.org/10.1038/s41598-025-92243-x	24 dogs	39 Mammary tumors	NIRF-ICG
Chiti et al 2025 https://doi.org/10.1111/vco.13058	48 dogs	60 MCT	NIRF-ICG + preoperative LPS
Griffin et al 2025 https://doi.org/10.1111/vsu.14242	6 dogs	6 Thyroid carcinoma	NIRF-ICG + CTL + MB
Griffin et al 2025 https://doi.org/10.1111/vsu.14187	1 dog	Primary pulmonary carcinoma	NIRF-ICG
Monti et al 2025 https://doi.org/10.1111/vsu.14289	18 dogs	18 Solid malignant tumors	NIRF-ICG + CTL

Note: NIRF-ICG: near-infrared fluorescence with indocyanine green; MB: methylene blue; CEUS: Contrasted-enhanced ultrasound; LPS: lymphoscintigraphy; CTL: computed tomography lymphography; MCT: mast cell tumor; AGASACA: Apocrine gland anal sac adenocarcinoma.

In humans, lymphoscintigraphy (LPS) is considered the "gold standard" for SLN detection and removal (Somashekhar et al., 2020; Stoffels et al., 2015). Nevertheless, legislative restrictions, radiation exposure, and the need for specialized facilities and personnel for radiopharmaceutical handling have prompted the search for alternative methods. In this context, fluorescence imaging has emerged as a potential ideal substitute for radioactive tracers in human medicine (Bargon et al., 2022; Kedrzycki et al., 2021).

Over recent years, there has been increasing interest in using NIRF-ICG for SLN mapping in several human cancers. Initially, NIRF-ICG was used in combination with LPS (Van Den Berg et al., 2012; Verbeek et al., 2014), because it is a more effective intraoperative guidance technique than other dyes, such as methylene blue. Subsequently, numerous studies compared the two techniques to assess whether NIRF-ICG could replace the gold standard (Bargon et al., 2022; Kedrzycki et al., 2021; Stoffels et al., 2015; Tagaya et al., 2010; Wishart et al., 2012). Years of research have demonstrated that NIRF-ICG is largely comparable to LPS and can be used as an alternative in cases where LPS is unavailable, particularly in breast cancer and other human solid tumors (Bargon et al., 2022; Kedrzycki et al., 2021; Wishart et al., 2012).

In veterinary medicine, LPS remains scarcely available due to logistical and regulatory constraints. In contrast, NIRF-ICG represents an accessible and promising tool that does not require legal authorization or radioactive infrastructure. The increased interest in fluorescence imaging (Korpita et al., 2022; Morris et al., 2019; Mullen et al., 2024; Suh et al., 2015) reflects both the need to find an alternative to LPS that reduces radiation exposure for patients and staff, and the practical advantages of using NIRF-ICG in clinical and research settings, particularly in dogs and cats.

Precisely because NIRF-ICG is a guided technique that uses a single tracer for both the mapping and surgical exploration phases, it is particularly well-suited as a potential replacement for LPS. The use of a single tracer ensures greater consistency between mapping and detection, which is especially relevant when lymph nodes are small and difficult to distinguish from the surrounding fatty tissue, situations where a guided approach like NIRF-ICG can significantly improve surgical precision.

In addition to the study of the use of NIRF-ICG as a method for sentinel lymph node mapping in patients with clinically unaltered lymph nodes, as demonstrated by the works published during my PhD period, and building on the clinical and research expertise of my supervisor and the surgical oncology team, I explored the feasibility of SLN mapping and removal in canine malignancies associated with the presence of enlarged regional lymph nodes.
Although this line of research was not originally planned, it emerged as a relevant and realistic scenario encountered in routine clinical practice. Moreover, it represents a novel and largely unexplored area in small animal surgery, with only limited data available even in human medicine.
For these reasons, we aimed to address this gap, to expand current knowledge, and provide preliminary evidence to support future surgical decision-making in everyday veterinary oncology practice.

It is reported that in the presence of a malignant tumor, it is not rare to have an enlarged regional lymph node (eRLN). While the usefulness of SLN mapping in patients with non-palpable, normal-sized lymph nodes has been extensively investigated in canine oncology (Annoni et al., 2023; Chiti et al., 2025; Collivignarelli et al., 2021; Ferrari et al., 2021; Ferraris et al., 2023), no veterinary data are currently available on SLN mapping in the presence of regional lymph node enlargement.

The occurrence of a malignant tumor with eRLN often prompts clinicians to enhance preoperative staging to rule out both nodal and distant metastases. Once distant metastases are excluded, excision

of the eRLN, regardless of its neoplastic or non-neoplastic status, is recommended to achieve definitive staging and may improve the effectiveness of adjuvant treatment (Alvarez-Sanchez et al., 2023; Baginski et al., 2014; Chiti et al., 2021; Collivignarelli et al., 2021; Grimes et al., 2017; Liptak and Boston, 2019; Stefanello et al., 2024; Wan et al., 2021).

The presence of an eRLN necessitates its excision due to the potential for metastatic involvement. Nonetheless, in veterinary medicine, there is a lack of evidence regarding the clinical relevance of performing sentinel lymph node (SLN) mapping in such cases.

In human oncology, it is reported that lymph node enlargement, whether due to metastatic infiltration or inflammatory disorders, can interfere with normal lymphatic drainage and affect tracer distribution. Alterations in lymphatic flow may block or redirect the tracer, leading to incomplete or absent uptake in the enlarged node(s), and sometimes result in the rerouting of the tracer to a so-called neo-sentinel lymph node (neo-SLN), a secondary node that assumes the sentinel role following disruption of the primary drainage pathway (Bassi et al., 2006.; Goyal et al., 2005; Lam et al., 2009; Leijte et al., 2009; Liao and Von Der Weid, 2014; Monaco et al., 2012).

Understanding and identifying neo-SLNs is critical, as metastatic spread may not follow the expected anatomical pathways (Proulx et al., 2013). While the influence of metastatic or inflammatory lymphadenopathy on lymphatic drainage has been investigated in human medicine (Goyal et al., 2005; Leijte et al., 2009; Monaco et al., 2012), this aspect remains largely unexplored in veterinary surgical oncology.

1.3. The use of NIRF-ICG for tumor fluorescence-guided surgery

Achieving histologically tumor-free surgical margins is essential for the successful treatment of solid malignant tumors (Bellamy and Berlato, 2022; Bray et al., 2023; Milovancev et al., 2019). Complete tumor excision significantly reduces the risk of local recurrence and is therefore critical not only for surgical success but also for improving oncologic prognosis and overall survival. This objective is of great interest in both human and veterinary medicine.

As a result, several technological advances have aimed to develop imaging systems capable of providing more precise information regarding the completeness of tumor removal (Cheng et al., 2022; Dornbusch et al., 2021a, 2021b; Holt et al., 2020). In veterinary medicine, surgical planning is supported by advanced diagnostic imaging such as computed tomography (CT). However, most imaging modalities are still limited to preoperative planning (e.g., CT), with no real-time feedback during surgery. Other techniques, such as Optical Coherence Tomography (OCT), for instance, are primarily employed after tumor excision to support histopathological assessment, rather than to guide the surgeon intraoperatively (Cheng et al., 2022; Dornbusch et al., 2021a, 2021b; Holt et al., 2020). This lack of intraoperative imaging guidance leaves a critical gap between preoperative planning and postoperative evaluation. In this context, the adoption of tumor fluorescence-guided surgery (TFGS) is emerging in human medicine as a promising approach to address this gap.

Over the past 20 years, NIRF-ICG has been investigated for use in humans for real-time intraoperative guidance in tumor removal (Brookes et al., 2021; Gong et al., 2023; Nicoli et al., 2021). The use of ICG in guided surgery is called **"second window**" and it is based on the intravenous administration of the free-ICG standard hours before the surgery. The mechanism by which free-ICG highlights tumor tissue is related to the abnormal and poorly organized vasculature typical of tumor neoangiogenesis (Egloff-Juras et al., 2019). This leads to increased extravasation and retention of high-molecular-weight substances within the tumor, a phenomenon known as **Enhanced Permeability and Retention (EPR)**, resulting in selective tumor staining (Egloff-Juras et al., 2019) (Figure 5).

The accumulation of fluorescence in the neoplastic tissue allows the visualization of the tumor and the distinction from the surrounding healthy tissue. This "second window" use of free-ICG is an important tool in the surgical management of malignancies in humans in different solid tumors, in particular sarcomas, head and neck tumors, or breast cancers, but also visceral tumors such as pulmonary tumors, colorectal cancers, hepatic tumors, or gynecologic cancers (Brookes et al., 2021;

Gong et al., 2023; Huang et al., 2023; Ishizawa et al., 2009; Jiang et al., 2015; Nicoli et al., 2021; Veys et al., 2018).

Figure 5. Second window use of ICG for EPR effect and tumor visualization

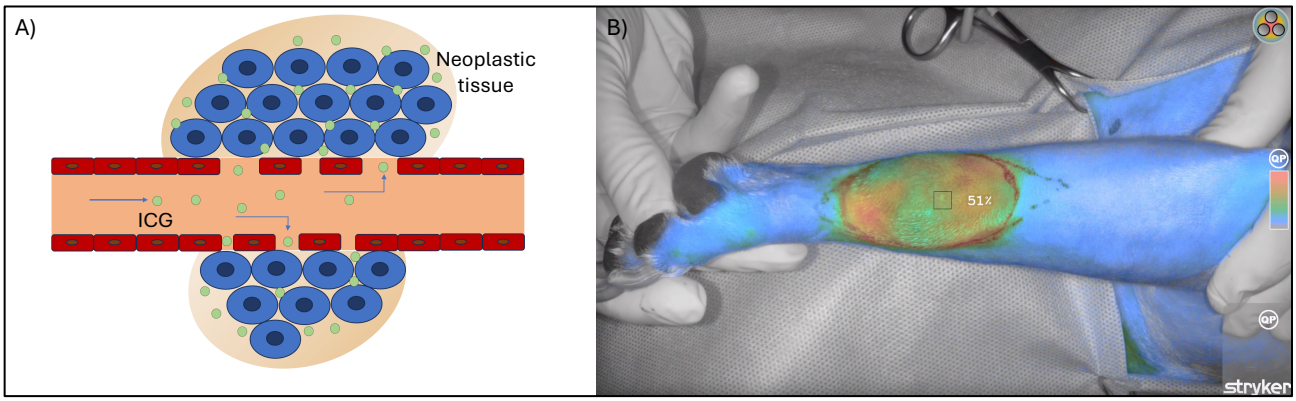

Note: A) Graphical representation of the Enhanced Permeability and Retention (EPR) effect of ICG. Following intravenous administration, ICG extravasates through the permeable tumor vasculature and accumulates within the neoplastic tissue, where it is retained.

B) Intraoperative fluorescence imaging of a tumor in a dog, 24 hours after IV injection of ICG. The dog underwent tumor excision at our Veterinary Teaching Hospital using a SPY-PHI QP System (Stryker) as the NIRF imaging device. The tumor is stained by fluorescence, while the surrounding tissue has retained minor fluorescence.

In human medicine, there is a growing focus on the development of targeted fluorophores (Keating et al., 2017). Targeted molecules have a specific affinity for tumor tissue. However, despite the promising results, the target fluorophores are not clinically available in both humans and small animals. Clinical studies in humans using targeted agents remain limited, with most translational and clinical applications still relying on non-targeted, ICG-based approaches (Keating et al., 2017). This is partly due to the wider availability and regulatory approval of ICG in clinical practice compared to targeted probes.

In contrast, canine studies have predominantly focused on targeted fluorophores (Bartholf DeWitt et al., 2016; Beer et al., 2025; Eward et al., 2013; Favril et al., 2020; Fidel et al., 2015), with relatively few reports using free-ICG (Favril et al., 2020; Holt et al., 2015; Newton et al., 2020). Notably, targeted probes are often studied in canine models as a translational step toward human application, as well as in murine models during early-phase research.

Table 2 provides an overview of the current state of the literature in both human and canine medicine, offering a comparative snapshot of TFGS applications using both free-ICG and targeted fluorophores.

Table 2. Overview of major human and canine publications on TFGS employing free-ICG and targeted fluorophores

TFGS with free-ICG		
Humans	**Studies**	**Tumor (number)**
	Ishizawa et al 2014; https://doi.org/10.1002/cncr.24291	Hepatic tumors (26)
	Veys et al 2018; https://doi.org/10.1371/journal.pone.0197857	Breast tumors (8)
	Predina et al 2019; https://doi.org/10.1002/cncr.31851	Mediastinal tumors (25)
	Newton et al 2019; https://doi.org/10.1016/j.jamcollsurg.2018.11.003	Thoracic tumors (41)
	Adbealfeez et al 2021; https://doi.org/10.3389/fped.2021.689612	Pediatric tumors (55)
	Seo et al 2021; https://doi.org/10.1002/jhbp.1037	Liver metastases (1)
	Pop et al 2021; https://doi.org/10.1016/j.ejso.2020.09.036	Breast tumors (50)
	Brookes et al 2021; https://doi.org/10.3390/cancers13246284	Sarcomas (39)
	Nicoli et al 2021; https://doi.org/10.1097/SLA.0000000000003857	Sarcomas (11)
	Gong et al 2023; https://doi.org/10.3390/cancers15030582	Sarcomas (18)
	Huang et al 2023; https://doi.org/10.1002/jso.27306	Sarcomas (70)
Dogs	**Studies**	**Tumor (number)**
	Reynolds et al 1999	Mammary tumors (2)
	Madajewski et al 2012; https://doi.org/10.1158/1078-0432.CCR-12-1188	Soft tissue sarcoma (3)
	Favril et al 2020; https://doi.org/10.1136/vr.105554	Various solid tumors (9)
	Newton et al 2020; https://doi.org/10.1371/journal.pone.0234791	Mammary tumors (41)
	Sakurai et al 2022; https://doi.org/10.1186/s12917-022-03467-2	Hepatic tumors (104)
Humans and dogs	**Studies**	**Tumor (number)**
	Holt et al 2014; https://doi.org/10.1371/journal.pone.0103342	Lung cancer (8 dogs; 5 humans)
	Holt et al 2015; https://doi.org/10.1117/1.JBO.20.7.076002	Sarcomas (15 dogs; 2 humans)
TFGS with Targeted fluorophores		
Humans	**Studies**	**Tumor (number)**
	Van Dam et al 2011; https://doi.org/10.1038/nm.2472	Ovarian cancer (10)
	Lamberts et al 2017; https://doi.org/10.1158/1078-0432.CCR-16-0437	Breast cancer (20)
	Gao et al 2018; https://doi.org/10.1158/0008-5472.CAN-18-0878	Head and neck SCC (21)
	Van Keulen et al 2019; https://doi.org/10.2967/jnumed.118.222810	Head and neck (14)
	Steinkamp et al 2021; https://doi.org/10.2967/jnumed.120.245696	Sarcomas (15)
Dogs	**Studies**	**Tumor (number)**
	Eward et al 2013; https://doi.org/10.1007/s11999-012-2560-8	MCT (4) and STS (6)
	Fidel et al 2015; https://doi.org/10.1158/0008-5472.CAN-15-0471	Various solid tumors (28)
	Bartholf DeWitt et al 2016; https://doi.org/10.1111/vsu.12487	MCT (7) and STS (12)
	Favril et al 2020; https://doi.org/10.18632/oncotarget.27633	Various solid tumors (24)
	Beer et al 2025; https://doi.org/10.1007/s00259-024-06953-x	STS (20)
Humans and dogs	**Studies**	**Tumor (number)**
	Keating et al 2017; https://doi.org/10.1002/cncr.30419	Lung cancer (10 dogs; 3 humans)
	Kennedy et al 2022; https://doi.org/10.1158/1078-0432.CCR-22-1215	Lung cancer (4 dogs; 2 humans)

There is a significant heterogeneity of published data about ICG dosage and administration timing (ranging from directly during the surgery to some days before surgery) (Table 3). This variability is evident in both human and canine studies, highlighting the lack of a standardized protocol for TFGS. In general, in dogs, the majority of studies utilize relatively high doses (3-7.5 mg/kg) of ICG (Favril et al., 2020; Holt et al., 2020, 2015; Madajewski et al., 2012; Newton et al., 2020).

Moreover, despite the wide range of time intervals explored, administration approximately 24 hours prior to surgery is the most frequently adopted protocol, especially in studies aiming to enhance tumor delineation through passive accumulation of the dye in neoplastic tissues (Favril et al., 2020; Holt et al., 2020, 2015; Madajewski et al., 2012; Newton et al., 2020; Sakurai et al., 2022). The differences in timing and dosage across studies reflect varying methodological approaches, as well as differences in tumor types included in the studies (Table 2-3). This heterogeneity complicates direct comparison across studies and underscores the need for consensus guidelines to optimize the use of ICG in canine surgical oncology.

Furthermore, consensus exists across human studies regarding the necessity of developing robust fluorescence quantification strategies to improve the accuracy and reproducibility of TFGS (de Muynck et al., 2023).
Quantification of the fluorescence intensity is essential to objectively distinguish the neoplastic from the non-neoplastic tissue. The quantification is most expressed as the tumor-to-background ratio (TBR) or signal-to-background ratio (SBR). However, there is considerable variability in the literature in the cut-off values considered indicative of neoplastic tissue, across both veterinary and human studies, even if, the most reported thresholds for distinguishing healthy from neoplastic tissue is a value of 2 (Gong et al., 2023; Holt et al., 2015; Huang et al., 2023; Newton et al., 2020). (Table 3)

In some studies, fluorescence quantification is not performed at all, and when it is, it is often carried out retrospectively using image analysis software in post-processing, rather than in real time. However, real-time intraoperative quantification is crucial, as it allows the surgical team to make informed decisions during the procedure, directly supporting the surgeon’s decision-making process (Predina et al., 2019).

Table 3. The ICG dose, timing, and the fluorescent intensity assessment in human and canine studies

Human data				
Study	**Tumor**	**ICG dose**	**Timing**	**TBR or SBR**
Ishizawa et al 2014	Hepatocellular Carcinoma	0.5 mg/kg	2 weeks before	Not reported*
Veys et al 2018	Breast tumors	0.25 mg/kg	Intraoperative	1.3
Predina et al 2019	Mediastinal tumors	5 mg/kg	24 h before	5.3§
Newton et al 2019	Thoracic tumors	5 mg/kg	24 h before	2
Adbealfeez et al 2021	Pediatric tumors	1.5 mg/kg	24 h before	Not reported
Seo et al 2021	Liver metastases	0.5 mg/kg	2 days before	Not reported
Pop et al 2021	Breast tumors	0.25 mg/kg	Anesthesia time	1.3
Brookes et al 2021	Sarcomas	1 mg/kg	16-24 h before	Not reported
Nicoli et al 2021	Sarcomas	2 mg/kg	16-24 h before	Not reported
Gong et al 2023	Sarcomas	2-2.5 mg/kg	3 h before	2
Huang et al 2023	Sarcomas	0.5 mg/kg	1-3 h before	2
Canine data				
Study	**Tumor**	**ICG dose**	**Timing**	**TBR or SBR**
Reynolds et al 1999	Mammary tumors	1 mg/kg	0-2 h before	Not reported
Madajewski et al 2012	Soft tissue sarcoma	7.5 mg/kg	24 h before	Not reported
Holt et al 2014	Pulmonary tumors	5 mg/kg	24 h before	6.7§
Holt et al 2015	Soft tissue sarcoma	3 mg/kg	24 h before	2
Newton et al 2020	Mammary tumors	3 mg/kg	20 h before	1.2
Favril et al 2020	Various solid tumors	5 mg/kg	24 h before	1.4§
Sakurai et al 2022	Hepatic tumor	0.5 mg/kg	12-24 h before	Not reported

Note: * Calculated the fluorescence intensity but not the ratio

§ This value of TBR is a result of the study, not used intraoperatively as a cut-off

As demonstrated by the current state-of-the-art analysis, despite the increasing interest in NIRF-ICG in canine surgery, the current literature on this topic remains limited and fragmented (Table 2-3). While targeted fluorophores show promising results in human medicine, their use is still largely experimental and less accessible in veterinary settings. In contrast, NIRF imaging with free-ICG represents a more affordable and widely available option, making it highly relevant for clinical use in dogs. There is a clear need to expand and integrate canine data to establish clinically meaningful applications of NIRF-ICG in canine oncology.

1.4. NIRF-ICG lymphography in cadavers for anatomical study:

In the last decades, lymphography in cadavers has been performed in various animal species as anatomical and translational models for investigating human lymphedema and other lymphatic disorders (Ito and Suami, 2015; Soto-Miranda et al., 2013; Suami et al., 2016, 2013, 2007).
Numerous techniques have been described to assess superficial lymphatic drainage patterns in both human and animal cadavers (Ito and Suami, 2015; Shinaoka et al., 2019, 2018; Soto-Miranda et al., 2013; Suami et al., 2016, 2013, 2007). Among these, NIRF-ICG has emerged as the most widely adopted and effective technology, due to its minimally invasive nature, real-time visualization capabilities, and high sensitivity in detecting lymphatic vessels and nodes (Suami and Shinaoka, 2019). Table 4 reports an overview of the last 20 years of lymphography studies in humans and animals.

Table 4. Overview of the last 20 years of lymphography studies in humans and animals

Studies	Species	Lymphography (number of cases)	Technique
Suami et al 2005 https://doi.org/10.1097/01.prs.0000163325.06437.b0	Human (cadaver)	Upper limb (1)	Radiographic + blue dye
Suami et al 2008 https://doi.org/10.1097/01.prs.0000293753.93274.21	Dogs (cadaver)	Torso (7)	Radiographic + ink
Suami et al 2012 https://doi.org/10.1097/PRS.0b013e3182402c6d	Dogs (cadaver)	Forelimb (6)	Radiographic + ink
Suami et al 2013 https://doi.org/10.1371/journal.pone.0069222	Dogs (4 cadaver + 2 alive and then euthanized)	Whole body (6)	Radiographic + ink + NIRF-ICG
Soto-Miranda et al 2013 https://doi.org/10.1002/ar.22699	Rabbits (2 alive + 8 cadavers)	Whole body (8)	NIRF-ICG
Ito and Suami, 2015 https://doi.org/10.1097/PRS.0000000000001460	Swine (cadaver)	Whole body (6)	Radiographic + ink + NIRF-ICG
Suami et al 2016 https://doi.org/10.1016/j.jss.2016.05.029	Dogs (alive)	Forelimb (2)	Radiographic + NIRF-ICG
Nakajima et al 2018 https://doi.org/10.1038/s41598-018-25383-y	Mice (alive and then euthanized)	Hind limbs (19)	NIRF-ICG
Shinaoka et al 2018 https://doi.org/10.1097/PRS.0000000000004315	Human (cadaver)	Lower limbs (10)	NIRF-ICG
Shinaoka et al 2019 https://doi.org/10.1097/PRS.000000000000598	Human (cadaver)	Lower limbs (53)	NIRF-ICG
Sanchez-Margallo et al 2020 https://doi.org/10.1371/journal.pone.0241992	Dogs (cadaver)	Laparoscopic lymphography of medial iliac lymph nodes (6)	NIRF-ICG
Lu et al 2023 https://doi.org/10.2460/ajvr.23.07.0168	Cats (alive)	Hind limbs (14)	NIRF-ICG +/- MB

In human medicine, there is considerable interest in studying lymphography due to its relevance in understanding the potential lymphatic complications associated with oncologic surgeries involving lymphadenectomy, such as lymphedema (Suami et al., 2016, 2005). The scarcity of human cadavers, along with ethical concerns, limits the feasibility of such research in humans, which is why animal cadavers are more commonly used for these anatomical and lymphographic investigations (Bala Ganesh et al., 2024). Among all studied animal species, the dog has been the most extensively considered in this context, due to its classification as a "large animal" and its suitability as a model both for lymphatic system physiology and for developing and refining surgical techniques (Sánchez-Margallo et al., 2020).

In veterinary medicine, however, there is no dedicated research, and much of our knowledge about the lymphatic anatomy relies on translational studies. One of the most significant contributions to the veterinary clinical practice and also to research is the study by Suami et al. (2013). This study used NIRF-ICG to assess the lymphography of the whole body of 4 healthy canine cadavers and identified 10 cutaneous lymphatic drainage territories, referred to as ''lymphosomes" (Figure 6).

Figure 6. Lymphosomes reported in Suami's study (2013)

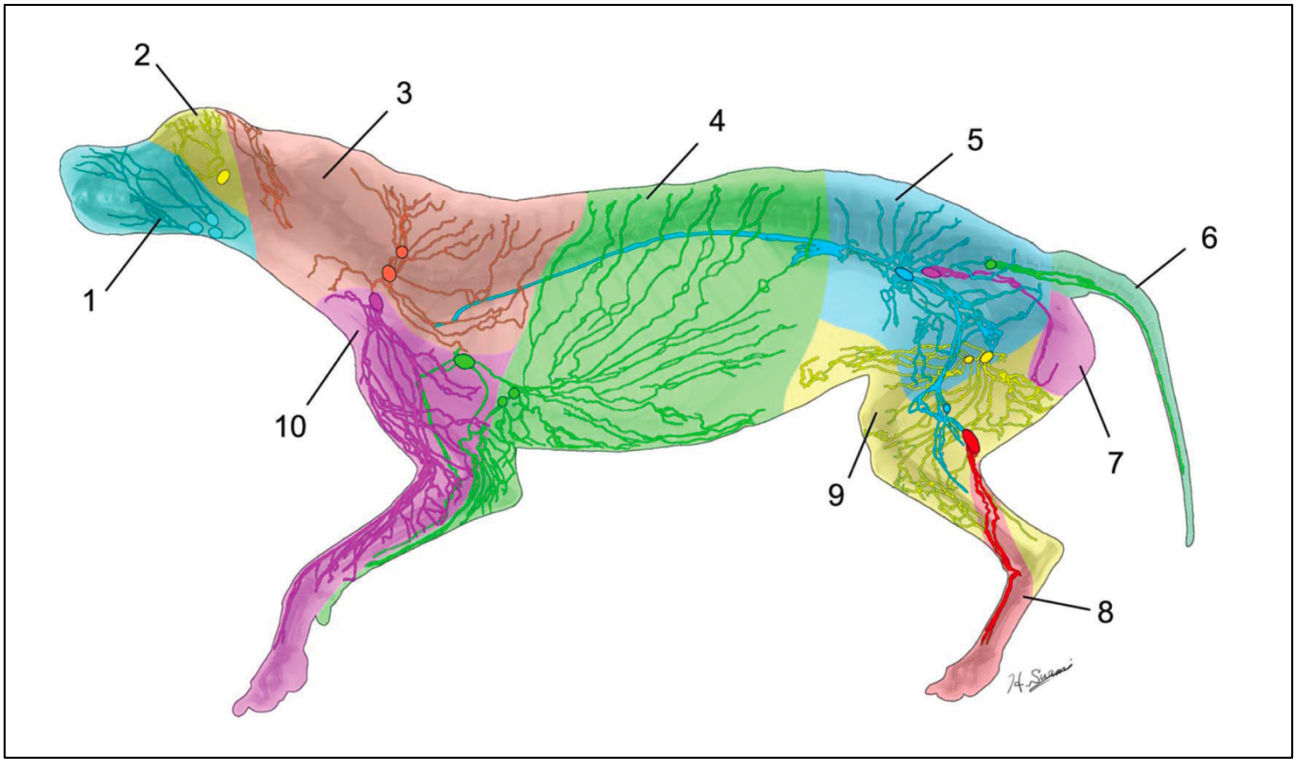

Note: 1, submandibular; 2, parotid; 3, dorsal superficial cervical; 4, axillary; 5, medial iliac; 6, lateral sacral; 7, hypogastric; 8, popliteal; 9, superficial inguinal; 10, ventral superficial cervical (Suami et al., 2013)

To date, these lymphosomes are routinely used in small animals' surgical oncology to determine the regional lymphocentrum (LC) responsible for draining specific anatomical areas affected by

neoplasia (Chiti et al., 2021; Ferrari et al., 2020). This approach has provided a more rational and anatomy-based method for draining lymph node identification and staging in dogs, improving the accuracy of oncologic surgical planning in cases where no SLN mapping has been performed. These anatomical predictions have been compared with the actual sentinel LC identified intraoperatively in various neoplastic conditions, thus validating the translational potential of cadaveric models (Chiti et al., 2021; Ferrari et al., 2020).

In contrast to the canine data, the feline lymphatic system remains poorly documented. Only a limited number of descriptive anatomical studies are available (Tobón Restrepo et al., 2022, 2021), and existing lymphographic research in cats is either outdated or narrowly focused on specific anatomical districts (Ratzlaff 1970; Tobón Restrepo et al., 2022, 2021; Wong et al., 1991.). To date, no lymphographic studies have comprehensively described the cutaneous lymphatic territories in cats, and detailed mapping of superficial lymphatic pathways from distinct body regions is still lacking. As a consequence, clinical studies involving lymph node assessment in feline oncology often rely on extrapolated data from canine models (Chiti et al., 2022), which may not accurately reflect the anatomical and physiological characteristics of the feline lymphatic system, potentially leading to misidentification or oversight of sentinel lymph nodes.

Furthermore, the study conducted on dogs highlighted the lymphatic territories but did not define the anatomical boundaries of these regions (Suami et al., 2013). As a result, the interpretation of border areas and overlaps between different lymphosomes is challenging from a clinical perspective and cannot be precisely applied to all individuals.

Recent advancements in sentinel lymph node mapping and surgical excision techniques in dogs have highlighted the complexity of the superficial lymphatic network in the head and hind limb regions. These areas pose significant challenges due to their variable and intricate lymphatic architecture, which can contribute to mapping inconsistencies or technique failure, even when using advanced imaging tools such as NIRF-ICG (Chiti et al., 2022; Suami et al., 2013).

In light of the limited available data and the growing clinical need for precise lymphatic mapping in feline patients, continued exploration in this field is warranted.

1.5. General aim:

The use of NIRF-ICG has attracted increasing interest in human medicine, particularly in general and oncological surgery, where it is employed for sentinel lymph node mapping, assessment of tissue perfusion, and intraoperative visualization of anatomical structures. In recent years, this technology has started to emerge in the field of small animal surgery as well, where it has promising results for similar applications. The real-time imaging capabilities of NIRF-ICG make it an attractive tool for improving surgical precision and outcomes in canine and feline patients.

Nevertheless, despite this rising attention, the body of published data regarding NIRF-ICG in small animal patients remains scarce. Most of the current knowledge is derived from human studies or limited veterinary case reports, which may not fully translate to the anatomical and physiological characteristics of small animals.

This highlights a significant gap in the existing literature and underlines the need for dedicated research to evaluate the applications of NIRF-ICG imaging in small animals' routine surgical practice.

In this context, the present PhD project is developed in 3 research lines of which the purposes are summarized below:

1. **NIRF-ICG in sentinel lymph node removal**
   Study the feasibility and utility of NIRF-ICG in SLN detection and removal, and its combined use with lymphoscintigraphy and comparison in performance.

2. **NIRF-ICG for tumor fluorescence-guided surgery**
   Study the feasibility and utility of NIRF-ICG in real-time intraoperative tumor visualization for decision making on excision surgical dose

3. **NIRF-ICG lymphography in cadavers for anatomical study**
   Use the NIRF-ICG technique for ex vivo lymphography study in feline cadavers, especially in anatomical regions recognized for having unpredictable drainage

1.6. References:

Alander, J.T., Kaartinen, I., Laakso, A., Pätilä, T., Spillmann, T., Tuchin, V. V., Venermo, M., Välisuo, P., 2012. A Review of indocyanine green fluorescent imaging in surgery. Int J Biomed Imaging. https://doi.org/10.1155/2012/940585

Alius, C., Oprescu, S., Balalau, C., Nica, A.E., 2018. Indocyanine green enhanced surgery; principle, clinical applications and future research directions. Journal of Clinical and Investigative Surgery 3, 1–8. https://doi.org/10.25083/2559.5555/31.18

Alvarez-Sanchez, A., Townsend, K.L., Newsom, L., Milovancev, M., Gorman, E., Russell, D.S., 2023. Comparison of indirect computed tomographic lymphography and near-infrared fluorescence sentinel lymph node mapping for integumentary canine mast cell tumors. Veterinary Surgery 52, 416–427. https://doi.org/10.1111/vsu.13929

Annoni, M., Borgonovo, S., Aralla, M., 2023. Sentinel lymph node mapping in canine mast cell tumours using a preoperative radiographic indirect lymphography: Technique description and results in 138 cases. Veterinary and Comparative Oncology 21, 469–481. https://doi.org/10.1111/vco.12906

Arz, R., Seehusen, F., Meier, V.S., Nolff, M.C., 2022. Indocyanine-based near-infrared lymphography for real-time detection of lymphatics in a cat with multiple mast cell tumours. Journal of Feline Medicine and Surgery Open Reports 8. https://doi.org/10.1177/20551169221074961

Baginski, H., Davis, G., Bastian, R.P., 2014. The Prognostic Value of Lymph Node Metastasis with Grade 2 MCTs in Dogs: 55 Cases (2001-2010). Journal American Animal Hospital Association 50, 89–95. https://doi.org/10.5326/JAAHA-MS-5997

Bala Ganesh, K.A., Panda, P., Gurawa, T., Gopalakrishna, P.K., Jagadeesan, S., Vishnumukkala, T., 2024. Ethics on academic procurement of cadavers. Bioinformation 20, 872–876. https://doi.org/10.6026/973206300200872

Bargon, C.A., Huibers, A., Young-Afat, D.A., Jansen, B.A.M., Borel-Rinkes, I.H.M., Lavalaye, J., van Slooten, H.J., Verkooijen, H.M., van Swol, C.F.P., Doeksen, A., 2022. Sentinel lymph node mapping in breast cancer patients through fluorescent imaging using indocyanine green the influence trial. Annals of Surgery 276, 913–920. https://doi.org/10.1097/SLA.0000000000005633

Bartholf DeWitt, S., Eward, W.C., Eward, C.A., Lazarides, A.L., Whitley, M.J., Ferrer, J.M., Brigman, B.E., Kirsch, D.G., Berg, J., 2016. A Novel Imaging System Distinguishes Neoplastic

from Normal Tissue During Resection of Soft Tissue Sarcomas and Mast Cell Tumors in Dogs. Veterinary Surgery 45, 715–722. https://doi.org/10.1111/vsu.12487

Bassi, K.K., Seenu, V., Ballehaninna, U.K., Parshad, R., Chumber, S., Dhar, A., Gupta, S.D., Kumar, R., Srivastava, A., 2006. Second echelon node predicts metastatic involvement of additional axillary nodes following sentinel node biopsy in early breast cancer. Indian Journal of Cancer **43**, 103–109.

Beer, P., Grest, P., Krudewig, C., Staudinger, C., Ohlerth, S., Rohrer Bley, C., Jarosch, A., Ech-Cherif, H., Markkanen, E., Park, B., Nolff, M.C., 2025. Evaluation of a targeted anti-αvβ3 integrin near-infrared fluorescent dye for fluorescence-guided resection of naturally occurring soft tissue sarcomas in dogs. European Journal of Nuclear Medicine and Molecular Imaging52, 1137–1148. https://doi.org/10.1007/s00259-024-06953-x

Beer, P., Rohrer-Bley, C., Nolff, M.C., 2022. Near-infrared fluorescent image-guided lymph node dissection compared with locoregional lymphadenectomies in dogs with mast cell tumours. Journal of Small Animal Practice 63, 670–678. https://doi.org/10.1111/jsap.13529

Bellamy, E., Berlato, D., 2022. Canine cutaneous and subcutaneous mast cell tumours: a narrative review. Journal of Small Animal Practice. 63, 497–511, https://doi.org/10.1111/jsap.13444

Bray, J., Eward, W., Breen, M., 2023. Evaluating the relevance of surgical margins. Part one: The problems with current methodology. Veterinary and Comparative Oncology 21(1), 1–11. https://doi.org/10.1111/vco.12865

Brookes, M.J., Chan, C.D., Nicoli, F., Crowley, T.P., Ghosh, K.M., Beckingsale, T., Saleh, D., Dildey, P., Gupta, S., Ragbir, M., Rankin, K.S., 2021. Intraoperative near-infrared fluorescence guided surgery using indocyanine green (ICG) for the resection of sarcomas may reduce the positive margin rate: An extended case series. Cancers (Basel) 13(24), 6284. https://doi.org/10.3390/cancers13246284

Buote, N.J., 2024. Looking to the Future; Veterinary Robotic Surgery. Veterinary Clinics of North America - Small Animal Practice. 54(2) https://doi.org/10.1016/j.cvsm.2024.02.008

Cheng, E., Jennings, R.N., Chen, C.L., Biggo, M.R., Erickson, A.K., Dornbusch, J.A., Linn, S.C., Lapsley, J., Alva, B.M., Lorbach, J.N., Premanandan, C., Selmic, L.E., 2022. Optical coherence tomography for surgical margin evaluation of excised canine cutaneous and subcutaneous tumours. Veterinary and Comparative Oncology 20, 836–845. https://doi.org/10.1111/vco.12844

Chiti, L.E., Beer, P., Ohlerth, S.M., Hartnack, S., Nolff, M.C., 2025. SHINE – Validation of Near Infrared Fluorescence Lymphography Against Lymphoscintigraphy for Sentinel Lymph Node

Biopsy in Dogs With Mast Cell Tumours. Veterinary and Comparative Oncology 23, 320–329. https://doi.org/10.1111/vco.13058

Chiti, L.E., Gariboldi, E.M., Ferrari, R., Luconi, E., Boracchi, P., De Zani, Donatella, Zani, Davide, Manfredi, M., Spediacci, C., Grieco, V., Giudice, C., Recordati, C., Ferrari, F., Stefanello, D., 2023. Surgical complications following sentinel lymph node biopsy guided by γ-probe and methylene blue in 113 tumour-bearing dogs. Veterinary and Comparative Oncology 21, 62–72. https://doi.org/10.1111/vco.12861

Chiti, L.E., Gariboldi, E.M., Stefanello, D., De Zani, D., Grieco, V., Nolff, M.C., 2022. Sentinel Lymph Node Mapping and Biopsy in Cats with Solid Malignancies: An Explorative Study. Animals 12 (23). https://doi.org/10.3390/ani12223116

Chiti, L.E., Stefanello, D., Manfredi, M., Zani, D.D., De Zani, D., Boracchi, P., Giudice, C., Grieco, V., Di Giancamillo, M., Ferrari, R., 2021. To map or not to map the cN0 neck: Impact of sentinel lymph node biopsy in canine head and neck tumours. Veterinary and Comparative Oncology 19, 661–670. https://doi.org/10.1111/vco.12697

Collivignarelli, F., Tamburro, R., Aste, G., Falerno, I., Signore, F. Del, Simeoni, F., Patsikas, M., Gianfelici, J., Terragni, R., Attorri, V., Carluccio, A., Vignoli, M., 2021. Lymphatic drainage mapping with indirect lymphography for canine mammary tumors. Animals 11(4). https://doi.org/10.3390/ani11041115

Dai, Z.Y., Shen, C., Mi, X.Q., Pu, Q., 2023. The primary application of indocyanine green fluorescence imaging in surgical oncology. Frontiers in Surgery 10, 1077492. https://doi.org/10.3389/fsurg.2023.1077492

de Muynck, L.D.A.N., White, K.P., Alseidi, A., Bannone, E., Boni, L., Bouvet, M., Falconi, M., Fuchs, H.F., Ghadimi, M., Gockel, I., Hackert, T., Ishizawa, T., Kang, C.M., Kokudo, N., Nickel, F., Partelli, S., Rangelova, E., Swijnenburg, R.J., Dip, F., Rosenthal, R.J., Vahrmeijer, A.L., Mieog, J.S.D., 2023. Consensus Statement on the Use of Near-Infrared Fluorescence Imaging during Pancreatic Cancer Surgery Based on a Delphi Study: Surgeons' Perspectives on Current Use and Future Recommendations. Cancers (Basel) 15(3), 652. https://doi.org/10.3390/cancers15030652

Dobson, J.M., 2019. Significant advances in veterinary oncology – 60 years on. Journal of Small Animal Practice. https://doi.org/10.1111/jsap.13076

Dornbusch, J.A., Cocca, C., Jennings, R., Samuelson, J., Vieson, M., Huang, P.C., Boppart, S.A., Wavreille, V.A., Selmic, L.E., 2021a. The feasibility and utility of optical coherence tomography directed histopathology for surgical margin assessment of canine mast cell tumours. Vet Comp Oncol 19, 616–623. https://doi.org/10.1111/vco.12654

Dornbusch, J.A., Selmic, L.E., Huang, P.C., Samuelson, J.P., McLaughlin, E.M., Wavreille, V.A., Ogden, J.A., Abrams, B., Kalamaras, A., Green, E., Hostnik, E.T., Every, L., Fuerst, J.A., Jennings, R., Premanandan, C., Lorbach, J.N., Linn, S.C., Alex, A., Sorrells, J.E., Yang, L., Boppart, S.A., 2021b. Diagnostic accuracy of optical coherence tomography for assessing surgical margins of canine soft tissue sarcomas in observers of different specialties. Veterinary Surgery 50, 111–120. https://doi.org/10.1111/vsu.13510

Egloff-Juras, C., Bezdetnaya, L., Dolivet, G., Lassalle, H.P., 2019. NIR fluorescence-guided tumor surgery: New strategies for the use of indocyanine green. International Journal of Nanomedicine 14, 7823–7838. https://doi.org/10.2147/IJN.S207486

Eiger, S.N., Bertran, J., Reynolds, P.S., Regier, P., Case, J.B., Ham, K., Mison, M., Fox-Alvarez, W.A., 2024. Use of near-infrared fluorescence angiography with indocyanine green to evaluate direct cutaneous arteries used for canine axial pattern flaps. Veterinary Surgery 53, 1073–1082. https://doi.org/10.1111/vsu.14121

Eward, W.C., Mito, J.K., Eward, C.A., Carter, J.E., Ferrer, J.M., Kirsch, D.G., Brigman, B.E., 2013. A novel imaging system permits real-time in vivo tumor bed assessment after resection of naturally occurring sarcomas in dogs tumor, in: Clinical Orthopaedics and Related Research. Springer New York LLC, pp. 834–842. https://doi.org/10.1007/s11999-012-2560-8

Favril, S., Abma, E., Blasi, F., Stock, E., Devriendt, N., Vanderperren, K., De Rooster, H., 2018. Clinical use of organic near-infrared fluorescent contrast agents in image-guided oncologic procedures and its potential in veterinary oncology. Veterinary Record. 183(11), 354 https://doi.org/10.1136/vr.104851

Favril, S., Abma, E., Stock, E., Devriendt, N., Van Goethem, B., Blasi, F., Brioschi, C., Polis, I., De Cock, H., Miragoli, L., Oliva, P., Valbusa, G., Vanderperren, K., De Rooster, H., 2020. Fluorescence-guided surgery using indocyanine green in dogs with superficial solid tumours. Veterinary Record 187, 273. https://doi.org/10.1136/vr.105554

Favril, S., Brioschi, C., Vanderperren, K., Abma, E., Stock, E., Devriendt, N., Polis, I., De Cock, H., Cordaro, A., Miragoli, L., Oliva, P., Valbusa, G., Alleaume, C., Tardy, I., Maiocchi, A., Tedoldi, F., Blasi, F., De Rooster, H., 2020. Preliminary safety and imaging efficacy of the near-infrared fluorescent contrast agent DA364 during fluorescence-guided surgery in dogs with spontaneous superficial tumors, Oncotarget 11(24), 2310–2326. https://doi.org/10.18632/oncotarget.27633

Favril, S., Stock, E., Hernot, S., Hesta, M., Polis, I., Vanderperren, K., de Rooster, H., 2019. Sentinel lymph node mapping by near-infrared fluorescence imaging and contrast-enhanced ultrasound in healthy dogs. Veterinary and Comparative Oncology 17, 89–98. https://doi.org/10.1111/vco.12449

Ferrari, R., Boracchi, P., Chiti, L.E., Manfredi, M., Giudice, C., De Zani, D., Spediacci, C., Recordati, C., Grieco, V., Gariboldi, E.M., Stefanello, D., 2021. Assessing the risk of nodal metastases in canine integumentary mast cell tumors: Is sentinel lymph node biopsy always necessary? Animals 11, 82373. https://doi.org/10.3390/ani11082373

Ferrari, R., Chiti, L.E., Manfredi, M., Ravasio, G., De Zani, D., Zani, D.D., Giudice, C., Gambini, M., Stefanello, D., 2020. Biopsy of sentinel lymph nodes after injection of methylene blue and lymphoscintigraphic guidance in 30 dogs with mast cell tumors. Veterinary Surgery 49, 1099–1108. https://doi.org/10.1111/vsu.13483

Ferraris, E.I., Olimpo, M., Giacobino, D., Manassero, L., Iussich, S., Lardone, E., Camerino, M., Buracco, P., Morello, E.M., 2023. Sentinel lymph node mapping with computed tomography lymphography for mast cell tumours and a comparison between regional and sentinel lymph node histological status: Sixty-two cases. Vet Comp Oncol 21, 208–220. https://doi.org/10.1111/vco.12878

Fidel, J., Kennedy, K.C., Dernell, W.S., Hansen, S., Wiss, V., Stroud, M.R., Molho, J.I., Knoblaugh, S.E., Meganck, J., Olson, J.M., Rice, B., Parrish-Novak, J., 2015. Preclinical Validation of the Utility of BLZ-100 in Providing Fluorescence Contrast for Imaging Spontaneous Solid Tumors. Cancer Res 75, 4283–4291. https://doi.org/10.1158/0008-5472.CAN-15-0471

Gariboldi, E.M., Ubiali, A., Chiti, L.E., Ferrari, R., De Zani, D., Zani, D.D., Grieco, V., Giudice, C., Recordati, C., Stefanello, D., Auletta, L., 2023. Evaluation of Surgical Aid of Methylene Blue in Addition to Intraoperative Gamma Probe for Sentinel Lymph Node Extirpation in 116 Canine Mast Cell Tumors (2017–2022). Animals 13, 11854. https://doi.org/10.3390/ani13111854

Gibson, E.A., 2024. Augmenting Veterinary Minimally Invasive Surgery: Evidence-based Review of Foundational and Novel Devices and Technology. Veterinary Clinics of North America - Small Animal Practice, 54(4), 721–733. https://doi.org/10.1016/j.cvsm.2024.02.007

Gong, M.F., Li, W.T., Bhogal, S., Royes, B., Heim, T., Silvaggio, M., Malek, M., Dhupar, R., Lee, S.J., McGough, R.L., Weiss, K.R., 2023. Intraoperative Evaluation of Soft Tissue Sarcoma Surgical Margins with Indocyanine Green Fluorescence Imaging. Cancers (Basel) 15, 30582. https://doi.org/10.3390/cancers15030582

Goyal, A., Douglas-Jones, A.G., Newcombe, R.G., Mansel, R.E., 2005. Effect of lymphatic tumor burden on sentinel lymph node biopsy in breast cancer. Breast Journal 11, 188–194. https://doi.org/10.1111/j.1075-122X.2005.21591.x

Grimes, J.A., Secrest, S.A., Northrup, N.C., Saba, C.F., Schmiedt, C.W., 2017. Indirect computed tomography lymphangiography with aqueous contrast for evaluation of sentinel lymph nodes

in dogs with tumors of the head. Veterinary Radiology and Ultrasound 58, 559–564. https://doi.org/10.1111/vru.12514

Holt, D., Okusanya, O., Judy, R., Venegas, O., Jiang, J., DeJesus, E., Eruslanov, E., Quatromoni, J., Bhojnagarwala, P., Deshpande, C., Albelda, S., Nie, S., Singhal, S., 2014. Intraoperative near-infrared imaging can distinguish cancer from normal tissue but not inflammation. PLoS One 9. e103342. https://doi.org/10.1371/journal.pone.0103342

Holt, D., Parthasarathy, A.B., Okusanya, O., Keating, J., Venegas, O., Deshpande, C., Karakousis, G., Madajewski, B., Durham, A., Nie, S., Yodh, A.G., Singhal, S., 2015. Intraoperative near-infrared fluorescence imaging and spectroscopy identifies residual tumor cells in wounds. ournal of Biomedical Optics 20, 076002. https://doi.org/10.1117/1.jbo.20.7.076002

Holt, D., Singhal, S., Selmic, L.E., 2020. Near-infrared imaging and optical coherence tomography for intraoperative visualization of tumors. Veterinary Surgery; 49(1), 33–43 https://doi.org/10.1111/vsu.13332

Huang, H., He, S., Wei, R., Zhu, X., Deng, Z., Wang, Y., Guo, L., Lei, J., Cai, L., Xie, Y., 2023. Near-infrared (NIR) imaging with indocyanine green (ICG) may assist in intraoperative decision making and improving surgical margin in bone and soft tissue tumor surgery. ournal of Surgical Oncology 128, 612–627. https://doi.org/10.1002/jso.27306

Ishizawa, T., Fukushima, N., Shibahara, J., Masuda, K., Tamura, S., Aoki, T., Hasegawa, K., Beck, Y., Fukayama, M., Kokudo, N., 2009. Real-time identification of liver cancers by using indocyanine green fluorescent imaging. Cancer 115, 2491–2504. https://doi.org/10.1002/cncr.24291

Ito, R., Suami, H., 2015. Lymphatic territories (Lymphosomes) in Swine: An animal model for future lymphatic research, in: Plastic and Reconstructive Surgery. Lippincott Williams and Wilkins, pp. 297–304. https://doi.org/10.1097/PRS.0000000000001460

Jiang, J.X., Keating, J.J., De Jesus, E.M., Judy, R.P., Madajewski, B., Venegas, O., Okusanya, O.T., Singhal, S., 2015. Optimization of the enhanced permeability and retention effect for near-infrared imaging of solid tumors with indocyanine green, American Journal of Nuclear Medicine and Molecular Imaging 5, 390–400. https://doi.org/10.11648/j.ijnm.20150504.13

Keating, J.J., Runge, J.J., Singhal, S., Nims, S., Venegas, O., Durham, A.C., Swain, G., Nie, S., Low, P.S., Holt, D.E., 2017. Intraoperative near-infrared fluorescence imaging targeting folate receptors identifies lung cancer in a large-animal model. Cancer 123, 1051–1060. https://doi.org/10.1002/cncr.30419

Kedrzycki, M.S., Leiloglou, M., Ashrafian, H., Jiwa, N., Thiruchelvam, P.T.R., Elson, D.S., Leff, D.R., 2021. Meta-analysis Comparing Fluorescence Imaging with Radioisotope and Blue Dye-

Guided Sentinel Node Identification for Breast Cancer Surgery. Annals of Surgical Oncology. https://doi.org/10.1245/s10434-020-09288-7

Korpita, M.F., Mayhew, P.D., Steffey, M.A., Balsa, I.M., Giuffrida, M.A., Chohan, A.S., Johnson, E.G., 2022. Thoracoscopic detection of thoracic ducts after ultrasound-guided intrahepatic injection of indocyanine green detected by near-infrared fluorescence and methylene blue in dogs. Veterinary Surgery 51, O118–O127. https://doi.org/10.1111/vsu.13682

Lam, T.K., Uren, R.F., Scolyer, R.A., Quinn, M.J., Shannon, K.F., Thompson, J.F., 2009. False-negative sentinel node biopsy because of obstruction of lymphatics by metastatic melanoma: The value of ultrasound in conjunction with preoperative lymphoscintigraphy. Melanoma Research 19, 94–99. https://doi.org/10.1097/CMR.0b013e32832166b7

Lapsley, J., Hayes, G.M., Janvier, V., Newman, A.W., Peters-Kennedy, J., Balkman, C., Sumner, J.P., Johnson, P., 2021. Influence of locoregional lymph node aspiration cytology vs sentinel lymph node mapping and biopsy on disease stage assignment in dogs with integumentary mast cell tumors. Veterinary Surgery 50, 133–141. https://doi.org/10.1111/vsu.13537

Larose, P.C., Brisson, B.A., Sanchez, A., Monteith, G., Singh, A., Zhang, M., 2024. Near-infrared fluorescence cholangiography in dogs: A pilot study. Veterinary Surgery 53, 659–670. https://doi.org/10.1111/vsu.14007

Leijte, J.A.P., Van Derploeg, I.M.C., Valdés Olmos, R.A., Meweg, O.E., Horenblas, S., 2009. Visualization of tumor blockage and rerouting of lymphatic drainage in penile cancer patients by use of SPECT/CT. Journal of Nuclear Medicine 50, 364–367. https://doi.org/10.2967/jnumed.108.059733

Liao, S., Von Der Weid, P.Y., 2014. Inflammation-induced lymphangiogenesis and lymphatic dysfunction. Angiogenesis, 17, 325–334. https://doi.org/10.1007/s10456-014-9416-7

Liptak, J.M., Boston, S.E., 2019. Nonselective Lymph Node Dissection and Sentinel Lymph Node Mapping and Biopsy. Veterinary Clinics of North America - Small Animal Practice. 49(5), 793–807. https://doi.org/10.1016/j.cvsm.2019.04.003

Madajewski, B., Judy, B.F., Mouchli, A., Kapoor, V., Holt, D., Wang, M.D., Nie, S., Singhal, S., 2012. Intraoperative near-infrared imaging of surgical wounds after tumor resections can detect residual disease. Clinical Cancer Research 18, 5741–5751. https://doi.org/10.1158/1078-0432.CCR-12-1188

Manfredi, M., De Zani, D., Chiti, L.E., Ferrari, R., Stefanello, D., Giudice, C., Pettinato, V., Longo, M., Di Giancamillo, M., Zani, D.D., 2021. Preoperative planar lymphoscintigraphy allows for sentinel lymph node detection in 51 dogs improving staging accuracy: Feasibility and pitfalls. Veterinary Radiology and Ultrasound 62, 602–609. https://doi.org/10.1111/vru.12995

Marconato, L., Stefanello, D., Kiupel, M., Finotello, R., Polton, G., Massari, F., Ferrari, R., Agnoli, C., Capitani, O., Giudice, C., Aresu, L., Vasconi, M.E., Rigillo, A., Sabattini, S., 2020. Adjuvant medical therapy provides no therapeutic benefit in the treatment of dogs with low-grade mast cell tumours and early nodal metastasis undergoing surgery. Veterinary and Comparative Oncology 18, 409–415. https://doi.org/10.1111/vco.12566

Mattioli, G., Cino, M., Stefanello, D., Drudi, D., Morello, E.M., Pisani, G., Chiti, L.E., Pierini, A., Gariboldi, E.M., De Zani, D., Massari, F., Giacobino, D., Martano, M., 2025. Peripheral sentinel lymphadenectomy in 163 dogs: Postoperative surgical complications and comparison between intraoperative dissection techniques. Veterinary Surgery 54, 766–776. https://doi.org/10.1111/vsu.14246

Mattoon, J.S., Bryan, J.N., 2013. The future of imaging in veterinary oncology: Learning from human medicine. Veterinary Journal, 197(3), 541–552. https://doi.org/10.1016/j.tvjl.2013.05.022

Milovancev, M., Tuohy, J.L., Townsend, K.L., Irvin, V.L., 2019. Influence of surgical margin completeness on risk of local tumour recurrence in canine cutaneous and subcutaneous soft tissue sarcoma: A systematic review and meta-analysis. Veterinary and Comparative Oncology 17, 354–364. https://doi.org/10.1111/vco.12479

Monaco, S.E., Khalbuss, W.E., Pantanowitz, L., 2012. Benign non-infectious causes of lymphadenopathy: A review of cytomorphology and differential diagnosis. Diagn Cytopathol. https://doi.org/10.1002/dc.21767

Morales-Conde, S., Licardie, E., Alarcón, I., Balla, A., 2022. Indocyanine green (ICG) fluorescence guide for the use and indications in general surgery: Recommendations based on the descriptive review of the literature and the analysis of experience. Cirugía Española. https://doi.org/10.1016/j.ciresp.2021.11.018

Morris, K.P., Singh, A., Holt, D.E., Stefanovski, D., Singhal, S., Bosco, J., Capps, M., McCallum, M., Runge, J.J., 2019. Hybrid single-port laparoscopic cisterna chyli ablation for the adjunct treatment of chylothorax disease in dogs. Veterinary Surgery 48, O121–O129. https://doi.org/10.1111/vsu.13195

Morton, D.L., Wen, D.-R., Wong, J.H., Economou, J.S., Cagle, L.A., Storm, ; F Kristian, Foshag, L.J., Cochran, A.J., 1992. Technical Details of Intraoperative Lymphatic Mapping for Early Stage Melanoma.

Mullen, K.M., Regier, P.J., Perez-Rodriguez, V., Fox-Alvarez, W.A., Bertran, J., Colee, J., 2024. Use of real-time near-infrared fluorescence to assess gastric viability in dogs with gastric dilatation

volvulus: A case-control study. Veterinary Surgery 53, 684–694. https://doi.org/10.1111/vsu.14067

Newton, A., Predina, J., Mison, M., Runge, J., Bradley, C., Stefanovski, D., Singhal, S., Holt, D., 2020. Intraoperative near-infrared imaging can identify canine mammary tumors, a spontaneously occurring, large animal model of human breast cancer. PLoS One 15. e0234791 https://doi.org/10.1371/journal.pone.0234791

Nicoli, F., Saleh, D.B., Baljer, B., Chan, C.D., Beckingsale, T., Ghosh, K.M., Ragbir, M., Rankin, K.S., 2021. Intraoperative Near-infrared Fluorescence (NIR) Imaging with Indocyanine Green (ICG) Can Identify Bone and Soft Tissue Sarcomas Which May Provide Guidance for Oncological Resection. Annals of Surgery 273, E63–E68. https://doi.org/10.1097/SLA.0000000000003857

Predina, J.D., Keating, J., Newton, A., Corbett, C., Xia, L., Shin, M., Frenzel Sulyok, L., Deshpande, C., Litzky, L., Nie, S., Kucharczuk, J.C., Singhal, S., 2019. A clinical trial of intraoperative near-infrared imaging to assess tumor extent and identify residual disease during anterior mediastinal tumor resection. Cancer 125, 807–817. https://doi.org/10.1002/cncr.31851

Preziosi, A., Cirelli, C., Waterhouse, D., Privitera, L., De Coppi, P., Giuliani, S., 2024. State of the art medical devices for fluorescence-guided surgery (FGS): technical review and future developments. urgical Endoscopy 38(11), 6227–6236. https://doi.org/10.1007/s00464-024-11236-5

Proulx, S.T., Luciani, P., Christiansen, A., Karaman, S., Blum, K.S., Rinderknecht, M., Leroux, J.C., Detmar, M., 2013. Use of a PEG-conjugated bright near-infrared dye for functional imaging of rerouting of tumor lymphatic drainage after sentinel lymph node metastasis. Biomaterials 34, 5128–5137. https://doi.org/10.1016/j.biomaterials.2013.03.034

Quinlan, A.S.F., Wainberg, S.H., Phillips, E., Oblak, M.L., 2021. The use of near infrared fluorescence imaging with indocyanine green for vascular visualization in caudal auricular flaps in two cats. Veterinary Surgery 50, 677–686. https://doi.org/10.1111/vsu.13577

Ratzlaff MH. The superficial lymphatic system of the cat. Lymphology. 1970;3(4):151–9. PMID: 5503520.

Rosenthal, E.L., Warram, J.M., Bland, K.I., Zinn, K.R., 2015. The status of contemporary image-guided modalities in oncologic surgery. Annals of Surgery 261(1), 46–55. https://doi.org/10.1097/SLA.0000000000000622

Sakurai, N., Ishigaki, K., Terai, K., Heishima, T., Okada, K., Yoshida, O., Kagawa, Y., Asano, K., 2022. Clinical impact of near-infrared fluorescence imaging with indocyanine green on surgical

treatment for hepatic masses in dogs. BMC Veterinary Research 18, 467. https://doi.org/10.1186/s12917-022-03467-2

Sánchez-Margallo, F.M., Brun, M.V., Sánchez-Margallo, J.A., 2020. Identification of intra-abdominal lymphatics in canine carcasses by laparoscopic fluorescence lymphography with intradermal and intrapopliteal ICG administration. PLoS One 15(11), e0241992. https://doi.org/10.1371/journal.pone.0241992

Shinaoka, A., Koshimune, S., Yamada, K., Kumagishi, K., Suami, H., Kimata, Y., Ohtsuka, A., 2019. Correlations between Tracer Injection Sites and Lymphatic Pathways in the Leg: A Near-Infrared Fluorescence Lymphography Study. Plastic and Reconstructive Surgery 144, 634–642. https://doi.org/10.1097/PRS.0000000000005982

Shinaoka, A., Koshimune, S., Yamada, K., Kumagishi, K., Suami, H., Kimata, Y., Ohtsuka, A., 2018. A Fresh Cadaver Study on Indocyanine Green Fluorescence Lymphography: A New Whole-Body Imaging Technique for Investigating the Superficial Lymphatics. Plastic and Reconstructive Surgery 141, 1161–1164. https://doi.org/10.1097/PRS.0000000000004315

Somashekhar, S.P., Kumar, C.R., Ashwin, K.R., Zaveri, S.S., Jampani, A., Ramya, Y., Parameswaran, R., Rakshit, S., 2020. Can Low-cost Indo Cyanine Green Florescence Technique for Sentinel Lymph Node Biopsy Replace Dual Dye (Radio-colloid and Blue Dye) Technique in Early Breast Cancer: A Prospective Two-arm Comparative Study. Clinical Breast Cancer 20, e576–e583. https://doi.org/10.1016/j.clbc.2020.03.013

Soto-Miranda, M.A., Suami, H., Chang, D.W., 2013. Mapping superficial lymphatic territories in the rabbit. Anatomical Record 296, 965–970. https://doi.org/10.1002/ar.22699

Stefanello, D., Gariboldi, E.M., Boracchi, P., Ferrari, R., Ubiali, A., De Zani, D., Zani, D.D., Grieco, V., Giudice, C., Recordati, C., Caniatti, M., Auletta, L., Chiti, L.E., 2024. Weishaar's classification system for nodal metastasis in sentinel lymph nodes: Clinical outcome in 94 dogs with mast cell tumor. J Vet Intern Med 38, 1675–1685. https://doi.org/10.1111/jvim.16997

Steffey, M.A., Mayhew, P.D., 2018. Use of direct near-infrared fluorescent lymphography for thoracoscopic thoracic duct identification in 15 dogs with chylothorax. Veterinary Surgery 47, 267–276. https://doi.org/10.1111/vsu.12740

Stoffels, I., Dissemond, J., Pöppel, T., Schadendorf, D., Klode, J., 2015. Intraoperative fluorescence imaging for sentinel lymph node detection: Prospective clinical trial to compare the usefulness of indocyanine green vs technetium Tc 99m for identification of sentinel lymph nodes. ournal of the American Medical Association Surgery 150, 617–623. https://doi.org/10.1001/jamasurg.2014.3502

Suami, H., Scaglioni, M.F., Dixon, K.A., Tailor, R.C., 2016. Interaction between vascularized lymph node transfer and recipient lymphatics after lymph node dissection - A pilot study in a canine model. Journal of Surgical Research 204, 418–427. https://doi.org/10.1016/j.jss.2016.05.029

Suami, H., Shinaoka, A., 2019. The methodology of lymphatic anatomy studies in a cadaver model: an overview. Plastic and Aesthetic Research 6, 33. https://doi.org/10.20517/2347-9264.2019.46

Suami, H., Taylor, G.I., O'Neill, J., Pan, W.R., 2007. Refinements of the radiographic cadaver injection technique for investigating minute lymphatic vessels. Plastic and Aesthetic Research 120, 61–67. https://doi.org/10.1097/01.prs.0000263321.64228.53

Suami, H., Taylor, I., Pan, W.R., 2005. A new radiographic cadaver injection technique for investigating the lymphatic system. Plast Reconstr Surg 115, 2007–2013. https://doi.org/10.1097/01.PRS.0000163325.06437.B0

Suami, H., Yamashita, S., Soto-Miranda, M.A., Chang, D.W., 2013. Lymphatic Territories (Lymphosomes) in a Canine: An Animal Model for Investigation of Postoperative Lymphatic Alterations. PLoS One 8, e69222. https://doi.org/10.1371/journal.pone.0069222

Suh, Y.J., Choi, J.Y., Chai, Y.J., Kwon, H., Woo, J.W., Kim, S. jin, Kim, K.H., Lee, K.E., Lim, Y.T., Youn, Y.K., 2015. Indocyanine green as a near-infrared fluorescent agent for identifying parathyroid glands during thyroid surgery in dogs. Surgical Endoscopy 29, 2811–2817. https://doi.org/10.1007/s00464-014-3971-2

Tagaya, N., Nakagawa, A., Abe, A., Iwasaki, Y., Kubota, K., 2010. Non-Invasive Identification of Sentinel Lymph Nodes Using Indocyanine Green Fluorescence Imaging in Patients with Breast Cancer, The Open Surgical Oncology Journal. 2, 71–74. https://doi.org/10.2174/1876504101002010071

Tobón Restrepo, M., Espada, Y., Aguilar, A., Moll, X., Novellas, R., 2021. Anatomic, computed tomographic, and ultrasonographic assessment of the lymph nodes in presumed healthy adult cats: The head, neck, thorax, and forelimb. Journal of Anatomy 239, 264–281. https://doi.org/10.1111/joa.13429

Tobón Restrepo, M., Novellas, R., Aguilar, A., Moll, X., Espada, Y., 2022. Anatomic, computed tomographic, and ultrasonographic assessment of the lymph nodes in presumed healthy adult cats: the abdomen, pelvis, and hindlimb. Acta Veterinaria Scandinavica 64, 18. https://doi.org/10.1186/s13028-022-00638-x

Van Den Berg, N.S., Brouwer, O.R., Klop, W.M.C., Karakullukcu, B., Zuur, C.L., Tan, I.B., Balm, A.J.M., Van Den Brekel, M.W.M., Valdés Olmos, R.A., Van Leeuwen, F.W.B., 2012. Concomitant radio- and fluorescence-guided sentinel lymph node biopsy in squamous cell

carcinoma of the oral cavity using ICG-99mTc- nanocolloid. European Journal of Nuclear Medicine and Molecular Imaging 39, 1128–1136. https://doi.org/10.1007/s00259-012-2129-5

Verbeek, F.P.R., Troyan, S.L., Mieog, J.S.D., Liefers, G.J., Moffitt, L.A., Rosenberg, M., Hirshfield-Bartek, J., Gioux, S., Van De Velde, C.J.H., Vahrmeijer, A.L., Frangioni, J. V., 2014. Near-infrared fluorescence sentinel lymph node mapping in breast cancer: A multicenter experience. Breast Cancer Research and Treatment 143, 333–342. https://doi.org/10.1007/s10549-013-2802-9

Veys, I., Pop, C.F., Barbieux, R., Moreau, M., Noterman, D., De Neubourg, F., Nogaret, J.M., Liberale, G., Larsimont, D., Bourgeois, P., 2018. ICG fluorescence imaging as a new tool for optimization of pathological evaluation in breast cancer tumors after neoadjuvant chemotherapy. PLOS ONE 13, e0197857. https://doi.org/10.1371/journal.pone.0197857

Wan, J., Oblak, M.L., Ram, A., Singh, A., Nykamp, S., 2021. Determining agreement between preoperative computed tomography lymphography and indocyanine green near infrared fluorescence intraoperative imaging for sentinel lymph node mapping in dogs with oral tumours. Veterinary and Comparative Oncology 19, 295–303. https://doi.org/10.1111/vco.12675

Wishart, G.C., Loh, S.W., Jones, L., Benson, J.R., 2012. A feasibility study (ICG-10) of indocyanine green (ICG) fluorescence mapping for sentinel lymph node detection in early breast cancer. European Journal of Surgical Oncology 38, 651–656. https://doi.org/10.1016/j.ejso.2012.05.007

Wong, J.H., Cagle, L.A., Morton, D.L., Building, F.F., 1991. Lymphatic Drainage of Skin to a Sentinel Lymph Node in a Feline Model Annals of Surgery 214, 637–641. https://doi.org/10.1097/00000658-199111000-00013

Worley, D.R., 2014. Incorporation of sentinel lymph node mapping in dogs with mast cell tumours: 20 consecutive procedures. Veterinary and Comparative Oncology 12, 215–226. https://doi.org/10.1111/j.1476-5829.2012.00354.x

2. Intrapatient application of lymphoscintigraphy and near-infrared fluorescence in canine and feline sentinel lymph node mapping and removal

- The present study was published in BMC Veterinary Research (October 9th, 2025) https://doi.org/10.1186/s12917-025-05013-2
- Results of this study presented at Veterinary Society of Surgical Oncology (VSSO) Conference, April 20th-23th 2025, Banff, Canada
- PhD student role: first author and corresponding author

Elisa Maria Gariboldi [1], Alessandra Ubiali [1], Patrizia Boracchi [2], Ester Luconi [3], Roberta Ferrari [1], Luigi Auletta [1], Donatella De Zani [1], Davide Danilo Zani [1], Paola Roccabianca [1], Valeria Grieco [1], Chiara Giudice [1], Camilla Recordati [1] and Damiano Stefanello [1].

[1] Dipartimento di Medicina Veterinaria e Scienze Animali - Università degli Studi di Milano, Lodi, Italia
[2] Dipartimento di Scienze Biomediche e Cliniche, Università degli Studi di Milano, Milano, Italia
[3] Dipartimento di Scienze Biomediche per la Salute, Università degli Studi di Milano, Milano, Italia

Sentinel lymph node (SLN) extirpation has been proven to lead to a more accurate staging in canine and feline malignancies [1–4]. Different mapping techniques are reported in veterinary medicine, such as contrast enhanced-ultrasound, radiographic indirect lymphography, indirect computed tomography lymphography, indocyanine based near infrared lymphography, lymphoscintigraphy [5–11]. Most of these are exclusively pre-operative and therefore need an additional tracer for surgical exploration of the sentinel lymphocentrum (SLC) and SLN extirpation [12,13].

In humans, lymphoscintigraphy (LPS) is considered the standard care for SLN detection and extirpation [14,15]. However, law permission, radioactive exposure, and the need for specialized facilities and personnel for radiopharmaceutical management led to the search for alternative techniques. Based on current data published in humans, fluorescence may represent an ideal alternative to radioactive tracers for SLN identification [16–18]. The same concerns exist in small animal practice since LPS for SLN mapping and extirpation is only available in a few facilities. Conversely, although it necessitates specialized equipment, near-infrared fluorescence with indocyanine green (NIRF-ICG) is an emerging technique for SLN mapping and extirpation [3,12,13,19], that does not require legal authorization or dedicated facilities. In addition, fluorescence

imaging can be applied in various fields of small animal surgery, including minimally invasive procedures [20–23]. SLN detection rate of NIRF is analogous to LPS in dogs and cats. However, neither technique alone guarantees 100% detection [1,12,13,19,24]. Combining sentinel lymph node mapping techniques to enhance sentinel lymph node detection is desirable in small animals with solid malignant tumors and has been reported for other preoperative and intraoperative techniques [12,13]. Although an increase in the SLN detection rate is expected in the case of the combination of LPS and NIRF-ICG, data regarding this are absent in veterinary medicine. Moreover, there is a lack of intra-patient comparison data regarding the performance of these two techniques in SLC mapping and SLN extirpation in dogs and cats.

Based on the latter consideration and the lack of studies focusing on the comparison lymphoscintigraphy and NIRF, the present study aims to compare intra-patient LPS and NIRF-ICG performance in SLC mapping and SLN detection for its removal. Specifically, the purpose is to evaluate the performance and agreement of these two techniques in canine and feline malignant tumors during different phases: 1) the mapping for sentinel lymphocentrum (SLC) identification; 2) the guided surgical exploration of SLC for SLN detection for its removal.

2.1. Material and methods:

The characteristics of participants:

This observational study was conducted on client-owned dogs and cats with a cytological or histological diagnosis of solid malignant tumors at first presentation, characterized by non-palpable and/or normal-sized regional lymph nodes. These animals were eligible for curative-intent surgery and SLN extirpation and were referred to the Veterinary Teaching Hospital (VTH) of the Università degli Studi di Milano, Lodi, Italy from November 2022 to December 2023. The combined use of LPS and NIRF-ICG was recommended to ensure better identification, detection, and removal of SLC and SLN. Owners signed a written informed consent for all the procedures performed and data collection. This study does not involve animal experimentation, but owned dogs and cats and the methods applied in our study are already widely described and used in small animal clinical practice. All the procedures were performed in accordance with the Italian National legislation for animal welfare (DL 14th March 2014 n.26) and best standard of veterinary practice (Good Veterinary Practice from the Federation Veterinary Europe—Italian National Federation of the Veterinary' Orders [FNOVI] 29th January 2005).

Patients with scars from previous excision of a malignant neoplasm in the absence of lymphadenectomy were also included. Exclusion criteria were: client declined the use of both techniques or SLC surgical exploration, evidence of distant metastases, previous regional lymphadenectomy and neo-adjuvant oncological therapy.

The SLC was defined as the first lymphatic station that included one or more SLNs receiving drainage from the tumor or scar and was expected to be the first site of metastasis. The term "SLC" was used during the mapping phase because LPS and NIRF-ICG are not able to define the individual SLNs within the SLC prior to the intraoperative approach.

Technical Information:

Complete preoperative staging and curative-intent surgical procedures were conducted according to the current recommendation based on cytological or histological tumor diagnosis [25-27]. Draining lymph nodes were selected and removed based on the combined use of LPS and NIRF-ICG.

Data about patient signalment were recorded: species, breed, sex, age, body weight, body condition score (BCS) on a nine scale, and number of tumors (single or multiple presentation). The clinical variables of tumors/scars included: anatomical location, dimension, ulceration, the related regional lymphocentrum (RLC) (according to Suami et al 2013 [28]) and drainage to a single or multiple SLC. Anatomical locations were categorized as limbs (below the elbow/knee, excluding digits), trunk (upper the elbow/knee, included lumbar area, thoracic and abdominal mammary glands), head and neck, inguinal (perineal, genitals, and inguinal mammary glands), digits, and tail regions. Correspondence between identified SLC with RLC was defined as follows: total correspondence if all SLC corresponded with the expected RLC; non-correspondence if all SLC had different locations than the RLC; unpredictable if the RLC could not be determined due to overlap of more than one lymphosome [28,29]. Skin related to lymphosome, according to Suami's study (2013) [28], was categorized as pigmented or non-pigmented based on clinical appearance.

Data registered were: visualization of radioactive or fluorescent drainage, SLC fluorescence/radioactivity, migration time (in minutes calculated from the injection to the SLC identification), number of SLNs per SLC detected intra-operative by each technique, total number of hot/fluorescent SLNs, presence of residual fluorescence or radioactivity in the SLC after each SLN removal. The time of tumor/scar excision and SLN biopsy (both calculated as time in minutes from skin incision to last skin suture) were also recorded, and any intra-operative and post-operative complication of the lymphadenectomy or tumor excision was registered (if it occurred). Histopathological data collected were: tumor type, histological grade (when applicable), and metastatic status of SLN.

The LPS and NIRF-ICG mapping and intraoperative phase are detailed below and shown in Figure. 1 and 2

Figure 1. LPS mapping for SLC identification and guided surgical exploration for SLN detection

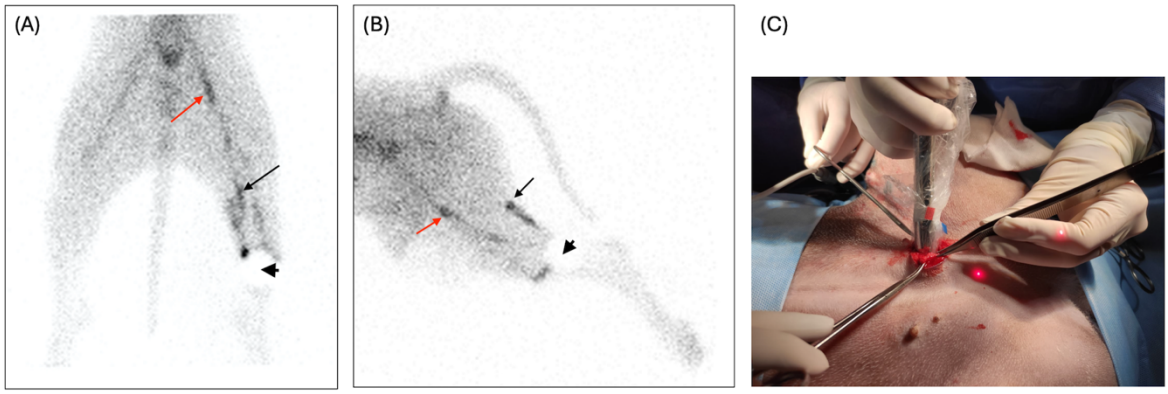

Figure 2. NIRF-ICG mapping for SLC identification and surgical guided exploration for SLN detection

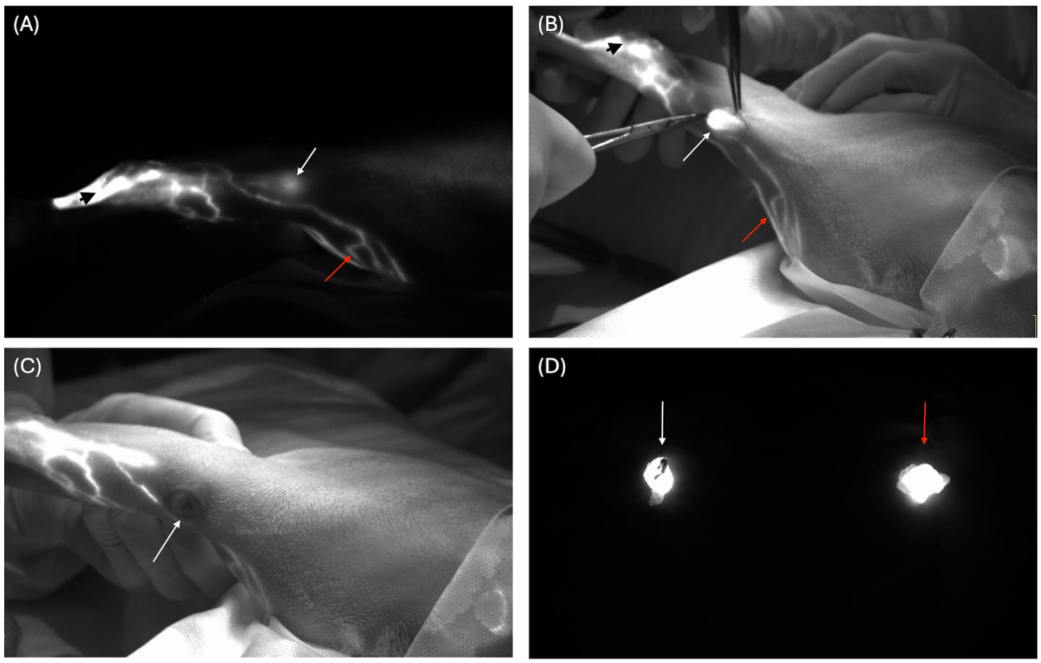

Mapping for SLC identification:

Both LPS and NIRF-ICG, were always performed on each animal on the same day of the surgery. These techniques were applied as described in previous studies [2,3,10,11,19,24]. The mapping for SLC identification with preoperative planar-LPS was performed as follows: a volume of 0,5 ml of technetium-99 metastable (99mTc) labeled nano-sized human serum albumin (Nanoalbumon; Radiopharmacy Laboratory Ltd, Budaörs, Hungary) with an activity ranged between 23 and 30 MBq

was intradermally and subcutaneously injected peritumorally in four sites at a distance of 1 to 2 mm from the gross margins of the tumor by the same operator (DDZ). Planar static images were immediately acquired using a single head gamma camera (Picker Prism 2000XP, Picker International, Highland Heights, Ohio). The average time elapsed between radiotracer injection and completion of planar image acquisition was approximately 12 minutes. The minimum time required for visualization of SLC uptake was 60 seconds, while the maximum time observed was 5 minutes. Following acquisition of planar images adequate for SLC identification, the patient was subsequently transferred to the operating room. Radiopharmaceutical mapping for SLC was then completed with the use of a handheld intraoperative gamma-probe (HIGP - Crystal probe SG04; Crystal Photonic GmbH, Berlin, Germany) connected to a display indicating the radioactive count (RC).

After planar-LPS, fluorescence lymphography was always performed in the operating room immediately before surgery. A volume of 0.2 ml (2.5 mg/ml) of ICG (Verdye, Diagnostic Green, Garrycastle, Ireland) plus 0.2 ml of 0.9% NaCl in a sterile syringe was injected in four quadrants peritumorally or around the scar by the surgeons (DS, RF) and a gentle massage was applied. A NIRF-camera (SPY-Elite Imaging system, Stryker, MIDA Tecnologia medica S.p.A) was positioned 20-30 cm above the surgical field and SLCs were determined by the images of fluorescence lymphography acquired and visualized on the display. Operating lights were turned to endoscopy mode during the explorative phase of the surgery. They were turned off for acquiring images during mapping and detection of surgical approach to the SLC, post-excisional surgical field check, and ex vivo evaluation of SLN.

In the absence of migration, the time of observation with the techniques was extended up to approximately 20-30 minutes. All lymphocentrums identified by at least one technique were considered SLC and surgically explored. The surgical approach to the SLC was established case by case according to tracers' guidance (maximum RC through the tissue above the SLC for the LPS and direct fluorescence of SLC for NIRF-ICG) and anatomic landmarks [30-33]. If mapping had suggested an intra-abdominal or intrathoracic SLC (e.g., medial iliac or sternal lymphocentrums), a routine celiotomy or thoracotomy would have been performed to visualize the lymphocentrum. Mapping for ICG and 99mTc was considered failed if no drainage or SLC focal uptake was detected by NIRF-camera or by LPS (planar-LPS with HIGP).

When, during mapping, the two techniques identified different SLCs, all of them were checked for both radioactivity and fluorescence. In the presence of simultaneous failures of both techniques, all RLC [28] were checked for both radioactivity and fluorescence. If no radioactivity or fluorescence was detected, the RLC was explored for nodal removal.

All the devices (RC display and imaging system screen showing fluorescence in monochromatic mode) were visible to the surgeons during all the procedures in the operating room. The presence of a "tumor shine-through effect", defined as the overlap of the SLC with tumor/scar radioactivity or fluorescence due to their anatomical proximity, was also recorded.

Guided surgical exploration of SLC for SLN detection:

Lymphadenectomy was performed before tumor/scar removal, except when tumor shine-through effect occurred or if SLC was in the same surgical field of tumor/scar. All procedures were performed by surgeons (DS, RF) with experience in sentinel lymph node extirpation (more than 20 SLN procedures) [34].

All lymph nodes identified by at least one tracer within the SLC were considered SLN and removed and submitted to histopathological analysis. A SLN was considered "hot" when its RC was at least 10% of the RC recorded for the corresponding tumor [11], "fluorescent" when detected by NIRF-camera and confirmed ex vivo by a signal-to-background ratio (SBR) > 1.1 [32]. The SBR was calculated as the ratio of the fluorescence intensity of the lymph node and the fluorescence intensity of the background (surrounding healthy tissues). To avoid the missing of additional SLN within a SLC, after each SLN removal, the surgical field was checked for further residual "hot" and/or fluorescent SLN and if present they were removed. Surgical exploration ended when the radioactive count in the surgical field was less than 10% of the hottest SLN extirpated, and no other fluorescent nodes were visible. The possible presence of ICG leakage, defined as diffuse nonspecific fluorescence in the surgical field due to ICG extravasation from broken lymphatic vessels, was also registered. At the end of surgery, radioactivity and fluorescence were evaluated in ex vivo SLNs. In addition, the surgeon subjectively reported after each SLN removal which technique gave the best surgical aid during intra-operative detection and classified in HIGP, NIRF-ICG, or equal performance.

Statistics:

Descriptive statistic was used to summarize the distribution of retrieved variables. For variables measured on a numerical scale, the distribution was summarized by the following quantities: minimum, first quartile, median, mean, third quartile, and maximum. For the variables measured on categorical scale the distribution was summarized by absolute frequencies and percentages.

For mapping and SLC identification, LPS (planar-LPS images with HIGP) and NIRF-ICG were compared. The percentage of tumors in which at least a lymphatic tract was detected was reported together with the corresponding 95% confidence interval for each technique (calculated by exact method).

The cases affected by tumor shine-through effect and those in which lymphadenectomy was performed *en bloc* with tumor removal (e.g., superficial inguinal SLN simultaneously removal during regional/unilateral mastectomy) were excluded from mapping comparison.

To evaluate the difference between the SLC detection probability with the two methods, a generalized linear model for the analysis of correlated observations was adopted [35]. Model response (dependent variable) was the binary variable related to the detection of the lymphatic network (coded 1 if detected and 0 if non detected),and the independent variable was the method (included as a binary variable coded 1 if NIRF and 0 for LPS). Model results were reported as prevalence detection ratio (with 95% confidence intervals and p-value of Wald Statistics).

The concordance between the two methods was estimated by Bangdiwala's agreement index B (and its 95% confidence intervals), which is appropriate in case of presence of cells with no observations. In this study, the absence of cells occurred when the lymphatic network was not detected using both techniques simultaneously. The index ranges between 0 (no agreement) and 1 (total agreement). [36]

Regarding SLN detection, HIGP and NIRF-ICG guidance were compared to identifying of SLN during SLC surgical exploration. The analysis focused on the percentage of hot and fluorescent extirpated SLNs, and the percentage of residual SLNs detected during post-excision surgical field checks by HIGP and/or NIRF-ICG. The statistical analysis for the comparison of the methods was performed by the previously described approaches.

An explorative analysis of the association between the selected variables and the detection of SLC or SLN for each method was performed for an empirical indirect comparison.

For each variable, the association was evaluated by the Fisher exact test, and the ratio between the percentage of detected SLC (or residual SLN) and the difference between the percentage of detected SLC (or residual SLN) in different categories were reported as measures for the strength of the association. The BCS was categorized as underweight (BCS < 4); normal weight (BCS = 4,5); overweight (BCS > 5). Considering the wide range of pet's body weight, this variable was arbitrarily categorized for statistical purposes into 3 classes: < 9 kg, 9-30 kg, and > 30 kg. For the same reasons, the SLN dimension was categorized into < 10 mm, 10-20 mm, and > 20 mm. The SLC anatomical locations were: head and neck (including parotid, mandibular, and retropharyngeal), superficial cervical, axillary (including axillary and accessory axillary), superficial inguinal, medial iliac, and popliteal. [28,29]

For the ratio and the difference between the percentage of detected SLC (or residual SLN), one of the categories was considered as a "reference" according to the clinical expected better performance of both techniques, for SLC (or residual SLN) detection. The superficial inguinal SLC and SLN anatomical location was considered a reference category among the lymphocentrums identified in

this study. According to the lymphosome map [28], the lymphatic territory related to the superficial inguinal SLC borders many other lymphatic territories. This anatomical location increases the likelihood of it being an SLC for malignancies developing in adjacent lymphosomes, making it a possible site frequently involved in mapping and SLN extirpation.

An explorative analysis of the association between the above-mentioned variables and the preferred method to detect SLN as surgical aid was performed using the same approach.

All analyses were performed using R Statistical Software (V 4.2.2 R Core Team 2022), packages Geepack [37], epiR [38], irrCAC [39].

2.2. Results:

Among 67 animals evaluated for surgical purposes during the study period, 13 were excluded because they underwent sentinel lymphadenectomy only guided by one technique (5 cats and 2 dogs underwent only NIRF-ICG, 6 dogs only LPS). A total of 54 animals (50 dogs and 4 cats) were included in the study. Six dogs underwent multiple mapping due to the presence of >1 tumors and scars (5 dogs had 2 mast cell tumors – MCT, and one dog had 2 mammary gland carcinomas). In the remaining cases the mapping was performed for a single tumor or scar. Overall, both tracers were used for SLC mapping and detection and surgical guided exploration in a total of 60 cases: 46 measurable tumors and 14 scars (4 of which with microscopic disease). Multiple SLCs (range 2-3) were detected in 16 tumors and 1 scar, while only one SLC was detected for each of the remaining 30 tumors and 13 scars. Eighty SLCs (76 peripheral and 4 intra-abdominal) were investigated, and a total of 113 SLNs were removed. Information about animals, tumors/scars, and SLC are summarized in Table 1- 3. In 47 (59%) SLC, there was correspondence with the expected RLC; in 18 (22%), there was no correspondence; and in 15 (19%), the RLC was unpredictable.

Table 1. Animals' signalment distributed in dogs and cats

	Animals (n=54)
Breed	13 (24.1%) Mixed breed 5 (9.2%) Boxer 3 (5.6%) Golden Retriever 3 (5.6%) Jack Russel Terrier 3 (5.6%) Labrador Retriever 23 (42.5%) Others canine breeds 4 (7.4%) Feline Domestic Shorthair
Age (years) Min - Max 1st Quart-3rd Quart Mean Median	 1.5-13.5 6.5-10.5 8.4 8
Sex	

	Animals (n=54)
Female Spayed Female Male Neutered Male	8 (14.8%) 25 (46.3%) 15 (27.8%) 6 (11.1%)
Bodyweight (kg) Min - Max 1st Quart-3rd Quart Mean Median	 3.4-54.3 9.8-31.8 23.2 22.1
BCS Underweight Normal weight Overweight	 0 38 (70.4%) 16 (29.6%)

Legend: BCS: body condition score

Table 2: Clinical and histopathological features of tumors and scars.

	Tumors (n = 46)	**Scars (n = 14)**
Anatomical location Trunk Head and neck Inguinal/genital Limbs	 22 7 10 7	 6 4 1 3
Maximum dimension (mm) Min - Max 1st Quart-3rd Quart Mean Median	 2-100 9.8-30 23 20	 -
Ulceration Yes No	 5 55	 -
Histopathological diagnosis (n=60)	26 cMCT: 4 PG1/KLG 21 PG2/KLG 1 PG3/KHG 6 sMCT: 3 infiltrative 1 circumscribed 2 combined 9 mammary gland carcinomas 1 G II STS 1 G II PWT 1 oral fibrosarcoma 2 feline cMCT LG	7 cMCT: 1 PG1/KLG 6 PG2/KLG 2 sMCT infiltrative 2 lip/oral melanoma 1 STS 1 feline cMCT LG 1 feline mammary gland carcinoma

Legend: cMCT: cutaneous mast cell tumor; sMCT: subcutaneous mast cell tumor; G: grade; PG: Patnaik grade; KLG: Kiupel low grade; KHG: Kiupel high grade); LG: low grade; STS: soft tissue sarcoma; PWT: perivascular wall tumor.

Table 3: Sentinel lymphocentrum (SLC) data.

	SLC draining measurable tumors (n = 65)	SLC draining scars (n = 15)
SLC anatomical location:		
Axillary (n=19)	17	2
Accessory axillary (n=4)	3	1
Medial iliac (n=4)	4	0
Superficial inguinal (n=23)	20	3
Mandibular (n=7)	3	4
Parotid (n=3)	2	1
Popliteal (n=6)	3	3
Superficial cervical (n=10)	9	1
Retropharyngeal (n=4)	4	0

Legend: SLC: sentinel lymphocentrum

In 13 tumors and 2 scars (25%), the skin covering the expected lymphosomes was pigmented. Five cases (8%) presented the tumor shine-through effect and in 3 of them the SLCs were *en-bloc* removed in association with the tumor, while in the 2 remaining cases the SLC was surgically explored after the tumor excision. In 2 other cases (both tumors on the third mammary gland), the SLC (superficial inguinal) was *en-bloc* excised during unilateral mastectomy even if no tumor shine-through effect was present.

The median surgical times for local tumor or scar removal (including cases where the SLC was in the same surgical field as the tumor) was 40 minutes (range 7-90 minutes). The median surgical times for SLC exploration and SLN removal was 21.5 minutes (range 5-60 minutes).

The only post-injection complication was peritumoral mild edema noticed in 16/60 (26.7%) cases (all MCT), and it was observed both after ^{99m}Tc and ICG injections. No intra-operative complications were registered. Five post-operative complications (6%) occurred at the SLC surgical site, 1 of them required surgical revision, whereas 13 complications (21.7%) took place at the tumor surgical site, 2 of which required surgical revision.

Mapping for SLC identification:

In all the tumors/scars included, the combined use of techniques led to the detection of at least one SLC. In 43 cases (71.7%), at least one tracer migrated to a single SLC, while in 17 cases (28.3%) to multiple SLCs (range: 2-4 SLCs per tumor) as detailed in Table 3. No lymphatic drainage or SLC focal uptake was detected during LPS mapping (planar-LPS with HIGP) in 1/60 case (2%) (one measurable MCT on the head and neck), and with NIRF-ICG mapping in 3/60 cases (5%) (one scar of a mammary gland carcinoma on the trunk and 2 measurable MCT one on the head and neck and one on the trunk). In 5 cases (8.3%) (4 tumors and one scar), the tumor shine-through effect was present with both techniques and in two of these tumors also exhibited lymphatic migration to an

another SLC. In 50/60 (83%) tumors/scars the two techniques detected the same SLCs during mapping, in 6/60 (10%) the agreement of the detection was partial and in 4/60 (7%) cases had no agreement. The time of SLC identification ranged from immediate to 12 minutes for the LPS and from immediate to 10 minutes for NIRF-ICG.

A total of 80 SLCs were identified using the combination of the techniques. Seven out of 80 SLCs were excluded because they received an *en-bloc* excision (which precluded the possibility of exploring the surgical approach to the SLC) and/or presented tumor shine-through effect. Among 73 SLCs included in this analysis, the SLC was identified in 67/73 (92%) using preoperative planar-LPS with HIGP, and 68/73 (93%) by NIRF-ICG. Within the 6 cases of LPS mapping failure, in only one SLC a hot SLN was removed. On the other hand, among the 5 NIRF-ICG mapping considered as failed, in 3 SLCs (2 superficial cervical and one superficial inguinal) the network was not visible percutaneously, but the fluorescence of SLC was detected only after or during surgical exploration. In 42/68 NIRF-ICG mapping (62%) lymphatic network and the SLC were directly visible percutaneously. In the remaining 26/68 (38%), only the lymphatic network leading to the SLC was visible. Specifically, 22/26 (83%) were peripheral SLCs and the SLC location was inferred with reasonable accuracy by projecting downward and slightly outward from the point where the lymphatic channel dives deep and disappears from the surgeon's view. In the remaining 4/26 (17%) non peripheric SLCs (all medial iliac SLCs) the fluorescent lymphatic network was visible on the lateral side of the trunk and then went deep, perforating the abdominal wall, and the SLC fluorescence was assessed after celiotomy.

Results of the comparison between preoperative planar-LPS with HIGP and NIRF-ICG mapping are summarized in Table 4. Considering 73 SLCs, both techniques agreed on identifying 62 (84.93%) and disagreed on 11 (15.07%). The strength of agreement, measured using the B index, was 0.838 (Table 4). Planar LPS with HIGP identified 91.78% of SLCs, while NIRF-ICG identified 93.15%; the difference between these percentages was not statistically significant (P = 0.754).

Table 4. Comparison among LPS and NIRF-ICG in identifying SLC (considered only the 73 SLCs included).

		NIRF-ICG		
		SLC identified	**SLC not identified**	**Total**
Planar-LPS with HIGP	**SLC identified**	62 (84.93%) 95%C.I.:74.64%-92.23%	5	67 (91.78%) 95%C.I.: 82.96%-96.92%
	SLC not identified	6	-	6 (8.22%)
	Total	68 (93.15%) 95%C.I.: 84.74%-97.74%	5 (6.85%)	73
C.I. confidence interval				

Agreement. Bangdiwala's B: 0.838 (95% C.I.: 0.743-0.934) Comparison between the percentage of identified SLC in the two techniques. Percentage ratio (NIRF-ICG vs Planar-LPS with HIGP): 1.015 (95%C.I.: 0.925 - 1.113) P= 0.754

No significant associations were found between mapping with preoperative planar-LPS with HIGP and NIRF-ICG and the variables considered: BCS, SLC location, weight, and skin pigmentation (Table 5).

Table 5: Association between detection of SLC with LPS vs NIRF-ICG with selected variables

		LPS (planar-LPS with HIGP) SLC Identified (n=67)	**NIRF-ICG** SLC Identified (n=68)
	Total number of SLC per category	Number identified per category (%)	Number identified per category (%)
BCS Normal Weight	52	49 (94.23%)	49 (94.23%)
*Overweight	21	18 (85.71%)	19 (90.48%)
		PR= 0.91 C.I. (0.75, 1.10) PD= -8.52 C.I. (-24.77, 7.74) P= 0.345	PR= 0.96 C.I. (0.82, 1.12) PD= -3.75 C.I. (-17.82, 10.31) P= 0.621
SLC location Axillary Accessory axillary Medial iliac Superficial Inguinal Mandibular Parotid Popliteal Superficial cervical Retropharyngeal	 19 4 4 18 7 3 4 10 4	 19 (100.00%) 4 (100.00%) 4 (100.00%) 17 (94.44%) 5 (71.43%) 3 (100.00%) 4 (100.00%) 9 (90.00%) 2 (50.00%)	 18 (94.74%) 4 (100.00%) 4 (100.00%) 16 (88.89%) 7 (100.00%) 3 (100.00%) 4 (100.00%) 8 (80.00%) 4 (100.00%)
		P=0.055	P=0.892
SLC location *Superficial Inguinal Axillary + Accessory Axillary	 18 23	 17 (94.44%) 23 (100%)	 16 (88.89%) 22 (95.65%)
		PR= 0.94 C.I. (0.84, 1.06) PD= -5.56 C.I. (-16.14, 5.03) P=0.439	PR= 0.93 C.I. (0.77, 1.12) PD= -6.76 C.I. (-23.50, 9.98) P=0.573
*Superficial Inguinal Head and neck	18 14	17 (94.44%) 10 (71.43%)	16 (88.89%) 14 (100.00%)
		PR= 1.32 C.I. (0.93, 1.88) PD= 23.02 C.I. (-2.91, 48.94) P=0.142	PR= 0.89 C.I. (0.75, 1.05) PD= -11.11 C.I. (-25.63, 3.41) P=0.492
* Superficial Inguinal Superficial cervical	18 10	17 (94.44%) 9 (90.00%)	16 (88.89%) 8 (80.00%)
		PR= 1.05 C.I. (0.83, 1.33) PD= 4.44 (-16.95, 25.84). P>0.99	PR= 1.11 C.I. (0.78, 1.58) PD= 8.89 C.I. (-19.84, 37.62) P=0.601
Weight			

< 9 kg 9-29.99kg >=30 kg	17 31 25	16 (94.12%) 27 (87.10%) 24 (96.00%)	16 (94.12%) 29 (93.55%) 23 (92.00%)
		P=0.557	P>0.99
*>=30 kg <9kg	25 17	24 (96.00%) 16 (94.12%)	23 (92.00%) 16 (94.12%)
		PR=1.02 C.I. (0.88, 1.18) PD=1.88 C.I. (-11.69, 15.45) P>0.99	PR=0.98 C.I. (0.83, 1.15) PD= -2.30 C.I. (-20.75, 13.33) P>0.99
*>=30 kg 9-29.99kg	25 31	24 (96.00%) 27(87.10%)	23(92.00%) 29(93.55%)
		PR= 1.10 C.I. (0.94, 1.29) PD= 8.90 C.I. (-5.18, 22.98) P= 0.367	PR= 0.98 C.I. (0.85, 1.14) PD= -2.12 (-17.55, 13.32). P>0.99
Skin pigmentation			
*No Yes	59 14	54 (91.53%) 13 (92.86%)	56 (94.92%) 12 (85.71%)
		PR= 0.99 C.I. (0.84, 1.16) PD=-1.33 C.I. (-16.58, 13.92) P>0.99	PR= 1.11 C.I. (0.89, 1.38) PD= 9.20 C.I. (-9.97, 28.37) P=0.242

Legend: PR: percentage ratio; PD: percentage difference; P: p-value of Fisher exact test; C.I.: 95% confidence interval; *reference category (numerator in PR and first term in the PD)

PR: the number of SLCs identified in 100 SLCs of the reference category is PR times the number of SLCs identified in 100 SLCs of the other category

PD: per 100 SLCs in the reference category, PD is the number of SLCs identified in excess (or reduction) compared to 100 SLCs in the other category

Guided surgical exploration of SLC for SLN detection:

Results of the comparison between HIGP and NIRF-ICG during SLC surgical exploration are summarized in Table 6. In all the included tumors/scars the combined intraoperative use of techniques led to the detection of at least one SLN within SLC. In 58/80 SLCs (72.5%), a single SLN was identified (in 5 SLCs only by NIRF and 5 SLCs only by HIGP) while 22/80 SLCs (27.5%) presented multiple SLNs (range, 2-4) and only one case was positive only by NIRF. A total of 113 SLNs were extirpated: 96/113 SLNs (85.0%) were both fluorescent and hot; 13/113 SLNs (11.5%) were fluorescent but non-hot; 4/113 SLNs (3.5%) were hot but non-fluorescent. The percentage of excised fluorescent nodes was significantly higher than that of hot nodes (percentage ratio=1.09, P=0.025). The agreement calculated with the B index was 0.841. (Table 6)

Table 6. HIGP and NIRF-ICG in identifying SLN during surgical exploration

		NIRF-ICG		
		Fluorescent SLN	**Non-fluorescent SLN**	**Total**
HIGP	**Hot SLN**	96 (84.96%)	4	100 (88.50%) 95%C.I.: 81.13%- 93.73%

		95%C.I.: 77.01%-90.99%		
	Non-hot SLN	13	-	13 (11.50%)
	Total	109 (96.46%) 95%C.I.: 91.18%-99.03%	4 (3.54%)	113
C.I. confidence interval Agreement. Bangdiwala's B: 0.841 (95% C.I.: 0.768-0.915) Comparison between the percentage of identified SLN in the two techniques. Percentage ratio (NIRF-ICG vs Planar-LPS with HIGP**):** 1.09 (95% C.I.: 1.011- 1.175) P= 0.025				

At histopathological analysis, 42/113 SLNs (37.2%) were metastatic (41 SLNs were metastatic from mast cell tumors and one from mammary gland carcinoma). Among the 6 SLCs that during mapping were identified exclusively by NIRF-ICG, 2 SLCs contained at least one metastatic SLN; among the 5 SLCs identified exclusively by planar lymphoscintigraphy with HIGP, 3 contained at least one metastatic lymph node. Details about SLN metastatic status and the presence of fluorescence and radioactivity are reported in Table 7.

Table 7. Metastatic status of SLNs and presence of fluorescence, radioactivity.

	Fluorescent – Hot	**Fluorescent – Non-hot**	**Hot – Non-fluorescent**	**Non-hot – Non-fluorescent**	**Total**
Metastatic	37	3	2	0	42
Non-metastatic	59	10	2	0	71
Total	96	13	4	0	**113**

A comparison of the techniques related to the guided surgical exploration was possible performed in 99/113 SLNs (87.6%). The remaining 14 nodes (from 5 SLCs) were removed *en-bloc* with the tumor due to their anatomical proximity, making guided surgical exploration not possible. Therefore, these nodes were excluded from the surgical exploration comparison, but the fluorescence and radioactivity of each SLN were evaluated *ex vivo*.

A total of 99 surgical fields were checked after the SLNs removal. The detection of a residual SLN was reported in 26/99 surgical fields (26.3%): in 18/26 of them (69.2%) the residual SLN was identified by both techniques, in 5/26 (19.2%) by NIRF-ICG only, and in 3/26 (11.6%) by HIGP only. All residual lymph nodes were always removed and underwent to histopathological analysis.

No statistically significant difference was found between HIGP and NIRF-ICG in the detection rate of a residual SLN during SLC exploration after the first SLN removal (percentage ratio=1.10; P=0.733). The concordance of the techniques in the post-excision check was 91.92%. The agreement calculated with the B index was 0.882. Details of post-excisional checks in both techniques are reported in Table 8.

Table 8. HIGP and NIRF-ICG in identifying residual SLN during surgical exploration

		NIRF-ICG		
		Identified residual SLN	**Not identified residual SLN**	**Total**
HIGP	**Identified residual SLN**	18 (18.18%) 95% C.I. 11.41%- 27.48%	3	21 (21.21%) 95%C.I. 13.89%-30.81%
	Not identified residual SLN	5	73(73.74%) C.I. 63.76%- 81.84%	78
	Total	23 (23.23%) 95%C.I. 15.58%-33.00%	76	99
C.I. confidence interval General Concordance 91/99 = 91.92% (95% C.I. 84.24% - 96.19%) Agreement. Bangdiwala's B: 0.882 (95% C.I.: 0.801-0.963) Comparison between the percentage of identified SLN in the two techniques. Percentage ratio (NIRF-ICG vs Planar-LPS with HIGP**):** 1.10 (95% C.I.: 0.650 - 1.846) P= 0.733				

The association between the investigated variables and the detection of a residual SLN by HIGP and NIRF-ICG during SLC surgical exploration is reported in Table 9. No significant associations were found in this analysis for HIGP surgical exploration. Considering the NIRF-ICG surgical field check, a significant association was found only with SLC anatomical location (P=0.004). Regarding SLC anatomical location, NIRF-ICG during guided surgical exploration identified more superficial inguinal residual SLN than axillary or accessory axillary residual SLN (P=0.024). The percentage of residual SLN identified in the superficial inguinal SLC was 26.77 higher than in axillary or accessory axillary SLC, and the percentage of identified superficial inguinal residual SLN was 7.79 times compared to those in axillary or accessory axillary.

Table 9. Association between detection of a residual SLN by HIGP and NIRF-ICG with selected variables

	Total number of SLN for category	**Residual SLN identified by HIGP** (n=21/26)	**Residual SLN identified by NIRF-ICG** (n=23/26)
BCS			
Normal Weight *Overweight	69 30	15 (21.74%) 6 (20.00%)	15 (21.74%) 8 (26.67%)
		PR= 0.92 (C.I. 0.40, 2.14) PD= -1.74 (C.I. -19.05, 15.57) P>0.99	PR= 1.23 (C.I.0.58, 2.58) PD= 4.93 (C.I.-13.65, 23.51) P=0.612
SLN location			
Axillary Accessory axillary Medial iliac Superficial Inguinal Mandibular Parotid Popliteal Superficial cervical Retropharyngeal	21 4 7 26 11 8 7 11 4	2 (9.52%) 1 (25%) 3 (42.9%) 6 (23.1%) 2 (18.2%) 5 (62.5%) 1 (14.3%) 1 (9.09%) 0 (0.00%)	0 (0.00%) 1 (25%) 3 (42,9%) 8 (30.8%) 4 (36.4%) 5 (62.5%) 1 (14.3%) 1 (9.09%) 0 (0.00%)
		P=0.09	**P=0.004**
SLN location			

*Superficial inguinal Axillary + accessory Axillary	26 25	6 (23.08%) 3 (12.00%)	8 (30.77%) 1 (4.00%)
		PR=1.92 (C.I. 0.54, 6.87) PD=11.08 (-9.53, 31.68) P=0.465	PR= 7.69 (C.I.1.04, 57.13) PD=26.77 (C.I.7.44, 46.10) **P=0.024**
*Superficial Inguinal Head and neck	26 23	6 (23.08%) 7 (30.43%)	8 (30.77%) 9 (39.13%)
		PR= 0.76 (C.I. 0.30, 1.93) PD= -7.36 (-32.17, 17.46) P=0.747	PR= 0.79 (C.I. 0.36, 1.70) PD=-8.36(C.I.-35.05, 18.33) P=0.564
*Superficial Inguinal Superficial cervical	26 11	6 (23.08%) 1 (9.09%)	8 (30.77%) 1 (9.09%)
		PR= 2.54 (0.34, 18.69) PD= 13.99 (-9.49, 37.46) P=0.649	PR= 3.38 (C.I. 0.48, 23.92) PD=21.68 (C.I.-2.88, 46.24) P=0.229
Weight			
<9kg 9-29.99kg >=30 kg	25 40 34	6 (24.00%) 7 (17.50%) 8 (23.53%)	8 (32.00%) 7 (17.50%) 8 (23.53%)
		P=0.7433	P=0.3874
*>=30 kg <9kg	34 25	8 (23.53%) 6 (24.00%)	8 (23.53%) 8 (32.00%)
		PR= 0.98 (C.I. 0.39, 2.47) RD= -0.47 (C.I. -22.46, 21.52) P>0.99	PR=0.74 (C.I. 0.32, 1.69) PD=-8.47(C.I.-31.66, 14.72) P=0.559
*>=30 kg 9-29.99kg	34 40	8 (23.53%) 7 (17.50%)	8 (23.53%) 7 (17.50%)
		PR= 1.34 (C.I.0.54, 3.33) PD= 6.03 (C.I.-12.46, 24.52) P=0.572	PR=1.34 (C.I.0.54, 3.33) PD=6.03 (-12.46, 24.52) P=0.572

Legend: PR: percentage ratio; PD: percentage difference; P: p-value of Fisher exact test C.I.: 95% confidence interval; *reference category: the numerator in PR and the first term in PD; Head and neck: mandibular + parotid+ retropharyngeal

PR: the number of SLNs identified in 100 SLNs of the reference category is PR times the number of SLNs identified in 100 SLNs of the other category

PD: per 100 SLNs in the reference category, PD is the number of SLNs identified in excess (or reduction) compared to 100 SLNs in the other category

The residual fluorescence caused by leakage of ICG after rupture of lymphatic vessels was recorded in 24/99 cases (24.2%).

During SLC surgical exploration, surgeons subjectively reported HIGP as more helpful in SLN detection and removal in 46 out of 99 cases (46.5%), NIRF-ICG in 24 out of 99 cases (24.2%), and both equally helpful in 29 out of 99 cases (29.3%). Considering the 70 cases where surgeons preferred only one of the two techniques, NIRF-ICG was preferred in 24/70 (34.29%) and HIGP in 46/70 cases (65.71%). Out of 24 cases of fluorescence leakage, NIRF and HIGP were equally helpful in 6 cases (25%) during SLC surgical exploration. In the remaining 18 cases, HIGP was more helpful in 13/24 cases (72.2%), while NIRF was more helpful in 5/24 cases (27.8%).

The association between the preferred technique and all the checked variables for these 70 cases is summarized in Table 10. The results of the association highlight that only the anatomical location of the SLC showed a significant association ($P < 0.01$). Regarding the comparison between superficial inguinal and axillary + accessory axillary nodes (P=0.054), NIRF-ICG was reported as the best tool for the removal of superficial inguinal nodes (7/23 = 30.43% vs. 1/19 = 5.25%, PR = 5.78), while HIGP was reported as the best tool for the removal of axillary + accessory axillary nodes (16/23 = 69.57% vs. 18/19 = 94.74%, PR = 0.73). About the comparison between superficial inguinal and head and neck nodes ($P < 0.001$), NIRF-ICG was reported as the best tool for the removal of head and neck nodes (7/23 = 30.4% vs. 13/15 = 86.67%, PR = 0.35), while HIGP was reported as the best tool for the removal of superficial inguinal nodes (6/23 = 26.09% vs. 2/15 = 13.33%, PR = 1.96). Medial iliac and popliteal lymphocentrum (and related SLNs) were excluded from the analysis with the reference categories (superficial inguinal) due to low numerosity (<10).

Table 10. **Association between surgical aid offered by HIGP and NIRF-ICG in SLN identification and investigated variables.**

	Number per category (99 SLN)	**Number preferred one of NIRF-ICG or HIGP** (70 SLN)	**Number NIRF-ICG preferred (%)** 24 SLN (34.29%)
BCS			
Normal weight *Overweight	69 30	46 24	17 (36.96%) 5 (20.83%)
			PR=0.56 C.I. (0.24, 1.34) PD= -16.12 (-37.54, 5.29) P=0.189
SLN location			
Axillary Accessory axillary Medial iliac Superficial inguinal Mandibular Parotid Popliteal Superficial cervical Retropharyngeal	21 4 7 26 11 8 7 11 4	18 1 1 23 7 6 4 8 2	0 (0.00%) 1 (100.00%) 1 (100.00%) 7 (30.43%) 7 (100.00%) 4 (66.67%) 1 (25.00%) 1 (12.50%) 2 (100.00%)
			P<0.001
*Inguinal Axillary + accessory axillary	26 25	23 19	7 (30.43%) 1(5.26%)
			PR= 5.78 (C.I. 0.78, 42.95) PD= 25.17 (3.85, 46.49) **P=0.054**
*Superficial Inguinal Head and neck	26 23	23 15	7 (30.43%) 13 (86.67%)
			PR= 0.35 (C.I. 0.18, 0.67) PD= -56.23 (C.I.-81.72, -30.75) **P <0.001**
*Superficial Inguinal	26	23	7 (30.43%)

Superficial cervical	11	8	1 (12.50%)
			PR= 2.43 (C.I. 0.35, 16.85) PD= 17.93 (C.I. -11.71, 47.58) P=0.642
Weight			
< 9 kg 9-29.99 kg >=30 kg	25 25 34	21 20 29	10 (47.62%) 7 (35.00%) 7 (24.14%)
			P= 0.2306
*>=30 kg < 9 kg	34 25	29 21	7 (24.14%) 10 (47.62%)
			PR= 0.51 (C.I. 0.23, 1.11) PD= -23.48 (C.I. -49.92, 2.95) P=0.131
*>=30 Kg 9-29.99 Kg	34 25	29 20	7 (24.14%) 7 (35.00%)
			PR= 0.69 (C.I.0.29, 1.66) PD= -10.86 (C.I. -36.93, 15.21) P=0.524
SLN size (mm)			
<10 10-20 >20	24 51 24	16 35 19	7 (43.75%) 11(31.43%) 6 (31.58%)
			P=0.6811
*>20 <10	24 24	19 16	6 (31.58%) 7 (43.75%)
			PR= 0.72 (C.I. 0.30, 1.71) PD= -12.17 (C.I.-44.23, 19.89) P=0.503
*>20 10-20	24 51	19 35	6 (31.58%) 11 (31.43%)
			PR= 1.00 (C.I. 0.44, 2.29) PD= 0.15 (C.I. -25.80, 26.10) P>0.99

Legend: C.I. 95% confidence interval; PR: percentage ratio; PD: percentage difference; *reference category: the numerator in PR and the first term in PD

PR: the number of suggested NIRF-ICG aid in 100 SLNs of the reference category is PR times the number of suggested NIRF-ICG aid in 100 SLNs of the other category

PD: per 100 SLNs in the reference category, PD is the number of Suggested NIRF-ICG AID in excess (or reduction) compared to 100 SLNs in the other category

2.3. Discussion:

The present study compared the two techniques using oncological cases that spontaneously presented at our VTH during the study period. The advantage of this study is that it is conducted in a daily clinical practice situation, mimicking the performance of the techniques used to identify SLC and SLN and related surgical guided removal. To better represent daily clinical practice in a referral small

animal veterinary oncologic centre, the study encompassed various tumor types, measurable macroscopic diseases or scars, and included both canine and feline species, drawing on recently published data [2–4,19,24,40].

The results of the present study confirm the high detection rate of SLC mapping for both techniques, as previously reported in the literature [2,19], and, when used in combination, the detection rate of SLB may further increase. In fact, the combined use of NIRF-ICG and LPS identifying at least one SLC and the detection and removal of at least one SLN for each tumor leading to a 100% detection rate. Conversely, while the combined use may provide complementary diagnostic benefits, the increased cost could represent the major limitation for the owners. The techniques were compared at two time points: mapping for SLC identification and guided surgical exploration of SLC for SLN detection. No statistical differences were found during SLC mapping between LPS and NIRF-ICG, and their detection rate was similar (respectively 92% and 93%). Despite the well-known ability of fluorescence to allow the surgeon to visualize lymphatic flow and SLCs through the skin in real-time [41], its recognized limit is the low visualization of deeper lymphatic networks and SLCs. Nevertheless, the absence of visualization of fluorescent lymphatic flow was observed in our study only in 5 SLCs, and in 3 of them, SLC fluorescence was detected during the surgical exploration phase. This indicates that, in these 3 cases, ICG reached the nodes, but lymphatic flows were too deep to be detected by the surgeons during the mapping phase before the surgical exploration. Albeit a few cases of tumors with a SLN medial iliac migration (n = 4), it should be noted that the two techniques had the same performance. Despite the depth of the SLC, the fluorescent flow was visible on the lateral side of the trunk and then went deep, perforating the abdominal wall as described in previous anatomical studies [42,43].

The comparison among techniques during the surgical exploration phase showed that excised SLN were significantly more frequently fluorescent than hot: this result follows with previous human and veterinary literature [12,44,45]. The hypothesized explanation is that the nanocolloidal formulation of 99mTc increases the tracer nodal retention, while low molecular weight of ICG allows a rapid transit through lymphatic vessels and short nodal retention [44]. The combined use of these two guiding techniques and the two tracers (99mTc and ICG) increases the number of extirped nodes and may maximize the chance of detecting nodal metastases [45]. Nevertheless, despite the higher number of fluorescent SLNs extirpated, the number of metastatic SLNs is comparable in the two techniques (Table 7), suggesting that fluorescence was associated with removal of an adjunctive number of SLNs. Therefore, the extirpation of a higher number of nodes seems not to produce an upper tumor stage migration as previously reported in human and veterinary literature [12,45].

Based on results of this study it is not possible to determine whether the additional lymph nodes removed can be considered or not second-tier nodes. Considering that in human oncology the specific definition and location of second tier lymph nodes can vary depending on the type of cancer and the anatomical region involved [46], at this moment the authors do not have such indications to correctly define the first and second tier in dogs. Further studies should focus on this aspect of advanced imaging techniques to better define the functional role of these nodes and to potentially adapt the human-derived staging system for veterinary use [47].

However, during SLC surgical exploration NIRF-ICG and LPS with HIGP performed similarly when checking the surgical field after the first SLN removal. The concordance of the two techniques, indeed, increased during the SLN removal phase. These results also underline that NIRF-ICG and HIGP guidance showed a greater advantage in the intraoperative phase by ensuring better extirpation of all SLNs linked to the tumor within an SLC [11,48].

As a part of the study, we also explored the opinions of the surgeons about the surgical aid provided by each technique in SLN extirpation. According to the surgeons, HIGP was considered the best tool in 46.5% while ICG in 24.2% of cases. It should be also noted that the surgical aid of both techniques was associated with the SLC anatomical location (Table 10). Indeed, HIGP and NIRF-ICG seem to offer different kinds of help. NIRF-ICG was considered the best tool during head and neck (parotid, retropharyngeal, and mandibular) SLC detection, probably due to the close proximity of the tumor/scar with most SLC that could increase the risk of tumor radioactive shine-through effects as previously reported in human literature [49]. Conversely, the use of HIGP was regarded as the best surgical aid mostly in axillary SLCs, according to the surgeons' opinions. A possible explanation could be due to the easy handling and high sensitivity of the probe: the probe can be inserted into the surgical field and can reach the deepest SLNs even in a small deep surgical field such as the axillary region. On the contrary, the type of NIRF-camera used for this study was placed above the surgical field, not directly handheld by the surgeon. Indeed, the visualization of the fluorescence was related to the anatomical conformation, laser angulation, and depth of the SLN. It is unknown to the authors if the use of a different NIRF-camera could improve their performance in this SLC location; however, it should be pointed out that recent research suggests a different approach for axillary SLC, using a minimally invasive endoscopic technique. This technique might be further refined with the addition of ICG [50].

Additionally, considering the surgeons' opinions, the use of HIGP was deemed more comfortable compared to NIRF-ICG in most of cases of fluorescence leakage. Indeed, the leakage of ICG, observed in 24 surgical fields, could produce fluorescent contamination of the surgical field, leading to unclear interpretations during the decision-making process in SLC exploration and SLN

extirpation. Even if fluorescent imaging interpretation has a quick learning-curve [51], HIGP probably ensures a more objective assessment of residual SLNs in the surgical field, especially for a surgeon at an early stage of the learning curve.

In human medicine, these techniques have mostly been compared for specific tumors in specific anatomical regions, such as breast cancer and head and neck tumors [17,45,49]. Our results cannot be equated with those mostly described for humans because we included different canine and feline solid malignant tumors with various anatomical locations. Conversely, our results could be compared with a study by Stoffels et al. (2015) on human cutaneous melanoma. In that study, the presence of cutaneous melanoma in various anatomical locations and, consequently, SLCs, showed that the use of NIRF-ICG could not replace the standard care use of LPS due to the lower detection rate and the consequent risk of missing most SLNs [14]. Although we investigated different anatomical locations, in our study, the detection rate of NIRF-ICG in mapping and its concordance with LPS were significantly higher compared to the human melanoma study, resembling findings in other canine and feline NIRF-ICG studies [3,12,13,19]. It could be assumed that even in the presence of different anatomical locations, fluorescence is more successful in dogs and cats rather than in humans. This difference between our results and the study of Stoffels et al. (2015), could be related to the obviously different anatomical conformation of humans and pets. Moreover, in humans, it is reported the worst performance of NIRF-ICG in obese patients, in whom fluorescence is visible only after skin incision [14,52,53]. On the contrary, in our study, NIRF-ICG did not show an association with BCS or the body weight of the included animals (Table 5, 9, and 10). According to the results in our sample population, it seems that, unlike in humans where obesity plays a role in the fluorescence visualization [14,52,53], in dogs and cats NIRF-ICG does not depend on BCS or body weight.

In contrast to human medicine, no comparative studies between LPS and NIRF-ICG are available in veterinary medicine regarding SLN mapping and extirpation. Despite LPS being considered the gold standard for SLN detection in humans, its role as a reference standard in dogs and cats has not been established. Based on this consideration, in our study, it was not possible to compare a technique with a gold standard [14,15]. Therefore, we evaluated the intra-patient performance and agreement between LPS and NIRF-ICG in SLN detection using the described statistical analysis.

The main limitation of this study is the low precision of the estimates, which is one of the consequences of the sample size. It was of interest to compare the association pattern for the pair of techniques to identify SLC and SLN. Although the appropriate method is a regression model, including the two techniques as independent variables and the selected variables as dependent variables, it was impossible to analyze data by this model because of the small sample size and the low number of non-detected SLC and SLN. Moreover, since no information was available regarding

a reference standard technique in veterinary medicine, we could not calculate the sample size for adequate statistical power to compare the techniques for identifying SLC and SLN and to obtain a pre-planned precision of the estimates for the concordance index. For this reason, all statistical analyses were performed only for exploratory purposes, and results of the statistical tests should be considered as a measure of "possible evidence" to be confirmed in studies with greater sample size.
Secondly, the study included a few endocavitary lymphocentrums, represented solely by medial iliac SLN, with no cases involving intrathoracic nodes; thus, no assumptions can be made regarding intrathoracic nodes. Furthermore, we enrolled predominantly cutaneous and subcutaneous tumors, precluding assumptions related to tumors in other locations (e.g., oral cavity or anal sac tumors). These limitations are beyond our control, as they depend on clinical referrals to the VTH during the study period.
In the intraoperative phase, the SLN detection and guided removal were similar. Even if NIRF-ICG selected more nodes than HIGP, the tumor staging did not change. Based on this phenomenon, future studies could explore if the additional non-hot but fluorescent nodes may represent second-tier nodes.
In this study, we did not standardize a maximum mapping time for SLN identification. The use of tracers such as technetium and indocyanine green allows real-time tracking of tracer migration from the tumor to the SLC, unlike radiological tracers (e.g., lipiodol, iohexol) that require radiographs or CT scans at predefined intervals to assess migration and cannot be evaluated intraoperatively [6,7,54]. As the mapping time can be influenced by multiple factors beyond the tracer's physicochemical properties and/or half-life of the tracer, we believe that a dedicated study on this aspect would be particularly valuable, especially in clinical settings with metastatic or enlarged lymph nodes [55].

In conclusion, despite some peculiar differences for each technique and the confirmed higher performance if combined, NIRF-ICG and LPS showed comparable performance in SLC mapping and SLN extirpation in canine and feline solid malignant tumors based on our results. Although more data on endocavitary nodes (abdominal and thoracic) should be collected, fluorescence can be considered a viable alternative to radiopharmaceuticals in daily clinical practice, particularly when the latter results not accessible. Finally, the results of this study could provide the opportunity to use the performance, and concordance estimates to plan a future study aimed at statistical inference.

2.4. References:

1. Worley DR. Incorporation of sentinel lymph node mapping in dogs with mast cell tumours: 20 consecutive procedures. Vet Comp Oncol. 2014;12:215–26. doi: 10.1111/j.1476-5829.2012.00354.x.
2. Chiti LE, Stefanello D, Manfredi M, Zani DD, De Zani D, Boracchi P, et al. To map or not to map the cN0 neck: Impact of sentinel lymph node biopsy in canine head and neck tumours. Vet Comp Oncol. 2021;19:661–70. doi: 10.1111/vco.12697.
3. Chiti LE, Gariboldi EM, Stefanello D, De Zani D, Grieco V, Nolff MC. Sentinel Lymph Node Mapping and Biopsy in Cats with Solid Malignancies: An Explorative Study. Animals. 2022;12. doi: 10.3390/ani12223116
4. Arz R, Seehusen F, Meier VS, Nolff MC. Indocyanine-based near-infrared lymphography for real-time detection of lymphatics in a cat with multiple mast cell tumours. JFMS Open Rep. 2022;8. doi: 10.1177/20551169221074961
5. Fournier Q, Thierry F, Longo M, Malbon A, Cazzini P, Bisson J, et al. Contrast-enhanced ultrasound for sentinel lymph node mapping in the routine staging of canine mast cell tumours: A feasibility study. Vet Comp Oncol. 2021;19:451–62. doi: 10.1111/vco.12647. Epub 2020
6. Annoni M, Borgonovo S, Aralla M. Sentinel lymph node mapping in canine mast cell tumours using a preoperative radiographic indirect lymphography: Technique description and results in 138 cases. Vet Comp Oncol. 2023;21:469–81. doi: 10.1111/vco.12906.
7. Randall EK, Jones MD, Kraft SL, Worley DR. The development of an indirect computed tomography lymphography protocol for sentinel lymph node detection in head and neck cancer and comparison to other sentinel lymph node mapping techniques. Vet Comp Oncol. 2020;18:634–44. doi: 10.1111/vco.12585.
8. Lapsley J, Hayes GM, Janvier V, Newman AW, Peters-Kennedy J, Balkman C, et al. Influence of locoregional lymph node aspiration cytology vs sentinel lymph node mapping and biopsy on disease stage assignment in dogs with integumentary mast cell tumors. Vet Surg. 2021;50:133–41. doi: 10.1111/vsu.13537
9. Grimes JA, Secrest SA, Northrup NC, Saba CF, Schmiedt CW. Indirect computed tomography lymphangiography with aqueous contrast for evaluation of sentinel lymph nodes in dogs with tumors of the head. Vet Radiol Ultrasound. 2017;58:559–64. doi: 10.1111/vru.12514
10. Manfredi M, De Zani D, Chiti LE, Ferrari R, Stefanello D, Giudice C, et al. Preoperative planar lymphoscintigraphy allows for sentinel lymph node detection in 51 dogs improving staging accuracy: Feasibility and pitfalls. Vet Radiol Ultrasound. 2021;62:602–9. doi: 10.1111/vru.12995

11. Gariboldi EM, Ubiali A, Chiti LE, Ferrari R, De Zani D, Zani DD, et al. Evaluation of Surgical Aid of Methylene Blue in Addition to Intraoperative Gamma Probe for Sentinel Lymph Node Extirpation in 116 Canine Mast Cell Tumors (2017–2022). Animals. 2023;13. doi: 10.3390/ani13111854.
12. Wan J, Oblak ML, Ram A, Singh A, Nykamp S. Determining agreement between preoperative computed tomography lymphography and indocyanine green near infrared fluorescence intraoperative imaging for sentinel lymph node mapping in dogs with oral tumours. Vet Comp Oncol. 2021;19:295–303. doi: 10.1111/vco.12675.
13. Alvarez-Sanchez A, Townsend KL, Newsom L, Milovancev M, Gorman E, Russell DS. Comparison of indirect computed tomographic lymphography and near-infrared fluorescence sentinel lymph node mapping for integumentary canine mast cell tumors. Vet Surg. 2023;52:416–27. doi: 10.1111/vsu.13929
14. Stoffels I, Dissemond J, Pöppel T, Schadendorf D, Klode J. Intraoperative fluorescence imaging for sentinel lymph node detection: Prospective clinical trial to compare the usefulness of indocyanine green vs technetium Tc 99m for identification of sentinel lymph nodes. JAMA Surg. 2015;150:617–23. doi: 10.1001/jamasurg.2014.3502
15. Somashekhar SP, Kumar CR, Ashwin KR, Zaveri SS, Jampani A, Ramya Y, et al. Can Low-cost Indo Cyanine Green Florescence Technique for Sentinel Lymph Node Biopsy Replace Dual Dye (Radio-colloid and Blue Dye) Technique in Early Breast Cancer: A Prospective Two-arm Comparative Study. Clin Breast Cancer. 2020;20:e576–83. doi: 10.1016/j.clbc.2020.03.013
16. Kedrzycki MS, Leiloglou M, Ashrafian H, Jiwa N, Thiruchelvam PTR, Elson DS, et al. Meta-analysis Comparing Fluorescence Imaging with Radioisotope and Blue Dye-Guided Sentinel Node Identification for Breast Cancer Surgery. Ann Surg Oncol. Springer Science and Business Media Deutschland GmbH; 2021. p. 3738–48. doi: 10.1245/s10434-020-09288-7.
17. Bargon CA, Huibers A, Young-Afat DA, Jansen BAM, Borel-Rinkes IHM, Lavalaye J, et al. Sentinel lymph node mapping in breast cancer patients through fluorescent imaging using indocyanine green the influence trial. Ann Surg. 2022;276:913–20. doi: 10.1097/SLA.0000000000005633.
18. Da Silva Sá R, Von Ah Rodrigues RF, Bugalho LA, Da Silva SU, Pinto Nazário AC. Evaluation of the efficacy of using indocyanine green associated with fluorescence in sentinel lymph node biopsy. PLoS One. 2023;18. doi: 10.1371/journal.pone.0273886.
19. Beer P, Rohrer-Bley C, Nolff MC. Near-infrared fluorescent image-guided lymph node dissection compared with locoregional lymphadenectomies in dogs with mast cell tumours. J Small Anim Pract . 2022;63:670–8. doi: 10.1111/jsap.13529.

20. Korpita MF, Mayhew PD, Steffey MA, Balsa IM, Giuffrida MA, Chohan AS, et al. Thoracoscopic detection of thoracic ducts after ultrasound-guided intrahepatic injection of indocyanine green detected by near-infrared fluorescence and methylene blue in dogs. Vet Surg. 2022;51:O118–27. doi: 10.1111/vsu.13682
21. Morris KP, Singh A, Holt DE, Stefanovski D, Singhal S, Bosco J, et al. Hybrid single-port laparoscopic cisterna chyli ablation for the adjunct treatment of chylothorax disease in dogs. Vet Surg. 2019;48:O121–9. doi: 10.1111/vsu.13195
22. Mullen KM, Regier PJ, Perez-Rodriguez V, Fox-Alvarez WA, Bertran J, Colee J. Use of real-time near-infrared fluorescence to assess gastric viability in dogs with gastric dilatation volvulus: A case-control study. Vet Surg. 2024; 53(4):684-694. doi: 10.1111/vsu.14067.
23. Suh YJ, Choi JY, Chai YJ, Kwon H, Woo JW, Kim SJ, et al. Indocyanine green as a near-infrared fluorescent agent for identifying parathyroid glands during thyroid surgery in dogs. Surg Endosc. 2015; 29(9):2811-7. doi: 10.1007/s00464-014-3971-2.
24. Ferrari R, Chiti LE, Manfredi M, Ravasio G, De Zani D, Zani DD, et al. Biopsy of sentinel lymph nodes after injection of methylene blue and lymphoscintigraphic guidance in 30 dogs with mast cell tumors. Vet Surg. 2020;49:1099–108. doi: 10.1111/vsu.13483.
25. Séguin B, Liptak JM. Updates in Surgical Oncology. Vet Clin North Am Small Anim Pract. 2024; 54(3):577-589. doi: 10.1016/j.cvsm.2023.12.010.
26. Meuten DJ, Moore FM, Donovan TA, Bertram CA, Klopfleisch R, Foster RA, et al. International Guidelines for Veterinary Tumor Pathology: A Call to Action. Vet Pathol. 2021; 58(5):766-794. doi: 10.1177/03009858211013712.
27. DE Almeida M, Gregório H, Pereira A, Queiroga FL. The Diagnostic Yield of Whole-body Computed Tomography in Dogs and Cats in the Oncology Setting. In Vivo. 2025; 39(3):1293-1302. doi: 10.21873/invivo.1393328.
28. Suami H, Yamashita S, Soto-Miranda MA, Chang DW. Lymphatic Territories (Lymphosomes) in a Canine: An Animal Model for Investigation of Postoperative Lymphatic Alterations. PLoS One. 2013;8. doi: 10.1371/journal.pone.0069222.
29. Baum H. The Lymphatic System of the Dog. 2021. University of Saskatchewan: Saskatoon, SK, Canada. https://openpress.usask.ca/k9lymphaticsystem/
30. Worden NJ, Bertran J, Watt MM, Reynolds PS, de Mello Souza CH, Maxwell EA, et al. Superficial anatomic landmarks can be used to triangulate the location of canine peripheral lymphocentrums: superficial cervical, axillary, and superficial inguinal. J Am Vet Med Assoc. 2023;261:490–9. doi: 10.2460/javma.22.11.0518.

31. Worden NJ, Bertran J, Reynolds PS, Chase EC, Crews CD, Ham K, et al. 2023. Geometric, landmark-guided technique reduces tissue trauma, surgery time, and subjective difficulty for canine peripheral lymphadenectomies: an educational crossover study. J Am Vet Med Assoc. 261(11):1-9. doi: 10.2460/javma.23.04.0206.
32. Verbeek FPR, Troyan SL, Mieog JSD, Liefers GJ, Moffitt LA, Rosenberg M, et al. Near-infrared fluorescence sentinel lymph node mapping in breast cancer: A multicenter experience. Breast Cancer Res Treat. 2014;143:333–42. doi: 10.1007/s10549-013-2802-9.
33. Wang Y, Peng Q, Sun P, Li X, Dong Y. Comparison of Sentinel Lymph Node Biopsy by Blue Dye Conjunction With Indocyanine Green or Radioisotope in Early-Stage Breast Cancer: A Prospective Single-Center Observational Study. Clin Med Insights Oncol. 2023;17. doi: 10.1177/11795549231201129.
34. Mcmasters KM, Wong SL, Chao C, Woo C, Tuttle TM, Noyes RD, et al. Defining the Optimal Surgeon Experience for Breast Cancer Sentinel Lymph Node Biopsy: A Model for Implementation of New Surgical Techniques. Ann Surg. doi: 10.1097/00000658-200109000-00003.
35. Lipsitz, Stuart R., Kyungmann Kim, Lueping Zhao. Analysis of repeated categorical data using generalized estimating equations. Stat Med. 13(11):1149-1163. doi: 10.1002/sim.4780131106
36. Shankar V, Bangdiwala SI. Observer agreement paradoxes in 2x2 tables: Comparison of agreement measures. BMC Med Res Methodol. 2014;14. doi: 10.1186/1471-2288-14-100.
37. Halekoh U, Højsgaard S, Yan J. The R Package geepack for Generalized Estimating Equations [Internet]. JSS Journal of Statistical Software. 2006. Available from: http://www.jstatsoft.org/
38. Stevenson MM, Marshall J, Sanchez J, Thornton R, Reiczigel J, Robison-Cox J. Title Tools for the Analysis of Epidemiological Data [Internet]. 2024. Available from: https://orcid.org/0000-0003-1890-9784
39. Kilem L. Gwet. Title Computing Chance-Corrected Agreement Coefficients (CAC) [Internet]. 2022. Available from: http://agreestat.com/
40. Gariboldi EM, Stefanello D, Nolff MC, De Zani D, Zani D, Grieco V, et al. Sentinel Lymph Node Biopsy Is Feasible in Dogs with Scars from Prior Local Excision of Solid Malignancies. Animals. 2022;12. doi: 10.3390/ani12172195
41. Favril S, Abma E, Stock E, Devriendt N, Van Goethem B, Blasi F, et al. Fluorescence-guided surgery using indocyanine green in dogs with superficial solid tumours. Veterinary Record. 2020; 187:273. doi: 10.1136/vr.105554

42. Suami H, O'Neill JK, Pan WR, Taylor GI. Perforating lymph vessels in the canine torso: Direct lymph pathway from skin to the deep lymphatics. Plast Reconstr Surg. 2008;121:31–6. doi: 10.1097/01.prs.0000293753.93274.21.
43. Sánchez-Margallo FM, Brun MV, Sánchez-Margallo JA. Identification of intra-abdominal lymphatics in canine carcasses by laparoscopic fluorescence lymphography with intradermal and intrapopliteal ICG administration. PLoS One. 2020;15. doi: 10.1371/journal.pone.0241992.
44. Schaafsma BE, Mieog JSD, Hutteman M, Van Der Vorst JR, Kuppen PJK, Löwik CWGM, et al. The clinical use of indocyanine green as a near-infrared fluorescent contrast agent for image-guided oncologic surgery. J Surg Oncol. 2011. p. 323–32. doi: 10.1002/jso.21943.
45. Wishart GC, Loh SW, Jones L, Benson JR. A feasibility study (ICG-10) of indocyanine green (ICG) fluorescence mapping for sentinel lymph node detection in early breast cancer. Eur J Surg Oncol. 2012;38:651–6. doi: 10.1016/j.ejso.2012.05.007.
46. Cozzaglio L, Doci R, Celotti S, Roncalli M, Gennari L. Gastric cancer: extent of lymph node dissection and requirements for a correct staging. Tumori. 2004; 90(5):467-72. doi: 10.1177/030089160409000505.
47. Mickelson MA. Updated Concepts in Oncologic Surgery: Apocrine Gland Anal Sac Adenocarcinoma and Mast Cell Tumors. Vet Clin North Am Small Anim Pract. 2022; 52(2):549-580. doi: 10.1016/j.cvsm.2021.12.008.
48. Stefanello D, Gariboldi EM, Boracchi P, Ferrari R, Ubiali A, De Zani D, et al. Weishaar's classification system for nodal metastasis in sentinel lymph nodes: Clinical outcome in 94 dogs with mast cell tumor. J Vet Intern Med. 2024;38:1675–85. doi: 10.1111/jvim.16997.
49. Van Den Berg NS, Brouwer OR, Klop WMC, Karakullukcu B, Zuur CL, Tan IB, et al. Concomitant radio- and fluorescence-guided sentinel lymph node biopsy in squamous cell carcinoma of the oral cavity using ICG-99mTc- nanocolloid. Eur J Nucl Med Mol Imaging. 2012;39:1128–36. doi: 10.1007/s00259-012-2129-5
50. Kuvaldina AB, Buote N, Campoy L, Porter I, Hayes GM. Development of a minimally invasive endoscopic technique for excisional biopsy of the axillary lymph nodes in dogs. Vet Surg. 2023;52:888–96. doi: 10.1111/vsu.13901
51. Tagaya N, Yamazaki R, Nakagawa A, Abe A, Hamada K, Kubota K, et al. Intraoperative identification of sentinel lymph nodes by near-infrared fluorescence imaging in patients with breast cancer. Am J Surg. 2008;195:850–3. doi: 10.1016/j.amjsurg.2007.02.032.
52. Tagaya N, Nakagawa A, Abe A, Iwasaki Y, Kubota K. Non-Invasive Identification of Sentinel Lymph Nodes Using Indocyanine Green Fluorescence Imaging in Patients with Breast Cancer. The Open Surg Oncol J. 2010. doi: 10.2174/1876504101002010071

53. Crane LMA, Themelis G, Arts HJG, Buddingh KT, Brouwers AH, Ntziachristos V, et al. Intraoperative near-infrared fluorescence imaging for sentinel lymph node detection in vulvar cancer: First clinical results. Gynecol Oncol. 2011; 120:291–5. doi: 10.1016/j.ygyno.2010.10.009
54. Brissot HN, Edery EG. Use of indirect lymphography to identify sentinel lymph node in dogs: a pilot study in 30 tumours. Vet Comp Oncol. 2017; 15(3): 740-753. doi:10.1111/vco.12214
55. Goyal A, Douglas-Jones AG, Newcombe RG, Mansel RE. Effect of lymphatic tumor burden on sentinel lymph node biopsy in breast cancer. Breast J. 2005;11(3):188-194. doi:10.1111/j.1075-122X.2005.21591.x

3. Nodal lymphatic mapping in 22 dogs bearing solid malignant tumors and enlarged regional lymph nodes: a descriptive study (2022-2025)

- The present study was submitted at The Veterinary Journal (July 11th, 2025) and under review at the time to submission of the present Thesis
- PhD student role: first author and corresponding author

Elisa Maria Gariboldi[a], Alessandra Ubiali[a], Roberta Ferrari[a], Luigi Auletta[a], Donatella De Zani[a], Davide Danilo Zani[a], Francesco Ferrari[a], Federica Alessandra Brioschi[a], Paola Roccabianca[a], Chiara Giudice[a], Valeria Grieco[a], Camilla Recordati[a] and Damiano Stefanello[a]

a. Dipartimento di Medicina Veterinaria e Scienze Animali - Università degli Studi di Milano, Lodi, Italia

The occurrence of a malignant tumor with an enlarged regional lymph node (eRLN) prompts clinicians to enhance preoperative staging to rule out both nodal and distant metastases. If distant metastases are excluded, excision of the eRLN – regardless of its neoplastic or non-neoplastic status – is recommended to achieve definitive staging and may improve the effectiveness of adjuvant treatment. (Alvarez-Sanchez et al., 2023; Baginski et al., 2014; Chiti et al., 2021; Collivignarelli et al., 2021; Grimes et al., 2017; Liptak and Boston, 2019; Stefanello et al., 2024; Wan et al., 2021). While the usefulness of mapping non-palpable and normal-sized sentinel lymph nodes (SLNs) has been extensively investigated in canine surgical oncology, (Annoni et al., 2023; Chiti et al., 2025; Collivignarelli et al., 2021; Ferrari et al., 2021; Ferraris et al., 2023) no data are currently available on SLN mapping in the presence of regional lymph node enlargement. In human oncology, lymph node enlargement—caused by neoplastic infiltration or inflammatory lymphatic disorders— can alter in the lymphatic flow. These alterations potentially interfere with the SLN mapping: the metastatic spread or inflammatory disease may disrupt the normal lymphatic drainage, blocking the tracers flow (Bassi et al., 2006; Goyal et al., 2005; Lam et al., 2009; Leijte et al., 2009; Liao and Von Der Weid, 2014; Monaco et al., 2012). This can cause incomplete or absent tracer uptake in the enlarged node/s and, in some cases, the rerouting of the tracer to a "neo-sentinel lymph node" (neo-SLN) (Goyal et al., 2005; Leijte et al., 2009). A neo-SLN refers to a new alternative lymph node that assumes this role after the original SLN pathway has been disrupted or altered. Understanding and identifying neo-

sentinel lymph nodes is important issue in human oncology because metastatic spread may not follow the original pathway (Bassi et al., 2006; Goyal et al., 2005; Leijte et al., 2009; Proulx et al., 2013).
The influence of metastatic or inflammatory lymphadenopathy in nodal drainage has been investigated in human medicine (Goyal et al., 2005; Leijte et al., 2009; Monaco et al., 2012) and remains unexplored in canine veterinary surgical oncology. In this context, the present study aims to describe the influence of eRLN (with neoplastic or non-neoplastic involvement) on nodal mapping and staging of SLN lymphography in dogs with solid malignancies and describe possible alterations of the nodal tracer distribution.

3.1. Materials and methods:

For this cross-sectional study, data from client-owned dogs bearing malignancies, referred to the Veterinary Teaching Hospital from May 2022 to May 2025 for tumor removal and sentinel lymph nodes excision, were retrospectively collected. All dogs had a cytological or histological diagnosis of a solid malignant tumor. Tumor at first presentation, recurrent tumor, or scars from previous tumor excision, in the absence of any lymphadenectomy, were included if presented at least a clinically eRLN. The lymph node was defined “enlarged’’ if it was larger than the contralateral one based on clinical palpation and/or imaging measurement (ultrasound and/or computed tomography). If available, the cytological status before surgery of the enlarged lymph node was recorded. The enlarged lymph node was considered the regional one according to Suami (Suami et al., 2013).
To be admitted to surgery a complete staging had to be performed based on tumor diagnosis and according to current recommendation. Only dogs without distant metastasis were enrolled. At the time of the surgery, all owners signed a written informed consent for the procedures and data collection. Dogs included in the present study underwent SLN mapping and removal guided by lymphoscintigraphy with Technetium-99 and/or near-infrared fluorescence with indocyanine green (NIRF-ICG). The SLN was defined as the first lymph node/s linked to primary tumor by lymphatic mapping and was thus expected to be first site of tracer uptake from afferent lymphatic vessels.
The SLN lymphography was performed with NIRF camera (SPY-PHI QP system, Stryker, MIDA Tecnologia medica S.p.A) (Alvarez-Sanchez et al., 2023; Beer et al., 2022; Wan et al., 2021) and/or lymphoscintigraphy (Picker Prism 200XP, Picker International, Highland Heights, OH, USA) associated with handheld intraoperative gamma probe (Crystal probe SG04; Crystal Photonic GmbH, Berlin, Germany) (Chiti et al., 2025; Ferrari et al., 2020; Manfredi et al., 2021). The NIRF and/or lymphoscintigraphy were performed on the same day of the surgery.

The lymphocentrum of the enlarged node was always explored, and all enlarged lymph nodes were excised regardless of tracer uptake. Moreover, any additional lymphocentrum detected by tracers were considered sentinel (SLC) and the SLNs were excised. Surgical exploration of the SLC was stopped when no more enlarged nodes were detected by palpation and no additional radioactive or fluorescent nodes were identified. Lymphadenectomy, if feasible, was performed before tumor excision and gloves and instruments were changed after the enlarged nodes manipulation, to avoid possible neoplastic contamination and seeding.

All the lymph nodes (enlarged and non-palpable/normal sized) extirpated from SLC identified by NIRF and/or lymphoscintigraphy mapping were evaluated ex-vivo to estimate qualitative distribution of radioactivity and fluorescence uptake. The qualitative nodal distribution of tracer uptake was classified as: total uptake (if the tracers were uniformly detectable in the whole lymph node), incomplete uptake (if a heterogeneous tracers' uptake was detected into the lymph node), and no uptake (if not any uptake was detected in the lymph node). In addition, nodal tracer rerouting was recorded (Goyal et al., 2005; Lam et al., 2009; Lützen et al., 2016). Rerouting was defined as the phenomenon in which the tracer is redirected to another lymph node within the same or a different SLC, resulting in incomplete or absent uptake in the enlarged lymph node and uptake in an additional sentinel lymph node (SLN). (Goyal et al., 2005; Lam et al., 2009; Lützen et al., 2016)

Excised tumors and all excised lymph nodes were formalin-fixed for histopathological analysis.

Patient signalment (breed, sex, age, bodyweight); clinical presentation (first presentation, recurrence, scar) of the tumor, anatomical location, size (major axis in mm), presence of ulceration, and histotype (with grading, if applicable) were collected. The following lymph nodes data were recorded: anatomical location of the lymphocentrums of the enlarged lymph node; enlarged lymph node fixed or not fixed to surrounding normal tissue; the number of the SLCs and the number of the SLNs detected by the tracers. The presence and description of possible rerouting and lymphatic flow alterations were recorded, as well. For each extirpated lymph node (both eRLN and non palpable/normal sized SLNs) dimension of major axis (mm), pattern of tracer uptake and nodal histological diagnosis were collected. Histological nodal status was classified as: metastatic from the enrolled tumor (for mast cell tumor – MCT early metastases and overtly metastasis) and non-metastatic (lymph nodes reactive or normal or bearing other lymphoproliferative malignancies). Occurrence of intra-operative complications or post-operative complications related to the lymphadenectomy were also recorded and classified as "minor" or "major" (Chiti et al., 2023; LeBlanc et al., 2021).

The retrieved variables were summarized with descriptive statistics reporting the number of patients and the % of the total cases within each category (breed, sex, eRLN identification, lymphographic

technique, and lymphatic pattern). Similarly, the number of SLC, the number of SLN, as well as the number of SLN within the enlarged and non-palpable/normal sized categories were reported. Normality for continuous variables was assessed with Shapiro-Wilk's W test and data were expressed as mean ± standard deviation for normally distributed variables and median (range) for non-normally distributed variables. Statistical analysis was performed with dedicated software (SPSS 29 for MacOS, SPSS Inc., Headquarters, Chicago, IL, USA) and significance was set at $p \leq 0.05$.

3.2. Results:

Among the 210 dogs with solid malignant tumors treated with surgery plus SLN mapping and removal, 22 presented eRLN suggestive of possible metastasis and met the inclusion criteria. Data about patient dogs, tumors, eRLN, lymphatic mapping results, nodal pattern of tracer uptake are summarized in Table 1.

Among the 22 included tumors, 12 (55%) were at first presentation, 6 (27%) were recurrence and 4 (18%) were scars from previous tumor excision. In 11 (50%) cases the tumors/scars were located in head and neck regions, in 4 (18%) in limbs, 3 (14%) in digit, 2 (9%) in trunk, 2 (9%) in perineal region. The tumors had a median size of 20 mm (10-100 mm). In 11 macroscopic tumors ulceration was present. The eRLN was assessed by clinical examination and palpation in 19 dogs (86%). In the remaining 3 dogs (14%) the enlarged lymph nodes were endocavitary and were detected by imaging techniques (abdominal ultrasound and/or total-body computed tomography). All eRLN were considered not fixed to surrounding tissue based either on clinical palpation and/or during surgical excision. The eRLN cytological diagnosis was available before surgery in 12 dogs (56%): 7 of them were metastatic (4 cutaneous mast cell tumors, 1 subcutaneous mast cell tumor, 1 rectal plasmacytoma and 1 oral malignant melanoma) while 5 of them were negative for metastasis (2 cutaneous mast cell tumors, 1 subcutaneous myxosarcoma, 1 soft tissue sarcoma, 1 squamous cell carcinoma). Three out of the latter resulted metastatic at histological exam.

For the lymphographies, NIRF alone was used in 13 (59%), lymphoscintigraphy alone in 6 (27%), and both techniques in 3 (14%). The SLC detection was achieved within the first 10-15 minutes after the tracers' injection regardless of the tracer used. Eleven lymphographies (50%) identified a single SLC, while in the remaining 11 (50%) multiple (2 - 4) SLCs were detected, for a total of 38 SLCs that were surgically explored.

Table 1. Comprehensive data about patient dogs, tumors, eRLN, lymphatic mapping results, nodal pattern of tracer uptake

Signalment	Histological diagnosis local tumor	Tumor anatomical location	Anatomical location of enlarged lymph node	Histological diagnosis eRLN	eRLN Uptake	Adjunctive non-palpable/normal sized lymph nodes and histological diagnosis	Pattern
Mixed breed, intact male, 15 years, 9,8 kg	Fibrosarcoma grade II	Left lower lip	Left mandibular	Metastatic	Total uptake	-	1A
			Left mandibular	Metastatic	Total uptake		
Labrador Retriever, intact male, 5 years, 42 kg	Cutaneous MCT Patnaik Grade 2/Kiupel Low Grade	Right lumbar region	Right medium iliac	HN3	Total uptake	-	1A
Labrador Retriever, intact male, 7 years, 48 kg	SCC	Nasal planum	Left mandibular	Non-metastatic (reactive)	Total uptake	-	1A
Schnauzer, intact male, 7 years, 16,4 kg	SCC	Third digit of the right forelimb	Right superficial cervical	Non metastatic (reactive)	Total uptake	-	1A
Whippet, spayed female, 8 years, 3,8 kg	Undifferentiated subcutaneous STS grade III	Third/fourth digit of the left forelimb	Left superficial cervical	Non-metastatic (reactive)	Total uptake	-	1A
Boxer, intact male, 6 years, 33,8 kg	Cutaneous MCT Patnaik Grade 2 Kiupel High Grade	Left shoulder region	Left superficial cervical	HN1 + small cell lymphoma	Incomplete uptake	-	1B
Mixed breed, neutered male, 14 years, 28,7 kg	Rectal plasmacytoma	Rectal mucosae	Right medium iliac	Metastatic	No uptake	-	1C
Mixed breed, spayed female, 12 years, 14 kg	OMM	Right caudal maxilla	Right mandibular	Metastatic	No uptake	-	1C
Cavalier King Charles Spaniel, spayed female, 8 years, 7,3 kg	AGASAC	Right anal sac	Sacral	Metastatic	Total uptake	-	1A
			Sacral	Metastatic	Incomplete uptake		1B
			Right medium iliac	Metastatic	No uptake		1C
Labrador Retriever, intact male, 7 years, 30,5 kg	Cutaneous MCT Patnaik Grade 2 Kiupel Low Grade	Third and fourth digit of the right forelimb	Right superficial cervical	HN2	Total uptake	Right superficial cervical (HN1)	2A
French bouledogue, intact male, 7 years, 13,8 kg	Cutaneous MCT Patnaik Grade 2 Kiupel Low Grade	Left hock	Left popliteal	HN2	Total uptake	Left inguinal (HN2)	2A
Mixed breed, spayed female, 13 years, 34 kg	Subcutaneous MCT	Left caudal thigh	Left inguinal	HN3	Total uptake	Left popliteal (HN2)	2A
			Left inguinal	HN3	Total uptake		
Mixed breed, neutered male, 11 years, 22,6 kg	Subcutaneous MCT	Right upper lip	Right mandibular	HN3	Total uptake	Right mandibular (HN2) Right retropharyngeal (HN2)	2A
French bouledogue, intact male, 9 years, 16 kg	Cutaneous MCT Patnaik Grade 3/Kiupel High Grade	Medial chin	Left mandibular	HN3	Total uptake	Left mandibular (HN2) Left retropharyngeal (HN2)	2A

French bouledogue, intact male, 11 years, 14,5 kg	Cutaneous MCT Patnaik Grade 2 Kiupel Low Grade	Left cheek	Left retropharyngeal	HN0 + T zone lymphoma	Total uptake	Left mandibular (HN0 + T zone lymphoma)	2A
			Right retropharyngeal	HN0 + T zone lymphoma	Total uptake		
Cocker Spaniel, intact male, 14 years, 28,5 kg	OMM	Left upper lip	Left mandibular	Metastatic	Total uptake	Left mandibular (Metastatic) Left mandibular (Metastatic)	2A
French bouledogue, spayed female, 10 years, 11,4 kg	Cutaneous MCT Patnaik Grade 3 Kiupel High Grade	Left hock	Left popliteal	HN2	Total uptake	Left inguinal (HN0)	2A
Jack Russel Terrier, neutered male, 15 years, 8,9 kg	Subcutaneous myxosarcoma Grade II	Right forelimb	Right superficial cervical	Metastatic	Total uptake	Right superficial cervical (Metastatic)	2A
Golden retriever, spayed female,10 years, 27,6 kg	OMM	Right maxilla	Right mandibular	Non-metastatic (reactive)	Total uptake	Right mandibular (Non-metastatic - reactive) Right mandibular (Non-metastatic -reactive) Right retropharyngeal (Non-metastatic - reactive) Left retropharyngeal (Non-metastatic - reactive)	2A
French bouledogue, spayed female, 8 years, 9,9 kg	Cutaneous MCT Patnaik Grade 3 Kiupel High Grade	Left lower eyelid	Left mandibular	HN3	Incomplete uptake	Left retropharyngeal (HN1)	2B*
Mixed breed, neutered male, 12 years, 30,7 kg	Subcutaneous MCT	Right upper lip	Right mandibular	HN0	Incomplete uptake	Right retropharyngeal (HN0) Left mandibular (HN2) Left mandibular (HN2)	2B*
			Right mandibular	HN0	Total uptake		
			Left mandibular	HN1	Total uptake		
Mixed breed, spayed female, 13 years, 11 kg	Cutaneous MCT Patnaik Grade 2 Kiupel High Grade	Right upper lip	Right mandibular	HN3	No uptake	Right retropharyngeal (HN3) Left mandibular (HN2) Left mandibular (HN0) Left retropharyngeal (HN0)	2C*
			Right mandibular	HN3	No uptake		

Legend: MCT= mast cell tumor; SCC=squamous cell carcinoma; STS= soft tissue sarcoma; OMM= oral malignant melanoma; AGASAC= apocrine gland anal sac adenocarcinoma; HN0: non-metastatic according to Weishaar et al 2014; HN1: pre-metastatic; HN2: early nodal metastasis; HN3 overtly metastasis. *Rerouting (according to Goyal et al., 2005; Leijte et al., 2009; Lutzen et al., 2016)

During exploration, 25 SLCs (66%) contained a single SLN while 13 SLCs (34%) contained multiple SLN (from 2 to 3). A total of 54 lymph nodes were removed: 30 (56%) were enlarged and 24 (44%) were non-palpable/normal sized. The eRLN and SLN tracer uptake is reported in Table 1-2. Notably, 5 out of 30 eRLNs (17%) showed no tracer uptake; all were metastatic, resulting in false-negative findings (Table2).

Based on the lymphatic mapping results observed, nodal pattern were categorized as follow (Figure 1-2; Table 2-4):

- Nodal pattern 1: In 9 lymphographies (41%), only the eRLNs (single or multiple) were identified by the tracers, and no adjunctive non-palpable/normal-sized SLNs were detected. In 5 lymphographies, the eRLNs showed total tracer uptake (pattern 1A); in 1, it showed incomplete uptake (pattern 1B); in 2, no uptake was observed (pattern 1C); and in 1 case with multiple eRLNs, tracer uptake varied among the nodes (including total, incomplete, and no uptake).
- Nodal pattern 2: In 13 lymphographies (59%), beyond the enlarged lymph nodes (single or multiple), at least one adjunctive non-palpable/normal-sized SLN was detected. In 10 of them, the eRLN had a total tracer uptake (pattern 2A), while in 3 of them the eRLN tracer uptake was incomplete (pattern 2B) or absent (pattern 2C) and the tracers were rerouted to a neo-SLN

Table 2. Histological nodal status of excised lymph nodes and their tracers' uptake.

Nodal tracer uptake	**Tot**	**Histological status**	
		Metastatic	**Non metastatic**
Enlarged lymph nodes removed:	**30**	**21**	**9**
Total uptake	21	14	7
Incomplete uptake	4	2	2
No uptake	5	5	-
Adjunctive non-palpable/normal sized SLNs removed:	**24**	**13**	**11**
Total uptake	18	12	6
Incomplete uptake	6	1	5

Table 3. The SLC distribution of the 24 adjunctive non-palpable/normal-sized SLNs and their histological status.

	N°/total (%)	Histological status of the lymph nodes	
		Metastatic	Non metastatic
TOT	**24**	**13**	**11**
In the same SLC of the eRLN	6 (25%)	3 (23%)	3 (30%)
In a different SLC of the eRLN	18 (75%)	10 (77%)	8 (70%)

Figure 1. Nodal pattern and distribution of tracer uptake with technetium and/or indocyanine green observed in the study

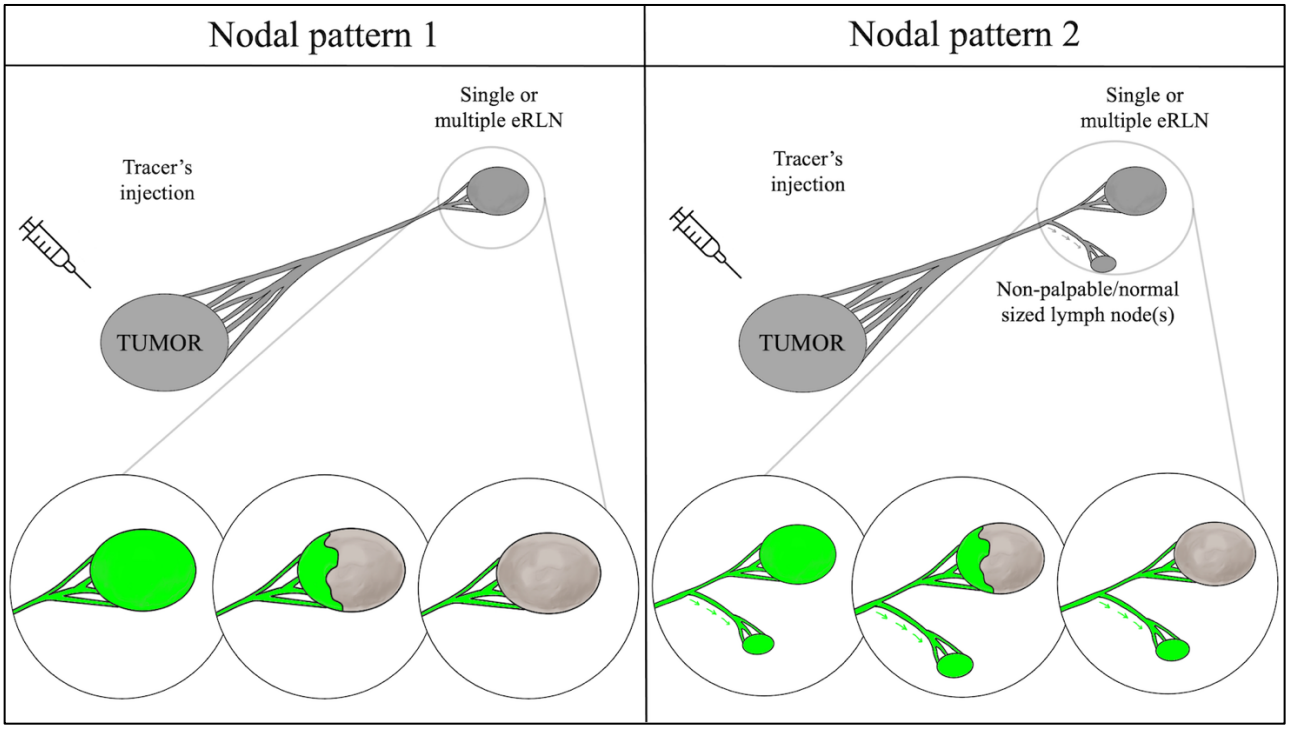

Pattern 1: the lymphography detected only the eRLN(s) from one or multiple lymphocentrum and no adjunctive non-palpable/normal-sized SLNs. The eRLN (single or multiple) presented different tracer uptake (total and/or incomplete and/or absence of tracer uptake). Pattern 2: beside the eRLN(s) the lymphography detected at least one non-palpable/normal-sized SLN in the same or in different SLC from the enlarged one. The eRLN presented one or different tracer uptake (total and/or incomplete and/or absence of tracer uptake).

Figure 2: An example of tracer uptake in lymph nodes with NIRF-ICG

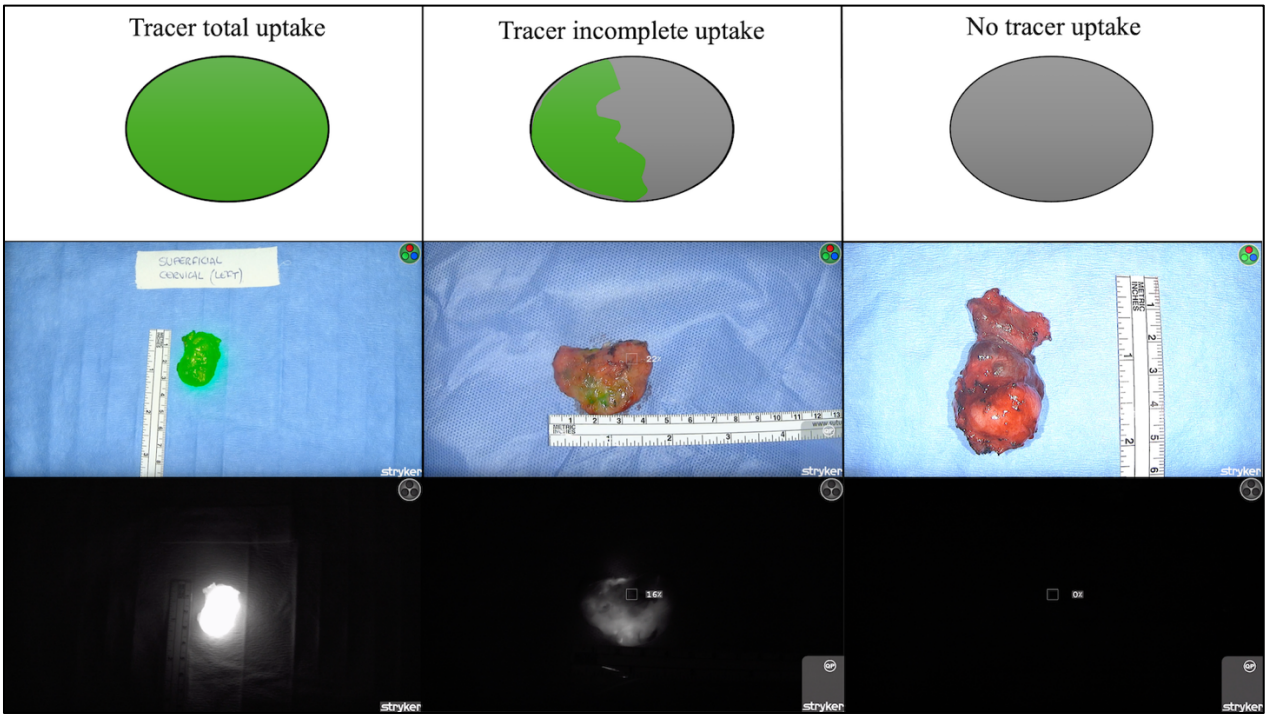

Example of 3 enlarged lymph nodes with different uptake patterns for NIRF-ICG (SPY-PHI overlay and monochromatic visualization mode).

Among the 24 non-palpable/normal-sized extirpated SLNs, 18 (75%) belonged to different adjunctive SLCs, while 6 SLNs (25%) were in the same SLC as the enlarged one (Table 4). Overall median dimension of extirpated SLNs was 20 (4 – 50) mm. The median size was 25 (15 – 50) mm for the eRLNs, and 15 (4 – 40) mm for non-palpable/normal-sized SLNs.

Out of the 54 extirpated lymph nodes, 34 (63%) were metastatic and 20 (37%) were non-metastatic. Among the latter, 4 were incidentally diagnosed at nodal histology as lymphoma (3 T-zone lymphoma and in 1 small-cell lymphoma).

Considering only the 30 eRLN, 21 (70%) were metastatic, and 9 (30%) were not (2 of them were diagnosed with nodal T-zone lymphoma, 1 with small-cell lymphoma and 6 were reported as reactive). Of the 24 non-palpable/normal-sized SLNs, 13 (54%) were metastatic, and 11 (46%) were not (1 was diagnosed as T-zone lymphoma). Among the 13 metastatic non-palpable/normal sized SLNs (10 SLNs metastatic for MCT, 2 for oral malignant melanoma and 1 for STS), 10 (77%) were detected in a different SLC from the one of the eRLN. In the present study population, retrieval of an adjunctive SLN did not change the staging of the dog. Presence or absence of nodal metastasis of enlarged and non-palpable/normal sized SLNs and nodal tracer uptake are summarized in Table 5.

No intra-operative complications were registered at the sites of lymphadenectomy, while post-operative complications were recorded in 10 dogs (45%), and included: seroma (8 dogs), abscess (1

dog), and transient lymphedema (1 dog). All complications were classified as minor and managed with medical therapy, including anti-inflammatory drugs (steroidal and non-steroidal, depending on the case) and antibiotics, as indicated by bacterial culture examination in the case complicated by the abscess.

3.3. Discussion:

The primary finding of the present study is that in 59% of the included dogs, mapping with ICG and/or Technetium-99 identified at least one non-palpable/normal-sized SLN in addition to the eRLN, regardless of whether the latter was metastatic or non-metastatic. Based on histopathological evaluation, 54% of the additional non-palpable/normal-sized SLNs were metastatic. These lymph nodes would not have been removed without mapping, and this indicates that metastatic spread may not be confined to the solely enlarged lymph nodes. (Goyal et al., 2005; Leijte et al., 2009). Even if among the 22 cases included in the study the oncologic stage did not change, these results highlight the relevance of lymph node mapping in assisting microscopic residual nodal metastatic disease identification in non-palpable/normal-sized SLN in dogs with solid malignancies and eRLN. Moreover, 75% of the adjunctive non-palpable/normal-sized SLNs were retrieved in different SLCs than the one of the eRLNs and most of them were metastatic (77%). This data supports the hypothesis that, in presence of malignancies, the lymphatic drainage may be unpredictable, and Technetium-99 and ICG can spread also to multiple SLCs, leading to the identification of more than one SLN linked with the tumor. The occurrence of multiple lymphatic drainage has drawn attention in both human and veterinary oncology, as a potential risk factor for nodal metastasis and as a possible prognostic indicator. (Ferrari et al., 2021; McHugh et al., 2006; Stefanello et al., 2024). Although the majority of non-palpable/normal-sized SLNs were retrieved from an SLC different from the one containing the enlarged lymph node, 25% were found within the same SLC as the enlarged lymph node. These findings should be carefully considered in relation to the intraoperative guidance of lymphoscintigraphy and/or NIRF-ICG that can assess both lymphatic mapping and surgical exploration. While pre-operative mapping might identify one or more SLC, the possibility to surgically identify and follow the same tracer (respectively Technetium-99 and ICG) during SLC exploration enhances the probability of removing multiple SLN with a high detection rate, as previously reported (Chiti et al., 2025; Gariboldi et al., 2023; Stefanello et al., 2024). In addition, intraoperative gamma probe and NIRF camera allowed the measurement of residual radioactivity/fluorescence that led to objective decision making during the dissection of the SLCs, since their absence indicates that there are no more SLN to be removed within the SLC (Chiti et al.,

2025; Gariboldi et al., 2023; Stefanello et al., 2024). This approach may help avoid missing metastatic non-palpable/normal-sized SLNs associated with the tumor, whether located in the same or a different SLC from the eRLN, thereby preventing incomplete staging and underestimation of metastatic disease extent. We can also hypothesize — although this needs to be confirmed in further studies — that the removal of additional non-palpable or normal-sized SLNs may reduce the risk of nodal relapse and/or distant tumor dissemination. In addition, considering that the surgical complications were in line with previous publications (Chiti et al., 2023; Mattioli et al., 2025), the surgeons might be encouraged to search for the SLN. Exploring more SLCs and remove more SLNs should not be considered a hazard when using a tracer that allows for an intraoperative guidance such as Technetium-99 or NIRF-ICG.

Regarding the second aim of the study, we were able to describe different nodal patterns and different qualitative tracers' uptakes in the removed lymph nodes. This confirms that the findings of altered nodal uptake reported in humans could also be observed in dogs with malignancies. Indeed, in several human cancers, like cutaneous melanoma, penile cancer and breast cancer, in presence of enlarged lymph nodes and possible metastatic invasion of lymphatic vessels, the lymphatic flow may result altered (Goyal et al., 2005; Lam et al., 2009; Leijte et al., 2009; Lützen et al., 2016; Nathanson and Mahan, 2011). Neoplastic invasion in the lymph node with related microscopic or macroscopic alteration or normal architecture may be associated with higher intranodal pressure leading to deviation of lymphatic flow ("rerouting") (Goyal et al., 2005; Nathanson and Mahan, 2011). Rerouting was not frequently observed in this sample population (3 cases all MCTs out of 22 lymphographies), and this seems to reflect what is reported in human literature (Bassi et al., 2006; Goyal et al., 2005; Leijte et al., 2009; Proulx et al., 2013). In the cases of rerouting, the enlarged lymph node was metastatic, and the tracer drainage was rerouted to another SLN. This was probably due to the tumor embolization blockage of the lymphatic afferent lymphatic vessels, mimicking the typical rerouting phenomenon defined in human literature. However, rerouting or drainage alteration may occur also in non-neoplastic lymph nodes in association with inflammatory abnormalities of flow and lymphatic dysfunction (Kandeel et al., 2013; Liao and Von Der Weid, 2014; Monaco et al., 2012).

It should be noted that in 10 cases, even if the eRLN exhibited a full tracer uptake, an additional SLN was identified. This could possibly represent simultaneous lymphatic drainage to multiple SLN (e.g., one enlarged and the other normal sized), although a rerouting scenario cannot be excluded. In such instances, increased intranodal pressure caused by metastatic burden may still allow tracer accumulation in the affected lymph node, while also promoting tracer diversion to a secondary, neo-sentinel lymph node (Nathanson and Mahan, 2011).

Regarding the tracer uptake (Technetium-99 and/or ICG) in the lymph nodes, five enlarged lymph nodes lacked uptake although they were all metastatic. To explain the absence of tracer uptake, it might be hypothesized, according to the literature, that when the microscopical architecture of the lymph node is fulfilled by the tumor, the tracer may fail to reach the lymph node, leading to false negatives results (Bassi et al., 2006; Goyal et al., 2005; Leijte et al., 2009; Nathanson and Mahan, 2011). In one study of Goyal et al. (2005) involving lymph nodes with breast cancer metastases, it was observed that radioactive tracer uptake decreased with increasing metastatic involvement. This could suggest that the absence of the tracer uptake in an enlarged lymph node may be related to the presence of metastasis. However, based on our results and the few cases included, we cannot establish a reliable correlation between tracer uptake and the presence or absence of metastasis. Further prospective studies are required to integrate data with quantification of tracers' uptake and association with neoplastic invasion of the lymph nodes.

The main limitation of this study is the small sample size, which nonetheless reflects the frequency of enlarged lymph nodes, that in the present study were observed in 22 out of the 210 dogs during daily clinical practice in the last 3 years at our VTH. This is the first study in canine surgical oncology that explores the influence of SLN mapping in the presence of eRLN, and lymph node tracers' uptake alteration. Therefore, further research involving a larger, more homogeneous population is needed to better understand the relationship between histotype, tumor characteristics, nodal pattern and tracer's uptake. Furthermore, collecting data about follow-up might define the prognostic inference of this neo-sentinel lymph nodes removal in presence of eRLN in different canine malignancies.

In conclusion, the mapping of SLN in presence of eRLN related to solid malignant tumors is strongly suggested and should be preferred over limiting excision to only the enlarged lymph node observed during clinical examination or diagnostic imaging (ultrasonography and /or computed tomography). In addition, the lymphatic mapping with ICG and Technetium-99 enhances the identification of possible neo-sentinel lymph nodes and help to avoid missing potentially residual microscopic neoplastic nodal disease.

3.4. References:

Alvarez-Sanchez, A., Townsend, K.L., Newsom, L., Milovancev, M., Gorman, E., Russell, D.S., 2023. Comparison of indirect computed tomographic lymphography and near-infrared fluorescence sentinel lymph node mapping for integumentary canine mast cell tumors. Veterinary Surgery 52, 416–427. https://doi.org/10.1111/vsu.13929

Annoni, M., Borgonovo, S., Aralla, M., 2023. Sentinel lymph node mapping in canine mast cell tumours using a preoperative radiographic indirect lymphography: Technique description and results in 138 cases. Vet Comp Oncol 21, 469–481. https://doi.org/10.1111/vco.12906

Baginski, H., Davis, G., Bastian, R.P., 2014. The Prognostic Value of Lymph Node Metastasis with Grade 2 MCTs in Dogs: 55 Cases (2001-2010). J Am Anim Hosp Assoc 50, 89–95. https://doi.org/10.5326/JAAHA-MS-5997

Bassi, K.K., Seenu, V., Ballehaninna, U.K., Parshad, R., Chumber, S., Dhar, A., Gupta, S.D., Kumar, R., Srivastava, A., 2006. Second echelon node predicts metastatic involvement of additional axillary nodes following sentinel node biopsy in early breast cancer. Indian J Cancer 43(3), 103–109. https://doi.org/10.4103/0019-509x.27931

Beer, P., Rohrer-Bley, C., Nolff, M.C., 2022. Near-infrared fluorescent image-guided lymph node dissection compared with locoregional lymphadenectomies in dogs with mast cell tumours. J Small Anim Pract 63, 670–678. https://doi.org/10.1111/jsap.13529

Chiti, L.E., Beer, P., Ohlerth, S.M., Hartnack, S., Nolff, M.C., 2025. SHINE – Validation of Near Infrared Fluorescence Lymphography Against Lymphoscintigraphy for Sentinel Lymph Node Biopsy in Dogs With Mast Cell Tumours. Vet Comp Oncol. 23(2):320-329 https://doi.org/10.1111/vco.13058

Chiti, L.E., Gariboldi, E.M., Ferrari, R., Luconi, E., Boracchi, P., De Zani, Donatella, Zani, Davide, Manfredi, M., Spediacci, C., Grieco, V., Giudice, C., Recordati, C., Ferrari, F., Stefanello, D., 2023. Surgical complications following sentinel lymph node biopsy guided by γ-probe and methylene blue in 113 tumour-bearing dogs. Vet Comp Oncol 21, 62–72. https://doi.org/10.1111/vco.12861

Chiti, L.E., Stefanello, D., Manfredi, M., Zani, D.D., De Zani, D., Boracchi, P., Giudice, C., Grieco, V., Di Giancamillo, M., Ferrari, R., 2021. To map or not to map the cN0 neck: Impact of sentinel lymph node biopsy in canine head and neck tumours. Vet Comp Oncol 19, 661–670. https://doi.org/10.1111/vco.12697

Collivignarelli, F., Tamburro, R., Aste, G., Falerno, I., Signore, F. Del, Simeoni, F., Patsikas, M., Gianfelici, J., Terragni, R., Attorri, V., Carluccio, A., Vignoli, M., 2021. Lymphatic drainage mapping with indirect lymphography for canine mammary tumors. Animals 11(4):1115. https://doi.org/10.3390/ani11041115

Ferrari, R., Boracchi, P., Chiti, L.E., Manfredi, M., Giudice, C., De Zani, D., Spediacci, C., Recordati, C., Grieco, V., Gariboldi, E.M., Stefanello, D., 2021. Assessing the risk of nodal metastases in canine integumentary mast cell tumors: Is sentinel lymph node biopsy always necessary? Animals 11(8):2373. https://doi.org/10.3390/ani11082373

Ferrari, R., Chiti, L.E., Manfredi, M., Ravasio, G., De Zani, D., Zani, D.D., Giudice, C., Gambini, M., Stefanello, D., 2020. Biopsy of sentinel lymph nodes after injection of methylene blue and lymphoscintigraphic guidance in 30 dogs with mast cell tumors. Vet Surg 49, 1099–1108. https://doi.org/10.1111/vsu.13483

Ferraris, E.I., Olimpo, M., Giacobino, D., Manassero, L., Iussich, S., Lardone, E., Camerino, M., Buracco, P., Morello, E.M., 2023. Sentinel lymph node mapping with computed tomography lymphography for mast

cell tumours and a comparison between regional and sentinel lymph node histological status: Sixty-two cases. Vet Comp Oncol 21, 208–220. https://doi.org/10.1111/vco.12878

Gariboldi, E.M., Ubiali, A., Chiti, L.E., Ferrari, R., De Zani, D., Zani, D.D., Grieco, V., Giudice, C., Recordati, C., Stefanello, D., Auletta, L., 2023. Evaluation of Surgical Aid of Methylene Blue in Addition to Intraoperative Gamma Probe for Sentinel Lymph Node Extirpation in 116 Canine Mast Cell Tumors (2017–2022). Animals 13(11):1854. https://doi.org/10.3390/ani13111854

Goyal, A., Douglas-Jones, A.G., Newcombe, R.G., Mansel, R.E., 2005. Effect of lymphatic tumor burden on sentinel lymph node biopsy in breast cancer. Breast J 11, 188–194. https://doi.org/10.1111/j.1075-122X.2005.21591.x

Grimes, J.A., Secrest, S.A., Northrup, N.C., Saba, C.F., Schmiedt, C.W., 2017. Indirect computed tomography lymphangiography with aqueous contrast for evaluation of sentinel lymph nodes in dogs with tumors of the head. Vet Radiol and Ultrasound 58, 559–564. https://doi.org/10.1111/vru.12514

Kandeel, A.A.S., Younes, J., Zaher, A.M., 2013. Significance of popliteal lymph nodes visualization during radionuclide lymphoscintigraphy for lower limb lymphedema. Indian J Nucl Med 28, 134–137. https://doi.org/10.4103/0972-3919.119540

Lam, T.K., Uren, R.F., Scolyer, R.A., Quinn, M.J., Shannon, K.F., Thompson, J.F., 2009. False-negative sentinel node biopsy because of obstruction of lymphatics by metastatic melanoma: The value of ultrasound in conjunction with preoperative lymphoscintigraphy. Melanoma Res 19, 94–99. https://doi.org/10.1097/CMR.0b013e32832166b7

LeBlanc, A.K., Atherton, M., Bentley, R.T., Boudreau, C.E., Burton, J.H., Curran, K.M., Dow, S., Giuffrida, M.A., Kellihan, H.B., Mason, N.J., Oblak, M., Selmic, L.E., Selting, K.A., Singh, A., Tjostheim, S., Vail, D.M., Weishaar, K.M., Berger, E.P., Rossmeisl, J.H., Mazcko, C., 2021. Veterinary Cooperative Oncology Group—Common Terminology Criteria for Adverse Events (VCOG-CTCAE v2) following investigational therapy in dogs and cats. Vet Comp Oncol 19, 311–352. https://doi.org/10.1111/vco.12677

Leijte, J.A.P., Van Derploeg, I.M.C., Valdés Olmos, R.A., Meweg, O.E., Horenblas, S., 2009. Visualization of tumor blockage and rerouting of lymphatic drainage in penile cancer patients by use of SPECT/CT. J Nucl Med 50, 364–367. https://doi.org/10.2967/jnumed.108.059733

Liao, S., Von Der Weid, P.Y., 2014. Inflammation-induced lymphangiogenesis and lymphatic dysfunction. Angiogenesis. https://doi.org/10.1007/s10456-014-9416-7

Liptak, J.M., Boston, S.E., 2019. Nonselective Lymph Node Dissection and Sentinel Lymph Node Mapping and Biopsy. Vet Clin North Am Small Anim Pract. https://doi.org/10.1016/j.cvsm.2019.04.003

Lützen, U., Zuhayra, M., Marx, M., Zhao, Y., Colberg, C., Knüpfer, S., Baumann, R., Kähler, K.C., Jünemann, K.P., Naumann, C.M., 2016. Value and efficiency of sentinel lymph node diagnostics in patients with penile carcinoma with palpable inguinal lymph nodes as a new multimodal, minimally invasive approach. Eur J Nucl Med Mol Imaging 43, 2313–2323. https://doi.org/10.1007/s00259-016-3482-6

Manfredi, M., De Zani, D., Chiti, L.E., Ferrari, R., Stefanello, D., Giudice, C., Pettinato, V., Longo, M., Di Giancamillo, M., Zani, D.D., 2021. Preoperative planar lymphoscintigraphy allows for sentinel lymph node detection in 51 dogs improving staging accuracy: Feasibility and pitfalls. Vet Radiol and Ultrasound 62, 602–609. https://doi.org/10.1111/vru.12995

Mattioli, G., Cino, M., Stefanello, D., Drudi, D., Morello, E.M., Pisani, G., Chiti, L.E., Pierini, A., Gariboldi, E.M., De Zani, D., Massari, F., Giacobino, D., Martano, M., 2025. Peripheral sentinel lymphadenectomy in 163 dogs: Postoperative surgical complications and comparison between intraoperative dissection techniques. Vet Surg 54, 766–776. https://doi.org/10.1111/vsu.14246

McHugh, J.B., Su, L., Griffith, K.A., Schwartz, J.L., Wong, S.L., Cimmino, V., Chang, A.E., Johnson, T.M., Sabel, M.S., 2006. Significance of multiple lymphatic basin drainage in truncal melanoma patients undergoing sentinel lymph node biopsy. Ann Surg Oncol 13, 1216–1223. https://doi.org/10.1245/s10434-006-9014-z

Monaco, S.E., Khalbuss, W.E., Pantanowitz, L., 2012. Benign non-infectious causes of lymphadenopathy: A review of cytomorphology and differential diagnosis. Diagn Cytopathol 40(10):925-938 https://doi.org/10.1002/dc.21767

Nathanson, S.D., Mahan, M., 2011. Sentinel lymph node pressure in breast cancer. Ann Surg Oncol 18, 3791–3796. https://doi.org/10.1245/s10434-011-1796-y

Proulx, S.T., Luciani, P., Christiansen, A., Karaman, S., Blum, K.S., Rinderknecht, M., Leroux, J.C., Detmar, M., 2013. Use of a PEG-conjugated bright near-infrared dye for functional imaging of rerouting of tumor lymphatic drainage after sentinel lymph node metastasis. Biomaterials 34, 5128–5137. https://doi.org/10.1016/j.biomaterials.2013.03.034

Stefanello, D., Gariboldi, E.M., Boracchi, P., Ferrari, R., Ubiali, A., De Zani, D., Zani, D.D., Grieco, V., Giudice, C., Recordati, C., Caniatti, M., Auletta, L., Chiti, L.E., 2024. Weishaar's classification system for nodal metastasis in sentinel lymph nodes: Clinical outcome in 94 dogs with mast cell tumor. J Vet Intern Med 38, 1675–1685. https://doi.org/10.1111/jvim.16997

Suami, H., Yamashita, S., Soto-Miranda, M.A., Chang, D.W., 2013. Lymphatic Territories (Lymphosomes) in a Canine: An Animal Model for Investigation of Postoperative Lymphatic Alterations. PLoS One 8(7):e69222. https://doi.org/10.1371/journal.pone.0069222

Wan, J., Oblak, M.L., Ram, A., Singh, A., Nykamp, S., 2021. Determining agreement between preoperative computed tomography lymphography and indocyanine green near infrared fluorescence intraoperative imaging for sentinel lymph node mapping in dogs with oral tumours. Vet Comp Oncol 19, 295–303. https://doi.org/10.1111/vco.12675

4. Real-time quantification during fluorescent-guided surgery with indocyanine green: a pilot study in canine soft tissue sarcomas and mast cell tumors

- The present study was submitted at Scientific Reports (September 11th, 2025) and under review at the time to submission of the present thesis
- PhD student role: first author and corresponding author

Elisa Maria Gariboldi[1], Alessandra Ubiali[1], Ester Luconi[2], Roberta Ferrari[1], Patrizia Boracchi[3], Paola Roccabianca[1], Silvia Dell'Aere[1], Chiara Giudice[1], Camilla Recordati[1], Valeria Grieco[1], Luigi Auletta[1], Francesco Ferrari[1], Federica Alessandra Brioschi[1] and Damiano Stefanello[1]

1: Department of Veterinary Medicine and Animal Sciences, University of Milan, Lodi, Italy
2: Department of Clinical Sciences and Community Health, University of Milan, Milan, Italy.
3: Department of Biomedical and Clinical Sciences, University of Milan, Milan, Italy

Achieving histologically tumor-free surgical margins is essential for the successful treatment of solid malignant tumors [1–3]. Despite improvements in the planning of surgery for canine soft tissue sarcoma (STS) and mast cell tumors (MCT) over the last decade [4,5] and updates in decision-making regarding radical versus wide versus marginal excision based on tumor size and location [2,3,6–10], accurately identifying tumor boundaries during surgery remains challenging. The need for the development of tools that assist surgeons during tumor excision and enhance surgical precision through real-time intraoperative assessment of the distinction between neoplastic and non-neoplastic tissue represents a new frontier in canine surgical oncology [4,11,12].

In human surgical oncology, tumor fluorescence-guided surgery (TFGS) using near-infrared fluorescence (NIRF) has emerged as a valuable intraoperative technique to differentiate neoplastic from non-neoplastic tissue and optimize resection [13–16]. Indocyanine green (ICG) is a non-target fluorophore that, after a defined interval from intravenous injection, shows passive accumulation in neoplastic tissue (allowing the so-called "second window" ICG) [17,18]. This phenomenon is attributed to the enhanced permeability and retention (EPR) effect, which results from aberrant tumor vascularization [17]. Taking advantage of EPR, promising results have been reported by the application

of NIRF-ICG in the surgical treatment of human soft tissue sarcomas and other solid tumors, with improved complete excision and reduced local recurrence rates [13,14,19].

Recently, research in small animal surgery has started exploring NIRF-ICG in different areas such as sentinel lymph node mapping, reconstructive surgery, and tissue perfusion assessment [20–23]. However, despite the rising interest in NIRF-ICG, its use for TFGS is still not well established in small animals' clinical practice and data on its application remain limited to translational medicine research [24–26], with some studies that have applied targeted fluorophores [11,27–30] or free-ICG [24,25] for TFGS in canine STS and MCT. Given the paucity of research on TFGS, combined with the predominance of translational medicine studies on canine tumors, there is to date a significant heterogeneity of published data on ICG dosage (ranging from 0.5 to 7.5 mg/kg) and administration timing (ranging from 1 to 24 hours before surgery). Furthermore, fluorescence quantification, most expressed as tumor-to-background ratio (TBR) or signal-to-background ratio (SBR), shows considerable variability both in the devices used and in the cut-off values reported across veterinary and human literature. Reported TBR or SBR thresholds for distinguishing healthy from neoplastic tissue range from 1.2 to 3 [13,14,19,24,25,31,32].

Hence, we designed a pilot study using a free-ICG dose of 0.5 mg/kg, an administration timing of 24 hours before surgery, and a TBR and SBR with a cut-off of 2 to address the following three objectives:

- To evaluate the real-time intraoperative feasibility of TFGS with NIRF-ICG in spontaneous canine STS and MCT;
- To compare the real-time quantification of the wound bed fluorescence after excision with the histopathological margins status of the excised tumor;
- To explore real-time fluorescence quantification guidance during tumor resection and intraoperative decision-making.

4.1. Material and methods:

Study population:

This observational pilot study was approved by the Institutional Ethical Committee for Animal Care of the University of Milan (OPBA 02-2025). This study enrolled client-owned dogs referred to the Veterinary Teaching Hospital of the University of Milan from February to August 2025 bearing spontaneous MCT (cutaneous and subcutaneous) and subcutaneous STS at first presentation or recurrence. Owners signed a written informed consent for ICG administration, surgical procedures, and data collection. All procedures were carried out in accordance with the Italian National legislation for animal welfare (DL 14th March 2014 n.26) and the best standards of veterinary clinical practice,

as defined by the Good Veterinary Practice guidelines of the Federation of Veterinarians of Europe and the Italian National Federation of Veterinary Orders (FNOVI, 29th January 2005) and in accordance with ARRIVE guidelines.

Dogs were included in the TFGS with NIRF-ICG if presenting with a macroscopical tumor mass, with a preoperative cytological or histological diagnosis of STS or MCT, eligible for curative intent surgery. Dogs presenting with simultaneous multiple tumors were included, as long as the tumors were located in distinct anatomical regions and on opposite sides of the body, thereby not involving the same surgical field. Exclusion criteria were: the presence of distant metastases and/or scars from previous tumor excision with residual microscopic disease. Tumors in which margin assessment with TFGS was deemed clinically irrelevant (i.e., limb or tail amputation for distally located tumors, where resection had to be performed at a considerable distance from the lesion) were also excluded.

Complete blood count with differential and serum biochemistry were always performed to assess general anesthesia risk and eligibility for the intravenous ICG administration protocol. Dogs with American Society Anesthesiologist physical status superior than 3 were excluded to avoid potential side effects associated with ICG administration [33].

ICG administration and surgical planning:

The solution of ICG (Verdye, DiagnosticGreen GmbH, Aschheim, Germany) was prepared with 10 ml of sterile water for injection, obtaining a concentration of 2.5 mg/ml. A dose of 0.5 mg/kg of ICG was administered intravenously 24 hours before the planned surgery. Occurrence of any adverse events during and after ICG intravenous administration were recorded and categorized in accordance with LeBlanc and coll. [34]. In all cases, sentinel lymph node mapping was performed prior to tumor excision using lymphoscintigraphy; peritumoral injections of methylene blue were avoided in sentinel lymph node mapping to prevent interference of the dye with tumor margin assessment.

Surgical dose adopted was classified as: radical (excision of an entire anatomical compartment); wide excision (2-3 cm lateral for STS and MCT >2 cm or proportional lateral margins for MCT < 2 cm only, and at least 1 involved fascial layers for deep margins including bone structures) [7,8]; planned narrow excision (if wide excision was not possible; the widest margins were applied based on tumor dimension and localization) [6,9,10,35,36]. On the day of surgery, wide clipping of the surgical area was performed, and the surgical field was prepared with sterile chlorhexidine-based scrubbing. Before NIRF-ICG application, the surgeons outlined the planned lateral skin excision with a sterile skin marker, considering the surgical dose, palpation findings of deeper tissue involvement, and, if available, pre-surgical computed tomography imaging, as usually performed. Electrocautery was deliberately avoided during tissue resection to prevent thermal artifact formation and deposition of

charred tissue remnants, which might compromise the accuracy of fluorescence imaging and subsequent analysis of the surgical bed [37]. All surgical procedures were performed by the same surgeon (DS) with several years of experience in clinical research of canine STS and MCT and in the use of NIRF technology. Occurrence of intra-operative or post-operative complications were recorded and classified according to Le Blanc and coll. [34].

NIRF technical information:

The NIRF device used was SPY-PHI QP% system (Stryker; MIDA, Tecnologia Medica S.p.a.) with a Portable Handheld Imager (SPY-PHI). The SPY-PHI has a dedicated sterile plastic drape to be intraoperatively handheld by the surgeons.

In addition to the white light visualization mode, the SPY-PHI QP% system (Stryker) allows three visualization modalities for fluorescence, defined as overlay mode, color maps mode, and contrast mode (Figure 1). These modalities can be freely selected and switched interchangeably during surgery, directly from the probe. The quantification of the fluorescence intensity of the regions of interest (ROI) in real-time is allowed by the QP% software (Stryker).

For this study, immediately before skin incision, the handheld camera was positioned 10–40 cm above the tissue of interest, and surgical lights were turned off when using the SPY-PHI device. At the beginning of each evaluation, the white balance was done, then the QP% software was calibrated using the tumor tissue as the reference baseline. All subsequent fluorescence measurements were quantified in relation to the baseline signal, ensuring case-by-case consistent and tumor-centered assessment throughout the procedure (Figure 2).

Using the QP% software, the fluorescence intensity of the tumor, each region of interest (ROI), and the background were recorded in real time. The ‘background’ was defined before excision as grossly normal-appearing tissue adjacent to the tumor, while the ‘signal’ was defined as the fluorescence intensity of a specific ROI. The tumor-to-background ratio (TBR) was calculated as the ratio of the tumor fluorescence intensity to that of the background and used to assess the feasibility of the procedure (see below). The signal-to-background ratio (SBR) was calculated as the ratio of the signal from a ROI to the background. The SBR was used for the decision-making of the dissection of skin and fascial plane, and to assess residual fluorescence in the wound bed. A TBR and SBR cut-off value of 2 was arbitrarily chosen, as it is, to the authors’ knowledge, the most frequently reported quantification threshold in both human and veterinary literature for distinguishing neoplastic from normal tissue. [19,26,31] (Figure 2).

Figure 1. Visualization modalities available for the SPY-PHI QP% system (Stryker)

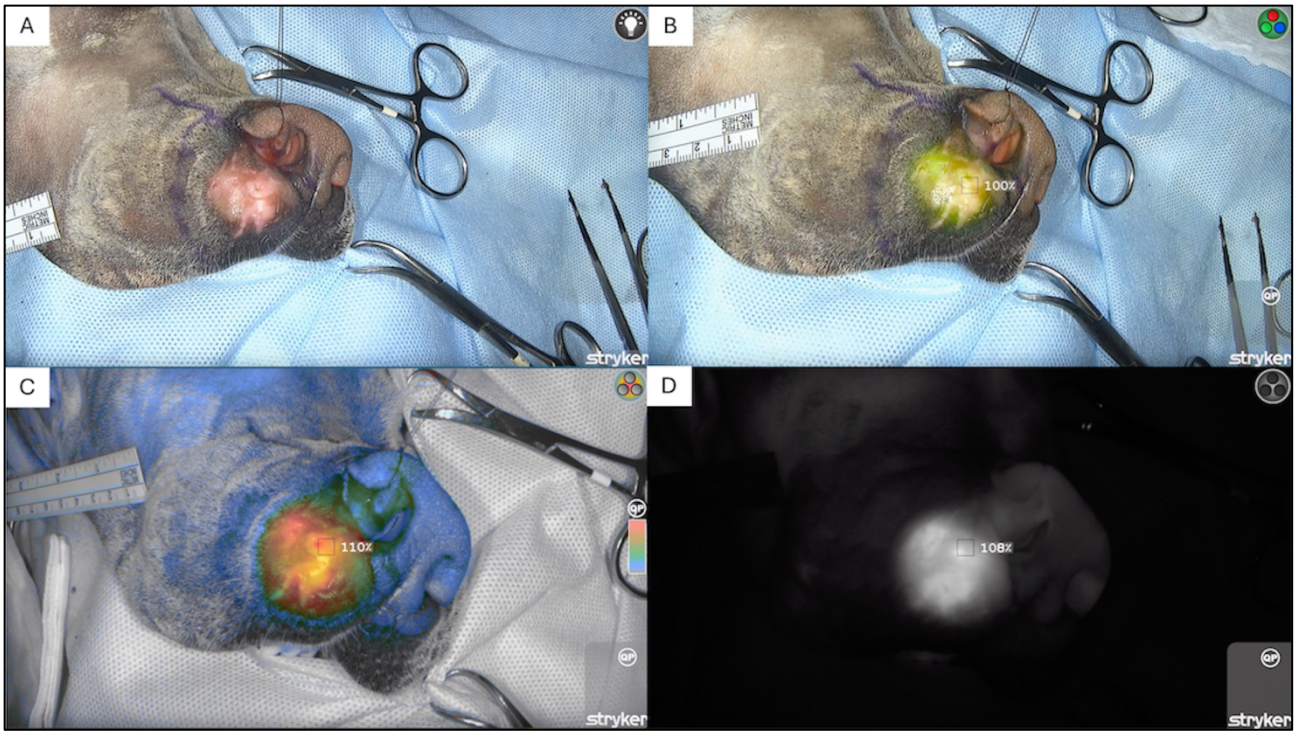

A. The white light visualization - SPY-PHI QP% system is used as a normal camera; B. the overlay mode – the fluorescence is represented with the overlaying green color. Increasing intensity of green color reflects increasing recorded fluorescence from the probe; C the color map mode – intensity of fluorescence is reported on a chromatic scale ranging from red (maximum fluorescence intensity) to blue (minimum fluorescence intensity). Grey color indicates absence of fluorescence.; D the contrast mode – intensity of fluorescence is represented on a monochromatic scale, higher fluorescence intensity is white, while the lower is black. All reported fluorescence intensities vary based on the set baseline.

Figure 2. Tumor-to-background ratio (TBR) and signal-to-background ratio (SBR) assessment in the two phases of TFGS.

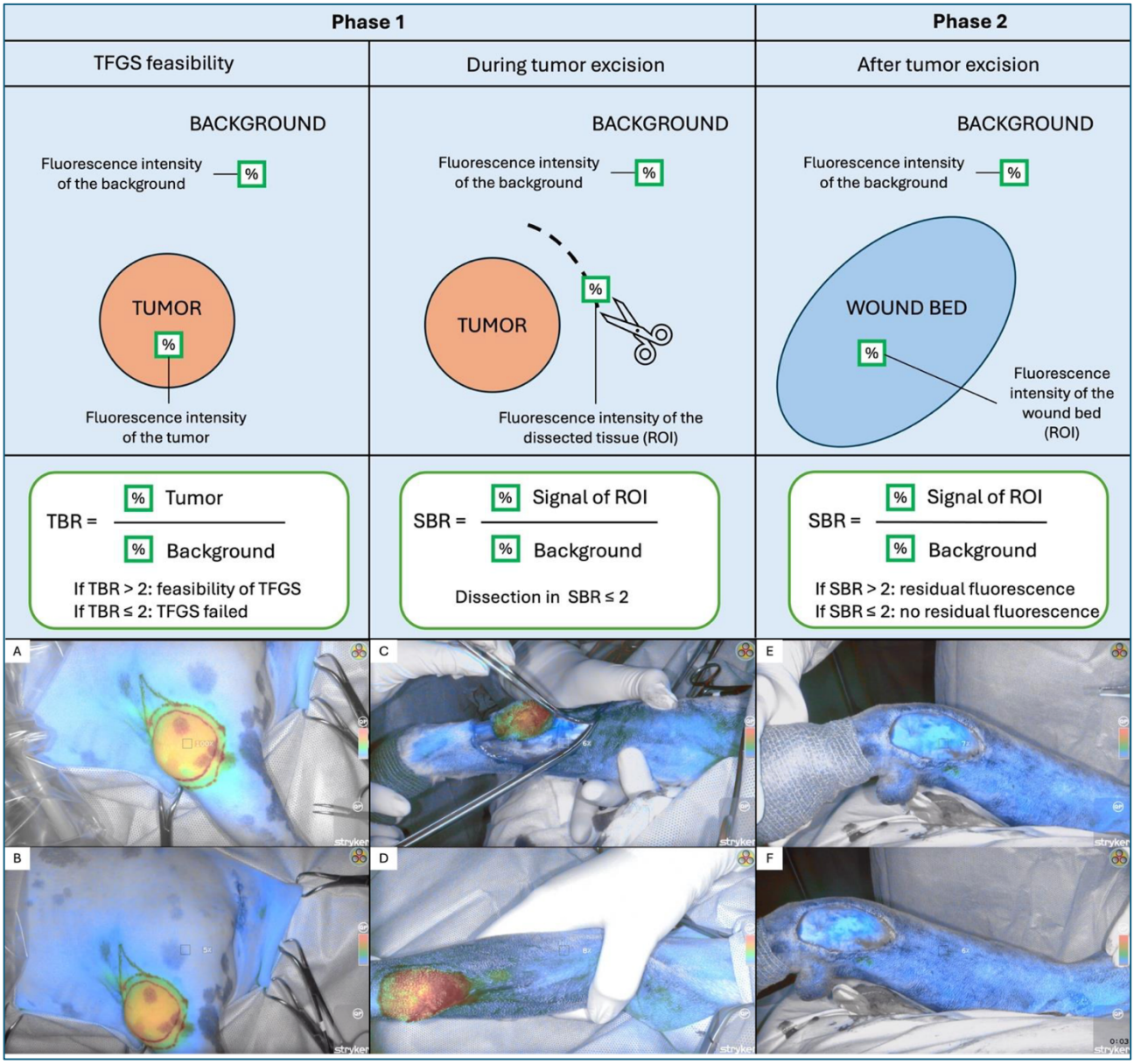

In this picture is reported the schematic representation of the real time calculation of TBR and SBR during the two phases of TFGS. All the clinical pictures reported are in color map modality.

A-B: The QP system is used to assess the TBR for the TFGS feasibility. A: The QP system is set on the tumor (100%); B: the relative background quantification is assessed (5%). The TBR is calculated as the ratio between the tumor and the background fluorescence quantification. In this particular case, TBR value resulted >2 (100%/5%= 20) therefore the technique was defined as successful.

C-D: the QP system is used to assess the SBR of the tissue to be dissected (ROI). During the excision the fluorescence intensity of the ROI (the site of dissection) (C) and the background (normal tissue) (D) is real-time assessed and the SBR calculated in order to perform the dissection in the SBR ≤ 2. In this particular case the is calculated as 6%/8%= 0.75)

E-F: the QP system is used to assess the SBR of the wound bed after the tumor removal. The wound bed fluorescence intensity (representing the ROI in this case) (E) and the background (F) are real time assessed and the SBR calculated. In this case the SBR is ≤ 2 (SBR = 7%/6%= 1,16) and the wound bed has no residual fluorescence.

TFGS procedure:

The TFGS procedure consisted of the following two phases:

Phase 1: Tumor surgical resection.

The tumor fluorescence was real-time quantitatively checked with the SPY-PHI. Using the QP% software, in order to assess the feasibility of the technique, the TBR was calculated. If the TBR was >2 (the tumor was considered distinguishable from the surrounding tissue and TFGS feasible). If TBR was ≤ 2, the TFGS was considered as failed, the surgery was performed as planned traditionally [38], and, therefore, the case was excluded from the following TFGS procedures. The SBR was used throughout the entire excision phase to guide the surgeons in tumor removal, thanks to the real-time quantification system, which was always intraoperatively available. Dissection around the tumor was performed, whenever possible, in tissues with SBR ≤ 2, as they displayed low fluorescence intensity and most likely non-neoplastic tissue. During all the excision phase, the real-time quantification system for TBR and SBR calculation was always available to guide the surgeons.

Furthermore, it was recorded whether TFGS led to the removal of small additional amounts of tissue in the lateral skin and/or subcutaneous fascia (≥ 0.5 cm) and/or deeper tissues (additional fascial plane), with respect to the area originally planned.

Phase 2: Wound bed fluorescence assessment before wound reconstruction

After the tumor removal, maintaining the original setting for QP% (100% on tumor fluorescence), the fluorescence quantification of the wound bed was checked with the SPY-PHI. Using the QP% software the SBR was calculated: the signal of the wound bed was compared to the background and an SBR > 2 was interpreted as residual fluorescence in the wound bed; an SBR ≤ 2 was interpreted as absence of residual fluorescence in the wound bed [24] (Figure 3). When residual fluorescence was present, it was classified as diffuse (if extensively diffuse on the tumor bed) or single spot (if only a single spot of fluorescence was visible). Wound bed residual fluorescence (spot or diffuse) was removed (adjunctive resection and /or incisional biopsy), if feasible and without increasing the risk of morbidity. All adjunctive tissues removed were individually submitted for histopathological evaluation.

The surgical aid of TFGS was evaluated by asking the surgeon whether NIRF imaging assisted intraoperative decision-making, leading to an increase in the planned resection (phases 1–2) [13]
After phases 1–2, the surgical procedure continued with wound reconstruction.

Figure 3. Examples of wound bed analysis for residual fluorescence.

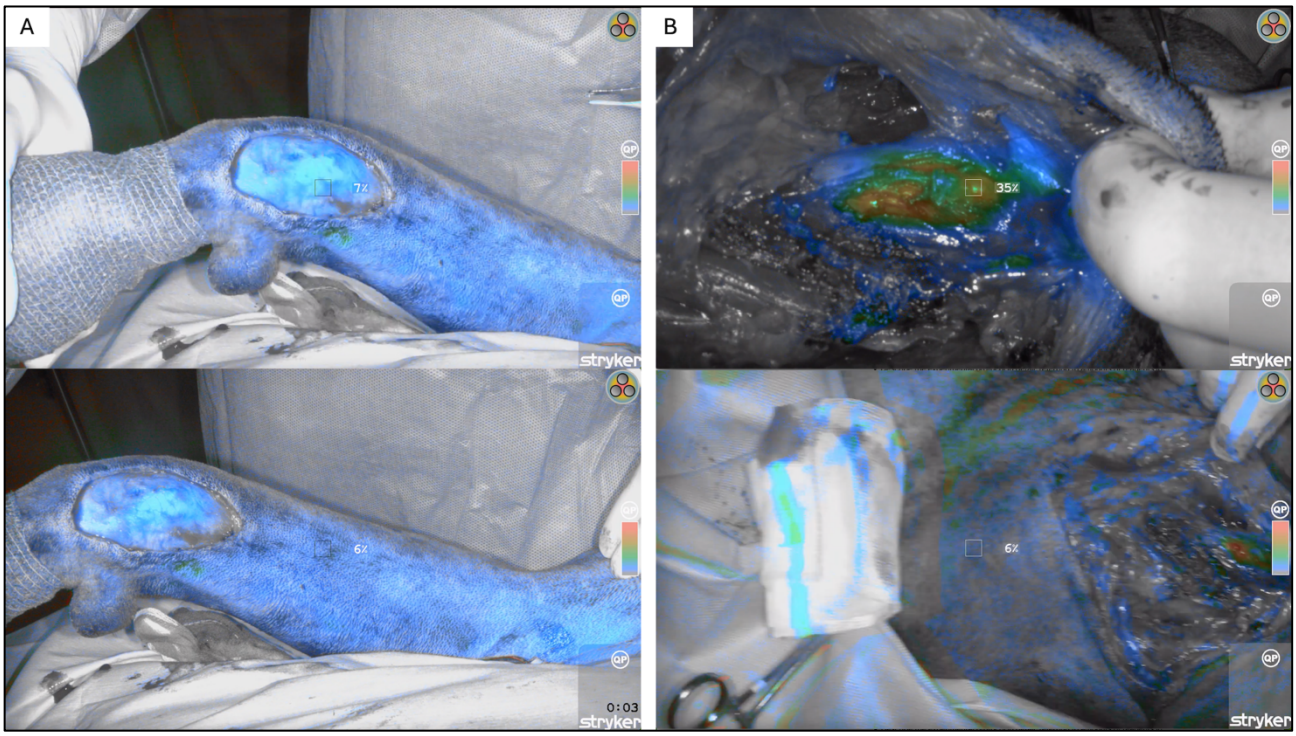

A: the wound bed has no residual fluorescence (SBR ≤ 2); B: the wound bed is positive for residual fluorescence (SBR > 2).

Histopathological analysis:

All specimens were promptly oriented by the surgeon post-excision and submitted for histopathological evaluation. For soft tissue sarcomas (STS), tumor grade was assessed [39,40]. For mast cell tumors (MCT), cutaneous forms were graded using both the Patnaik and Kiupel systems [41–43], while subcutaneous MCTs were classified according to Thompson et al. (2011) [44]. A complete longitudinal section was examined, and the status of surgical margins was assessed using 3-dimensional technique [45,46]. Histological margins were categorized as infiltrated and non-infiltrated.

Data collection and statistical analysis:

Recorded data about dogs signalment were the following: breed, sex, age, body weight, body condition score (BCS) on a five scale (classified in underweight if 1-2/5; normal weight if 3/5; overweight if 4-5/5). The clinical variables of tumors included: presentation (first or recurrence),

anatomical location (categorized as limbs - below the elbow/stifle, excluding digits; trunk - upper the elbow/stifle, included thoracic mammary glands; head and neck; inguinal - perineal, genitals, and inguinal mammary glands; digits; and tail), dimension (in millimeters), presence of tumor ulceration, pigmentation of the overlying skin, clinical skin mobility overlying the tumor and if tumor was fixed or not fixed to deeper fascia. Surgical data included: surgical dose (radical, wide excision or planned marginal excision); tumor surgical timing (calculated in minutes from skin incision to last skin suture); occurrence of intra or post-operative complication and grade [34].

Tumor's histopathological variables collected were: histotype, grade (when applicable), status of margins (infiltrated vs non-infiltrated).

Based on the TFGS, the following data were collected: occurrence of adverse events after ICG intravenous administration; the TBR of the tumor; the feasibility of the technique (defined as TBR > 2); whether the fluorescence confirmed or increased the resection (either during excision ≥0,5 cm of one or more lateral margins and/or deeper fascial plane, or via additional resection adjunctive fluorescent tissue in the wound bed); the SBR of the wound bed post-excision to confirm presence/absence of residual fluorescence.

The distribution of retrieved variables was synthesized by a descriptive statistic: for categorical variables, the frequency of each modality is reported as the % of the total cases, for continuous variables, was expressed as median (first quartile; third quartile) since the distribution were asymmetrical. The cumulative distributions of TBR for STS and MCT were compared using the exact two-sample Kolmogorov-Smirnov test. The null hypothesis of this test is that the two groups were sampled from the same population distribution. The same test was also used to compare the SBR of STS and MCT. Exact distributions for the two-sample (Smirnov) test are computed by the algorithm proposed by Schröer and Trenkler (1995)[47].

The performance of the TFGS to identify the status of the margins, was evaluated considering the histopathological marginal status of the reference standard (gold standard). The performance measures for each tumor category (STS and MCT) were sensitivity, specificity, positive and negative likelihood ratios (LR^+, LR^-) with their 95% confidence interval. For sensitivity and specificity, the confidence intervals were calculated according to Wilson [48]. This approach is recommended in cases of small sample size ($n < 40$) due to its superior coverage probability, especially when the proportion values (such as sensitivity or specificity) are not extremely close to 0 or 1 [49].

The LR^+ is the ratio between the presence of residual fluorescence given infiltrated histopathological margins and the probability of residual fluorescence given the non-infiltrated histopathological

margins. The higher the LR^+ value, the more effective fluorescence is in identifying positive margins. The LR^- is the ratio between the probability of an absence of residual fluorescence given the positive histopathological margins and the probability of the absence of residual fluorescence given the negative histopathological margins. The lower the LR^- value, the more effective fluorescence is in ruling out infiltrated margins. The strength of the effectiveness of fluorescence in identifying the histopathological status of the margins can be quantified according to the criteria suggested by Ebell [50]: $LR^+ \geq 10$ relevant (and often conclusive) result regarding the presence of infiltrated margins; $5 \leq LR^+ < 10 \rightarrow$ moderate indication of the presence of infiltrated margins; $2 \leq LR^+ < 5 \rightarrow$ weak indication of the presence of infiltrated margins. $LR^- \leq 0.1$ relevant (and often conclusive) result regarding the non-infiltrated margins $0.1 < LR^- \leq 0.2$ moderate indication of the non- infiltrated margins $0.2 < LR^- \leq 0.5$ weak indication of the non- infiltrated margins. For the likelihood ratios, confidence intervals were based on the formulae provided by Simel at al. [51]. All those computations were performed using the epi.tests function from the R package epiR, version 2.0.76 [52]. Based on reported infiltrated margins prevalence ranges for STS (16–69.5%) [1,9,10,53–55] and MCT (15–56%) [1,10,44,56–59] the positive predictive value (PPV) and negative predictive value (NPV) were calculated under three scenarios: using the point estimates of sensitivity and specificity, using the lower limits of their 95% CIs (representing a worst-case scenario), and using the upper limits of the CIs (best-case scenario). This was done to explore the impact of diagnostic accuracy variation across different prevalence levels. The confidence intervals for the predictive values were calculated according to Wilson.

Lastly, the diagnostic performance of residual fluorescence at the wound bed (SBR) without considering the cut-off value was evaluated using receiver operating characteristic (ROC) curve analysis. Given the small sample size, a non-parametric method based on smoothed empirical distribution functions was employed, as recommended by Jokiel-Rokita and Pulit (2013) [60]. To identify the best cut-off, the Youden index was considered. The Area under the ROC evaluated the discriminant ability of fluorescence.

All procedures performed during the TFGS with NIRF-ICG and combination with histologic results are summarized in Figure 4. All the analysis were performed with R software version 4.4.0. [61]

Figure 4. Decision making process during TFGS.

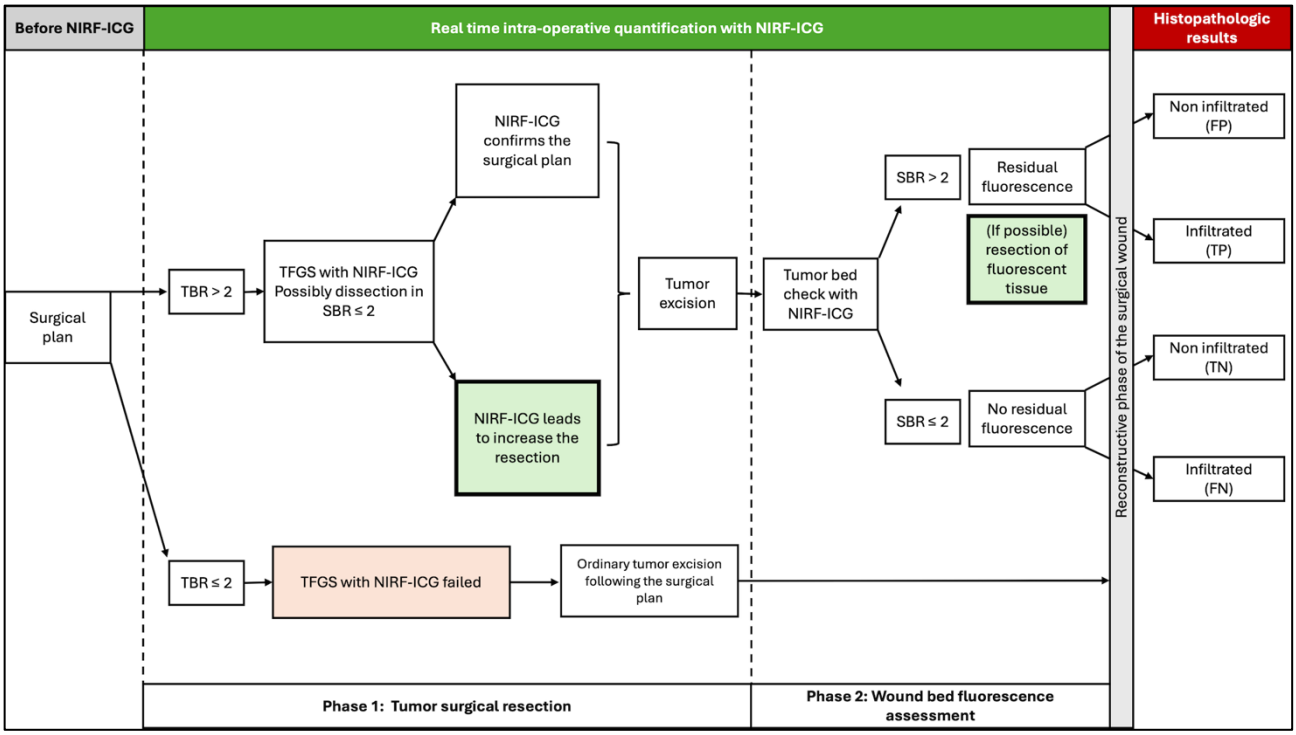

TBR= tumor to background ratio, SBR= signal to background ratio, NIRF-ICG=near infrared fluorescence with indocyanine green, FP=false positive, TP=true positive, TN=true negative, FN=false negative

4.2. Results:

Study population:

Among 30 animals evaluated for surgical purposes during the study period, 4 were excluded: 3 dogs had microscopic disease in the scar and 1 had local recurrence and distant metastasis. Twenty-six dogs met the inclusion criteria and were enrolled for the study. The most represented breed was the mixed breed (n=8; 31%) followed by Labrador Retriever (n=5; 19%) and Belgian Malinois (n=2; 8%). The remaining 11 (42%) dogs each belonged to a different breed. Thirteen dogs (50%) were spayed female, 7 (27%) intact males, 3 (11%) intact females and 3 (12%) neutered males. Median age was 8.4 years (range 2.5 – 14.2 years. IQR: 11 - 6.3). The median bodyweight was 23 kilograms (IQR 31 – 10 kg) and 14 dogs (54%) were normal weight, while 12 (46%) were overweight.

Twenty-four dogs presented single tumors while 2 dogs presented simultaneous multiple tumors (1 dog had simultaneously 1 STS and 1 MCT, and 1 dog had 2 simultaneous MCTs). A total of 28 tumors were included (14 MCTs and 14 STSs). Recorded clinical variables of the tumors are reported in Table 1.

Table1. **Tumors clinical variables**

Variables	STS (n = 14)		MCT (n = 14)	
	N°	%	N°	%
Presentation				
First presentation	11	79%	12	86%
Recurrence	3	21%	2	14%
Anatomical location				
Limb	9	64%	5	36%
Head and Neck	2	14%	3	21%
Inguinal/Perineal	0	0%	2	14%
Trunk	2	14%	4	29%
Digit	1	7%	0	0%
Ulceration				
No	10	71%	13	93%
Yes	4	29%	1	7%
Clinical skin mobility overlying the tumor				
No	6	43%	7	50%
Yes	8	57%	7	50%
Tumor clinically fixed to deeper fascia				
No	10	71%	13	93%
Yes	4	29%	1	7%
Skin pigmentation				
No	10	71%	13	93%
Yes	4	29%	1	7%
Tumor size (mm)				
Median	30		20	
IQ25%	20		12	
IQ75%	49		28	

NOTES: STS=Soft Tissue Sarcomas, MCT=Mast Cell Tumors

The performed surgical dose was wide excision in 19/28 (68%) tumors (10 STSs and 9 MCTs) and a planned narrow excision in 9/28 (32%) tumors (4 STS and 5 MCT). The median surgical time for STSs and MCTs excision was respectively 50 (IQR 94 – 40) minutes and 40 (IQR 30 – 55) minutes. Post-operative surgical complications emerged in 7/28 (25%) surgical sites of which 5 mild complications-Grade 1 (seroma and hematoma) and 2 moderate-Grade 2 (dehiscence) complications that required a surgical revision.

TFGS and surgical procedures:

No dogs showed adverse events during and after intravenous ICG administration.

Phase 1: tumor surgical resection

The technique resulted feasible in 14/14 (100%) STSs and in 11/14 (79%) MCTs. In 3/14 (21%) MCTs the TBR registered was < 2, making the fluorescence of the tumor undistinguishable from the background, therefore the technique was considered as failed. The 3 failed MCTs were excluded from the following analysis.

The median TBR of STS and MCT was 13 (IQR 26 – 9.4) and 5.8 (IQR 19 – 3.6) respectively. No statistical difference was present comparing populations of the 2 tumors in TBR values (p = 0.09).

During resection, the surgeon reported that the TFGS influenced the surgical procedure by increasing the planned resection of adjunctive tissue in 6/14 (43%) STSs and 4/11 (36%) MCTs. In all cases, the increased lateral margins recorded (minimum of 0.5 cm to a maximum of 0.8 cm) did not change the planned surgical dose category. The adjunctive lateral tissue resection involved only one of the margins in all cases. No increase of deeper margins was recorded in Phase 1.

Phase 2: Wound bed fluorescence assessment before surgical defect reconstruction:

The median SBR of STS and MCT was 1.1 (IQR 3.6 – 0.74) and 2 (IQR 5.4 – 1.3), respectively. No statistical difference was observed among the 2 tumor populations in SBR values (p = 0.3686). After tumor removal, 12 wound beds (6 STS and 6 MCT) had residual fluorescence. The qualitative and quantitative analysis of the fluorescence in the wound bed with NIRF-ICG after STS and MCT removal is reported in Table 2. Residual single-spot fluorescence was present in 9/12 wound bed (6 STSs and 3 MCTs): the surgeon performed adjunctive tissue resection in 8/9 wound bed (6/6 STSs and in 2/3 MCTs). This procedure on wound bed did not change the planned surgical dose category. In the remaining MCT case (carpal region), further resection was not feasible due to the proximity to functional neurovascular structures. Diffuse residual fluorescence was observed in 3/12 wound beds, but no biopsies or further resections were performed, due to the proximity to functional neurovascular structures.

The influence of the TFGS with NIRF-ICG on the intraoperative decision-making in Phase 1 and 2 is reported in Table 3. Overall, in 64% of STS and in 55% of MCT an increase of resection compared to the planned one was performed during the TFGS (Table 3).

Table 2. Wound bed qualitative and quantitative analysis with NIRF-ICG in STS and MCT population

Variables	**STS (n = 14)**		**MCT (n = 11)**	
Residual fluorescence				
No	8	57%	5	45%
Yes	6	43%	6	55%
Residual fluorescence distribution*				
Diffuse	0	0%	3	50%
Single spot	6	100%	3	50%

SBR on the wound bed		
Median	1.1	2
IQ25%	0.74	1.3
IQ75%	3.6	5.4

NOTES: STS=Soft Tissue Sarcomas, MCT=Mast Cell Tumors; SBR=Signal to Background ratio; SD= Standard Deviation, IQ Interquartile. * calculated in case of residual fluorescence

Table 3. Influence of the TFGS with NIRF-ICG on the surgery in STS and MCT population.

Variables	**STS (n = 14)**		**MCT (n = 11)**	
Phase 1: increase resection during excision				
No	8	57%	7	64%
Yes	6	43%	4	36%
Phase 2: increased wound bed tissue resection				
No	8	57%	9	82%
Yes	6	43%	2	18%
Overall increased tissue resection (Phase 1 + Phase 2)				
No	5	36%	5	45%
Yes	9	64%	6	55%

NOTES: STS=Soft Tissue Sarcomas, MCT=Mast Cell Tumors

Histopathological results:

Detailed histopathology analyses of the 14 MCT and 14 STS are reported in Table 4. Overall, 10/28 tumors had infiltrated margins (5 STSs and 5 MCTs). Among the 3 failed MCT cases were all subcutaneous MCT (2 combined pattern and 1 infiltrating pattern) and one of them had infiltrated margins.

Table 4. Histopathological characteristics of STS and MCT populations.

Tumor	**Histological characteristics**	**N°**	**%**
STS (n = 14)	**Histotype**		
	Undifferentiated		
	Grade III	2	14%
	Perivascular wall tumor		
	Grade I	5	36%
	Grade II	2	14%
	Grade III	2	14%
	Fibrosarcoma		
	Grade II	3	22%
	Status of margins:		

	Clean Infiltrated	9 5	64% 36%
MCT (n = 14)	**Cutaneous (n = 7)** Cutaneous MCT Patnaik II / Kiupel low **Status of margins**: Clean Infiltrated	7 5 2	100% 71% 29%
	Subcutaneous (n = 7) Infiltrative pattern Combined pattern **Status of margins**: Clean Infiltrated	4 3 4 3	57% 43% 57% 43%

NOTES: STS=Soft Tissue Sarcomas, MCT=Mast Cell Tumors

Based on the presence of residual fluorescence and the results of histopathological margins status of resected tumors, the sensitivity and specificity of NIRF-ICG in STS excision were respectively 80% and 78% and in MCT were respectively 60% and 50%. Table 5-6-7.

Table 5. Histological results and residual fluorescence in the wound bed.

Tumor		**Infiltrated margins**	**Clean margins**	**Total**
STS	**Residual fluorescence**	4 (True positive)	2 (False positive)	6
	No residual fluorescence	1 (False negative)	7 (True negative)	8
	Total	5	9	**14**
MCT	**Residual fluorescence**	3 (True positive)	3 (False positive)	6
	No residual fluorescence	2 (False negative)	3 (True negative)	8
	Total	5	6	**11**

Table 6. Diagnostic performance indicators of NIRF-ICG in the wound bed analysis for STS and MCT with 95% Wilson Confidence Intervals

Indicator	**STS**		**MCT**	
	Result	**95% Confidence Interval**	**Result**	**95% Confidence Interval**
Sensitivity	0.80	(0.38, 0.96)	0.60	(0.23, 0.88)
Specificity	0.78	(0.45, 0.94)	0.50	(0.19, 0.81)
Positive Predictive Value (PPV)	0.67	(0.30, 0.90)	0.50	(0.19, 0.81)
Negative Predictive Value (NPV)	0.88	(0.53, 0.98)	0.60	(0.23, 0.88)
Positive likelihood ratio (LR+)	3.60	(0.98, 13.19)	1.20	(0.41, 3.51)
Negative likelihood ratio (LR–)	0.26	(0.04, 1.54)	0.80	(0.21, 3.05)

Table 7. Wound bed fluorescence and histological status of margins in Phase 2

Tumor type	Pattern of residual fluorescence	Number of adjunctive resected tissue	Histological status of adjunctive resected tissue	Histological status of margins of resected tumor
STS	Single spot	2	Neoplastic	Infiltrated
STS	Single spot	1	Non-neoplastic	Non-infiltrated
STS	Single spot	3	Neoplastic	Infiltrated
STS	Single spot	3	Non-neoplastic	Non-infiltrated
STS	Single spot	2	Neoplastic	Infiltrated
STS	Single spot	3	Neoplastic	Infiltrated
MCT	Single spot	1	Non-neoplastic	Non-infiltrated
MCT	Single spot	1	Non-neoplastic	Infiltrated
MCT	Single spot	0	Not performed	Infiltrated
MCT	Diffuse	0	Not performed	Infiltrated
MCT	Diffuse	0	Not performed	Non-infiltrated
MCT	Diffuse	0	Not performed	Non-infiltrated

Considering the 8 wound beds in which adjunctive fluorescent tissue was resected (6 STS and 2 MCT), their histopathological evaluation found neoplastic tissue only in 4 STS all of which had also infiltrated margins in the excised tumor. (Table 7).

The LR^+ of the STS showed that the probability of having a fluorescent wound bed for infiltrative margins was 3.60 times the probability to have the same result for non-infiltrated margins; for MCT the LR^+ value was only 1.20, suggesting a best performance for STS.

The LR^- of the STS showed that the probability of non-fluorescent tumor bed for non-infiltrated margins was 3.85 times the probability to have the same result for infiltrate margins; for MCT the LR^- value was only 1.25, suggesting a best performance for STS.

Nevertheless, on the basis of the classification criteria reported in the method section, these results indicated that using only the fluorescence gave only a weak indication about the "real" status of margins, but the 95% confidence interval is wide for the LR^+ (0.98, 13.19) and LR^- (0.04, 1.54); considering the superior value of the confidence intervals there is an indication of a possible excellent performance of the test ($LR^+>10$ and $LR^-<0.1$) in STS. For MCT, the 95% confidence interval may suggest a good test performance (LR^+: 0.41, 3.51; LR^- 0.21, 3.05).

The trend of PPV for STS and MCT in function of the prevalence for different scenario of STS and MCT shows that for a higher value of sensibility and specificity the positive predictive value was higher for all the values of prevalence. The highest PPV for the same combination of sensibility and specificity is for a higher prevalence (Figure 5).

The trend of NPV for STS and MCT in function of the prevalence for different scenario of STS and MCT shows that for a higher value of sensibility and specificity the NPV was higher for all the values of prevalence. The highest NPV for the same combination of sensibility and specificity is for the lower prevalence (Figure 6).

The best cut-off according to Youden index for the STS was 0.548 (Sensibility=0.78 and Specificity=0.77, LR^{+}=3.39, LR^{-}=0.29). The area under the ROC curve for STS was 0.809. Therefore, the SBR in the wound bed has a good discriminative ability for the histological margin for this type of tumor. The area under the ROC curve for MCT was 0.506. Therefore, the SBR in the wound bed has a very poor discriminative ability for the histological status of margin for this type of tumor. Given the extremely poor discrimination, the best cut off was not considered (Figure 5-7).

Figure 5. **Positive Predictive Value in function to prevalence of infiltrated margins in STS and MCT**.

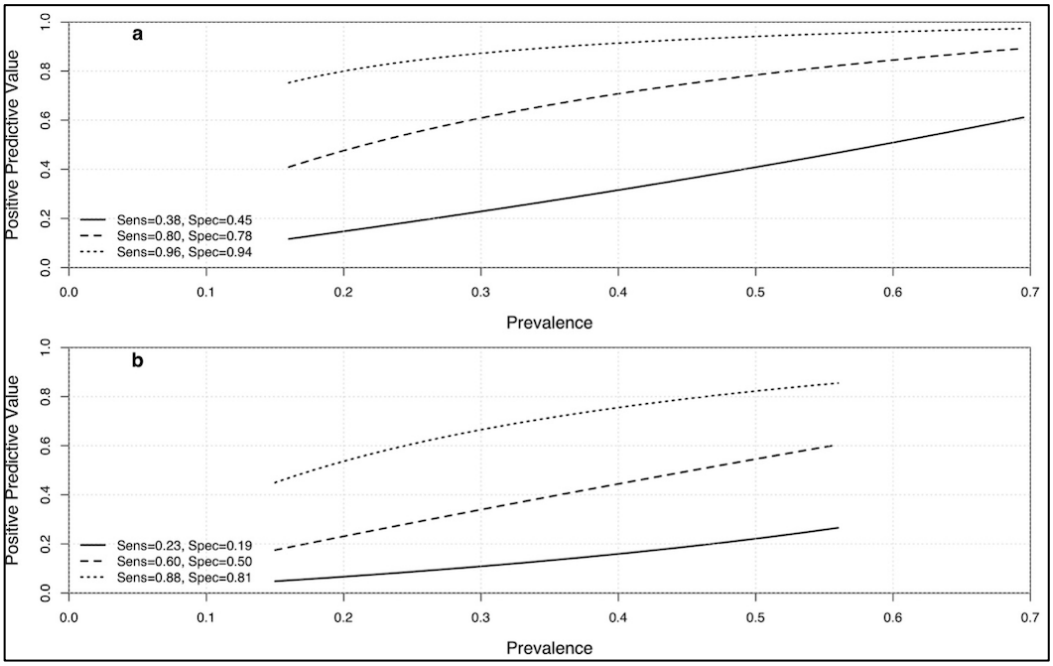

Panel ‘’a’’ shows the results for STS and panel ‘’b’’ shows the results for MCT. Sens=Sensitivity. Spec=specificity.

Figure 6. **Negative Predictive Value in function to prevalence of infiltrated margins in STS and MCT**.

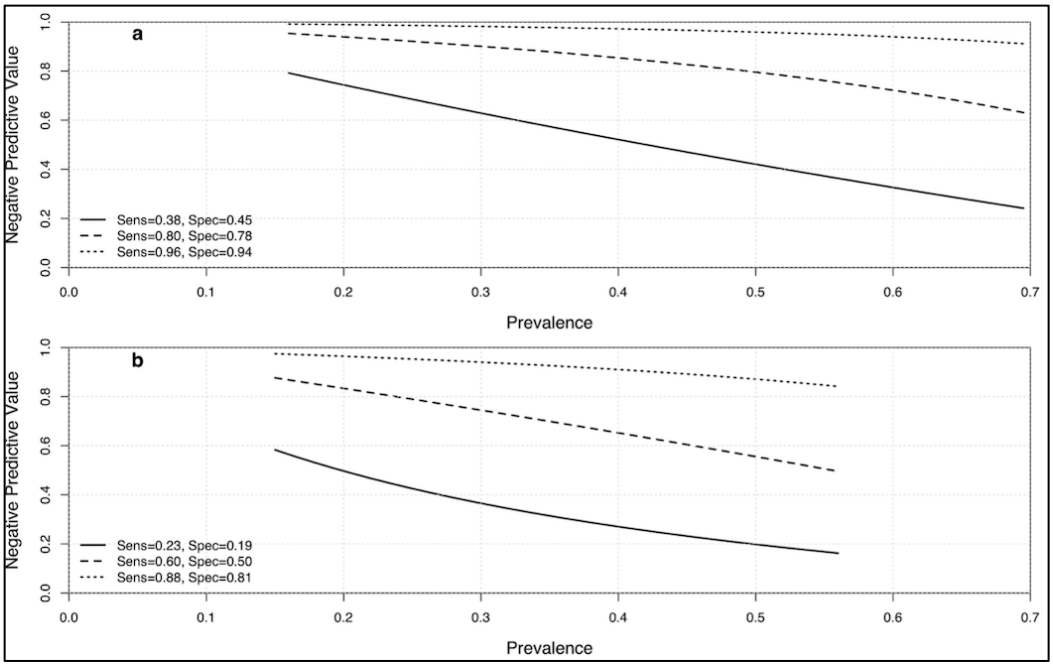

Panel ‘’a’’ shows the results for STS and panel ‘’b’’ shows the results for MCT. Sens=Sensitivity. Spec=specificity.

Figure 7. **ROC curve for infiltration margin identification by fluorescence in the wound bed in STS and MCT**.

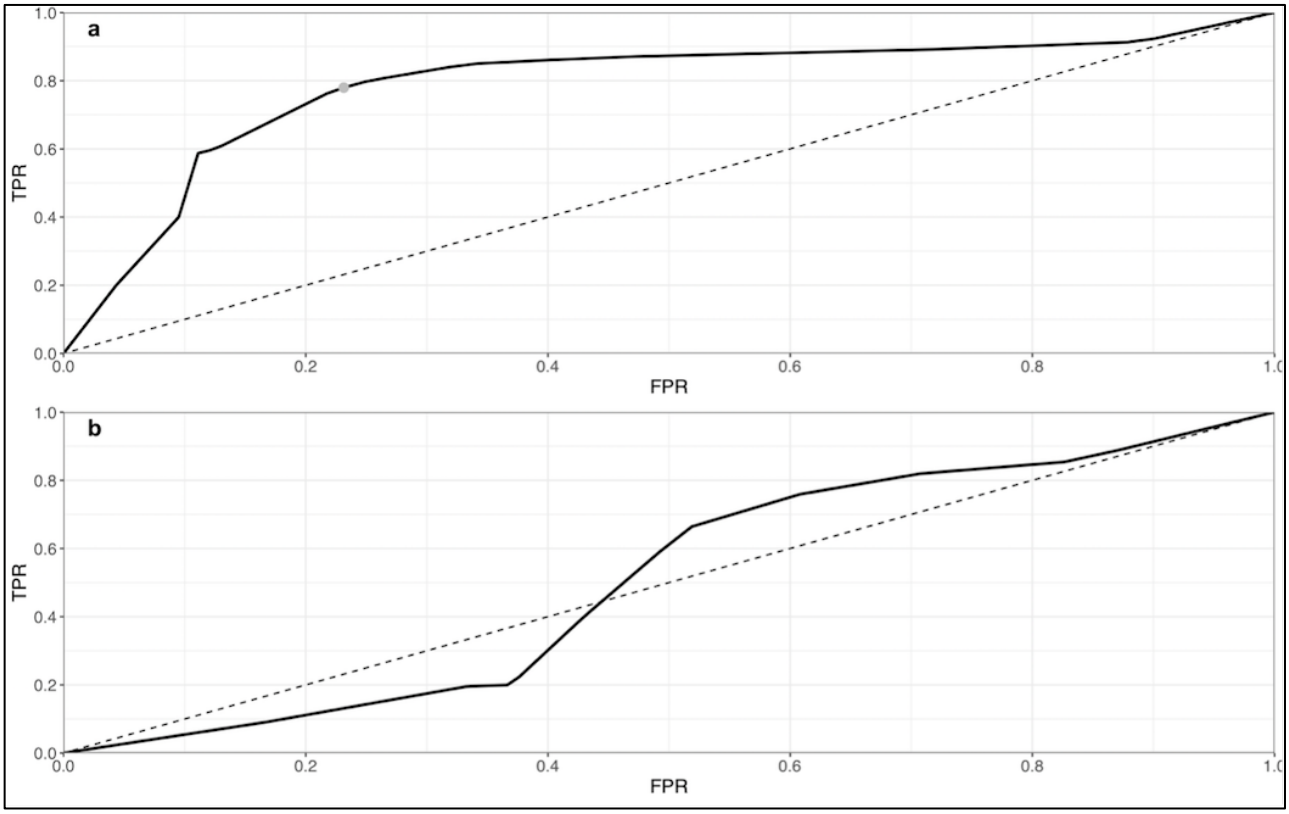

Panel ‘’a’’: STS. Panel ‘’b’’: MCT. TPR=True Positive Rate. FPR=False Positive Rate. The gray point in panel a identify the position of the Youden index.

4.3. Discussion:

Considering the growing interest and application of NIRF-ICG in small animal surgical oncology [20–23], this study aimed to investigate the clinical use of free-ICG in canine surgical oncology, particularly for STS and MCT, to increase the likelihood of complete tumor removal [2,3]. Targeted fluorophores are not currently in use in veterinary medicine clinical setting and few studies have investigated the use of free-ICG for TFGS [18,24,25] ; however, early research differ from our work as they employed higher doses of ICG and focused either on a single tumor histotype or on multiple histotypes with limited sample sizes [24–26]. None of these studies explored the performance of the technique across different spontaneous cancers. Given the recent advancements in commercially available NIRF technologies, updated information on standardized TFGS using free-ICG are warranted. The findings of this pilot study indicate that the use of free-ICG, combined with intraoperative real-time quantification of fluorescence at the applied dose and timing and TBR or SBR cut-off chosen, provide a substantial support to the surgeon during STS and MCT removal. Nonetheless, differences observed between these histotypes highlight the need for further assessments and more detailed discussion.

Regarding feasibility, the results of this study demonstrate that using a dose of 0.5 mg/kg of ICG administered intravenously 24 hours before surgery makes TFGS practicable for both STS and MCT. Feasibility was high for both histotypes, with 100% for STS and 79% for MCT. From the revision of literature, the ICG dose (0.5–7.5 mg/kg), timing of administration (1–24 hours preoperatively), TBR and SBR cut off (1.2-3) and fluorescence quantification devices, showed significant heterogeneity in both dog and human [13,14,18,19,24,25,62,63]. This variability poses a major challenge for standardizing and reproducing TFGS protocols. In small animal surgical oncology, the limited available data further complicates the establishment of consensus on optimal ICG parameters [64]. Previous studies in dogs have employed higher ICG doses (3–7.5 mg/kg) [24–26,62,65], whereas our study adopted a lower dose (0.5 mg/kg) that has been already validated in humans [19], possibly reducing dose per kilogram administered and consequently the costs related to the use of this fluorophore in daily clinical practice. The 24-hour timing from administration to surgery is frequently reported in both human and canine literature [13,14,25,65]; however, the optimal window should be defined based on tumor histotype in future studies. Despite the overall good feasibility, the technique's performance differed between the two tumor types: the TFGS proved consistently successful in all included STS cases, whereas a 21% (3/14) failure rate was observed in MCTs. It cannot be excluded that these neoplasms may require different administration protocols. Indeed, while the selected dose and timing proved consistently optimal for STS, MCTs may benefit from different parameters to allow the TGFS in all tumors. Moreover, the recorded TBR was higher in the STSs group compared to MCTs, although no

statistically significant difference was observed between the two distributions, possibly due to the limited sample size. This suggests that STSs are more easily distinguishable from surrounding tissues than MCTs at this dosage, timing and TBR, possibly due to differences in tumor biology affecting the EPR effect [66]. Increased vascular permeability in tumors allows ICG to extravasate and accumulate in the tumor microenvironment. However, in cases with marked peritumoral inflammation, common in MCTs due to mast cells degranulation and histamine release, ICG may accumulate extensively in peritumoral tissues thus, extending beyond the gross tumor margin and limiting the effectiveness of non-targeted NIRF agents like ICG [65].

The difference between STS and MCT were also observed in the assessment of wound bed residual fluorescence (SBR in Phase 2) and related to the histopathological status of margins. In the STS population, the technique demonstrated good precision in distinguishing among infiltrated and non-infiltrated margins. In detail, NIRF-ICG in STS cases showed good sensitivity and specificity, at 80% and 78%, respectively, whereas in MCTs had lower sensitivity and specificity values (60% and 50%, respectively) (Table 6; Figure 1-3). Nevertheless, the estimated performance of the test evaluating by LR values, was based on a very limited case series and should be revaluated to obtain a higher precision of the estimate. These findings suggest that, in MCTs, the ability of NIRF-ICG to accurately differentiate between infiltrated and non-infiltrated margins seems to be limited. This may be due to the same reason related to biological behavior of MCT that affected the results of TBR [65]. Moreover, ROC curve analysis further confirmed this discrepancy among tumor types. In STSs, the AUC value of 0.80 indicates good discriminative ability, meaning that infiltrated margins generally exhibited higher SBR values than non-infiltrated ones and that makes the NIRF-ICG a reliable intraoperative tool in STS cases. On the other hand, the AUC for MCTs was close to 0.50, indicating that the technique performed no better than chance in detecting residual neoplastic tissue in the wound bed. (Figure 3)

An adjunctive tissue resection based on intraoperative fluorescence signals detected before wound bed reconstruction, was performed in a total of 6 STS and 2 MCT cases (Table 3, Table 7). Histological analysis confirmed the presence of cancer in the fluorescent adjunctive tissue removed in 4 STS and all of these cases had infiltrated margins of the respective tumor removed. Because to date the result of histological status of the margins is not available immediately after tumor excision, the use of real time intraoperative quantitative assessment of fluorescence may help the surgeons to remove adjunctive neoplastic tissue otherwise not identifiable without this technology, contributing to reduce the burden of microscopic disease [13,15,63].

Among the objectives of this pilot study, we also explored the influence of TFGS with NIRF-ICG in intraoperative decision-making. The results showed that in 64% of STS and 55% of MCT an increased

tissue resection was performed in real-time based on the detection of intensity of fluorescence during excision of the tumors (Phase 1) and evaluation of the wound bed (Phase 2) (Table 5). These findings, together with the histopathological results and the higher sensitivity and specificity, suggest that TFGS may have greater clinical utility in STS compared to MCT at this dosage, timing and TBR. The good performance of TFGS in STS confirms what has been reported in the literature on human sarcomas, where the use of NIRF-ICG appears to be a useful technique to support surgical decision-making and improve the ability of obtaining non infiltrated margins in soft tissue and bone sarcoma surgery [13–15,19].

The influence of TFGS with NIRF-ICG on intraoperative decision-making should also be considered in light of the technology adopted in this study, which operates without the need for additional personnel beyond the surgical team and does not require external software or separate devices, as all functionalities are fully integrated into the intraoperative system. This integration enabled a quantitative evaluation of fluorescence intensity, through the calculation of TBR in Phase 1 and SBR in Phase 2, thus ensuring more accurate real-time intraoperative decision-making by the surgeons. Nevertheless, our results indicate that the TBR and SBR value seems to be appropriate and consistent with previously published results, in particular for STS [19,31]. The Youden index identified a cut-off value of 0.54 as the best balance between sensitivity and specificity (Figure 3). However, this threshold did not appear to offer superior diagnostic performance compared to the clinically established cut-off of 2. Given the small sample size, these findings should be interpreted with caution. Further studies involving larger cohorts are needed to validate the optimal diagnostic threshold and support its clinical applicability.

Despite the relatively small sample size, the number of cases included is comparable to that reported in previous studies in dogs [11,24–27]. This limitation inherently constrains the generalizability of our findings and underscores the need for confirmation in larger caseloads. Such studies should also explore potential differences in fluorescence performance across STS subtypes or grades, as well as between cutaneous and subcutaneous MCTs, and better quantify the extent of the increased margins. Furthermore, to improve standardization of dose, timing, and TBR for each histotype, dedicated pharmacokinetic studies of ICG are also warranted.

In conclusion, this study confirms the clinical applicability of TFGS using NIRF with free-ICG for the excision of canine STS and MCT. However, the technique demonstrated superior performance in STS, likely due to biological differences influencing ICG accumulation. In this context, the integration of intraoperative real-time quantification of NIRF-ICG into surgical decision-making may

represent an important first step toward future investigations aimed at optimizing free-ICG use for TFGS in canine surgical oncology and enhancing its use in daily clinical practice.

4.4. References:

1. Milovancev, M., Tuohy, J. L., Townsend, K. L. & Irvin, V. L. Influence of surgical margin completeness on risk of local tumour recurrence in canine cutaneous and subcutaneous soft tissue sarcoma: A systematic review and meta-analysis. *Vet Comp Oncol* **17**, 354–364 https://doi.org/10.1111/vco.12479 (2019).
2. Bray, J., Eward, W. & Breen, M. Evaluating the relevance of surgical margins. Part one: The problems with current methodology. *Vet Comp Oncol* vol. 21 1–11 Preprint at https://doi.org/10.1111/vco.12865 (2023).
3. Bellamy, E. & Berlato, D. Canine cutaneous and subcutaneous mast cell tumours: a narrative review. *JSAP* vol. 63 497–511 Preprint at https://doi.org/10.1111/jsap.13444 (2022).
4. Dornbusch, J. A. *et al.* The feasibility and utility of optical coherence tomography directed histopathology for surgical margin assessment of canine mast cell tumours. *Vet Comp Oncol* **19**, 616–623 https://doi.org/10.1111/vco.12654 (2021).
5. Lages, M. & Selmic, L. E. Exploring optical coherence tomography imaging depth to differentiate tissues at surgical margins. *Vet Comp Oncol* **19**, 763–769 https://doi.org/10.1111/vco.12745 (2021).
6. Stefanello, D. *et al.* Marginal excision of low-grade spindle cell sarcoma of canine extremities: 35 Dogs (1996-2006). *Vet Sug* vol. 37 461–465 Preprint at https://doi.org/10.1111/j.1532-950X.2008.00408.x (2008).
7. Fulcher, R. P. *et al.* Evaluation of a Two-Centimeter Lateral Surgical Margin for Excision of Grade I and Grade II Cutaneous Mast Cell Tumors in Dogs MCT Mast Cell Tumor. *JAVMA* vol. 228(2), 210–215. https://doi.org/10.2460/javma.228.2.210 (2006).
8. Saunders, H., Thomson, M. J., O'Connell, K., Bridges, J. P. & Chau, L. Evaluation of a modified proportional margin approach for complete surgical excision of canine cutaneous mast cell tumours and its association with clinical outcome. *Vet Comp Oncol* **19**, 604–615 https://doi.org/10.1111/vco.12630 (2021).
9. Del Magno, S. *et al.* Evaluation of the neoplastic infiltration of the skin overlying canine subcutaneous soft tissue sarcomas: An explorative study. *Vet Comp Oncol* **19**, 304–310 https://doi.org/10.1111/vco.12676 (2021).

10. Haine, D. L., Pittaway, R., Berlato, D. & Demetriou, J. Incomplete histological margins following planned narrow excision of canine appendicular soft tissue sarcomas and mast cell tumors, using the residual tumor classification scheme. *Vet Surg* **51**, 1078–1086 https://doi.org/10.1111/vsu.13852 (2022).
11. Bartholf DeWitt, S. *et al.* A Novel Imaging System Distinguishes Neoplastic from Normal Tissue During Resection of Soft Tissue Sarcomas and Mast Cell Tumors in Dogs. *Vet Surg* **45**, 715–722 https://doi.org/10.1111/vsu.12487 (2016).
12. Chen, Z. *et al.* Progresses in Fluorescence Imaging Guidance for Bone and Soft Tissue Sarcoma Surgery. *Frontiers in Oncology* vol. 12 Preprint at https://doi.org/10.3389/fonc.2022.879697 (2022).
13. Brookes, M. J. *et al.* Intraoperative near-infrared fluorescence guided surgery using indocyanine green (ICG) for the resection of sarcomas may reduce the positive margin rate: An extended case series. *Cancers (Basel)* **13**, https://doi.org/10.3390/cancers13246284 (2021).
14. Gong, M. F. *et al.* Intraoperative Evaluation of Soft Tissue Sarcoma Surgical Margins with Indocyanine Green Fluorescence Imaging. *Cancers (Basel)* **15**, https://doi.org/10.3390/cancers15030582 (2023).
15. Nicoli, F. *et al.* Intraoperative Near-infrared Fluorescence (NIR) Imaging with Indocyanine Green (ICG) Can Identify Bone and Soft Tissue Sarcomas Which May Provide Guidance for Oncological Resection. *Ann Surg* **273**, E63–E68 https://doi.org/10.1097/SLA.0000000000003857 (2021).
16. Atallah, I. *et al.* Role of near-infrared fluorescence imaging in head and neck cancer surgery: from animal models to humans. *Eur Arch Otorhinolaryngol* vol. 272 2593–2600 Preprint at https://doi.org/10.1007/s00405-014-3224-y (2015).
17. Fang, J., Nakamura, H. & Maeda, H. The EPR effect: Unique features of tumor blood vessels for drug delivery, factors involved, and limitations and augmentation of the effect. *Adv Drug Deliv Rev* vol. 63 136–151 Preprint at https://doi.org/10.1016/j.addr.2010.04.009 (2011).
18. Newton, A. D. *et al.* Optimization of Second Window Indocyanine Green for Intraoperative Near-Infrared Imaging of Thoracic Malignancy. *J Am Coll Surg* **228**, 188–197 (2019).
19. Huang, H. *et al.* Near-infrared (NIR) imaging with indocyanine green (ICG) may assist in intraoperative decision making and improving surgical margin in bone and soft tissue tumor surgery. *J Surg Oncol* **128**, 612–627 https://doi.org/10.1016/j.jamcollsurg.2018.11.003 (2023).

20. Beer, P., Rohrer-Bley, C. & Nolff, M. C. Near-infrared fluorescent image-guided lymph node dissection compared with locoregional lymphadenectomies in dogs with mast cell tumours. *JSAP* **63**, 670–678 https://doi.org/10.1111/jsap.13529 (2022).
21. Alvarez-Sanchez, A. *et al.* Comparison of indirect computed tomographic lymphography and near-infrared fluorescence sentinel lymph node mapping for integumentary canine mast cell tumors. *Vet Surg* **52**, 416–427 https://doi.org/10.1111/vsu.13929 (2023).
22. Eiger, S. N. *et al.* Use of near-infrared fluorescence angiography with indocyanine green to evaluate direct cutaneous arteries used for canine axial pattern flaps. *Vet Surg* **53**, 1073–1082 https://doi.org/10.1111/vsu.14121 (2024).
23. Mullen, K. M. *et al.* Use of real-time near-infrared fluorescence to assess gastric viability in dogs with gastric dilatation volvulus: A case-control study. *Vet Surg* **53**, 684–694 https://doi.org/10.1111/vsu.14067 (2024).
24. Holt, D. *et al.* Intraoperative near-infrared fluorescence imaging and spectroscopy identifies residual tumor cells in wounds. *J Biomed Opt* **20**, 076002 https://doi.org/10.1117/1.JBO.20.7.076002 (2015).
25. Favril, S. *et al.* Fluorescence-guided surgery using indocyanine green in dogs with superficial solid tumours. *Vet Rec* **187**, 273 https://doi.org/10.1136/vr.105554 (2020).
26. Newton, A. *et al.* Intraoperative near-infrared imaging can identify canine mammary tumors, a spontaneously occurring, large animal model of human breast cancer. *PLoS One* **15**, https://doi.org/10.1371/journal.pone.0234791 (2020).
27. Eward, W. C. *et al.* A novel imaging system permits real-time in vivo tumor bed assessment after resection of naturally occurring sarcomas in dogs tumor. in *Clin Orthop Relat Res* vol. 471 834–842 https://doi.org/10.1007/s11999-012-2560-8 (2013).
28. Fidel, J. *et al.* Preclinical Validation of the Utility of BLZ-100 in Providing Fluorescence Contrast for Imaging Spontaneous Solid Tumors. *Cancer Res* **75**, 4283–4291 https://doi.org/10.1158/0008-5472.CAN-15-0471 (2015).
29. Favril, S. *et al.* Preliminary Safety and Imaging Efficacy of the Near-Infrared Fluorescent Contrast Agent DA364 during Fluorescence-Guided Surgery in Dogs with Spontaneous Superficial Tumors. *Oncotarget* vol. 11(24), 2310–2326. https://doi.org/10.18632/oncotarget.27633 (2020).
30. Beer, P. *et al.* Evaluation of a targeted anti-αvβ3 integrin near-infrared fluorescent dye for fluorescence-guided resection of naturally occurring soft tissue sarcomas in dogs. *Eur J Nucl Med Mol Imaging* **52**, 1137–1148 https://doi.org/10.1007/s00259-024-06953-x (2025).

31. Keating, J. J. *et al.* Intraoperative near-infrared fluorescence imaging targeting folate receptors identifies lung cancer in a large-animal model. *Cancer* **123**, 1051–1060 https://doi.org/10.1002/cncr.30419 (2017).
32. Gao, R. W. *et al.* Determination of tumor margins with surgical specimen mapping using near-infrared fluorescence. *Cancer Res* **78**, 5144–5154 https://doi.org/10.1158/0008-5472.CAN-18-0878 (2018).
33. Hendrix, J. M., & Garmon, E. H. American Society of Anesthesiologists Physical Status Classification System. In *StatPearls*. StatPearls Publishing. (2025).
34. LeBlanc, A. K. *et al.* Veterinary Cooperative Oncology Group—Common Terminology Criteria for Adverse Events (VCOG-CTCAE v2) following investigational therapy in dogs and cats. *Vet Comp Oncol* **19**, 311–352 https://doi.org/10.1111/vco.12677 (2021).
35. Pratschke, K. M., Atherton, M. J., Sillito, J. A., & Lamm, C. G. Evaluation of a modified proportional margins approach for surgical resection of mast cell tumors in dogs: 40 cases (2008-2012). *JAVMA*, 243(10), 1436–1441. https://doi.org/10.2460/javma.243.10.1436 (2013).
36. Cockburn, E., Janovec, J., Solano, M. A. & L'Eplattenier, H. Marginal excision of cutaneous mast cell tumors in dogs was not associated with a higher rate of complications or prolonged wound healing than marginal excision of soft tissue sarcomas. *J Am Vet Med Assoc* **260**, 741–746 https://doi.org/10.2460/javma.21.05.0235 (2022).
37. Lagarto, J. L. *et al.* Electrocautery effects on fluorescence lifetime measurements: An in vivo study in the oral cavity. *J Photochem Photobiol B* **185**, 90–99 https://doi.org/10.1016/j.jphotobiol.2018.05.025 (2018).
38. Séguin, B. & Liptak, J. M. Updates in Surgical Oncology. *Vet Clin North Am Small Anim Pract* vol. 54 577–589 Preprint at https://doi.org/10.1016/j.cvsm.2023.12.010 (2024).
39. Roccabianca, P., Schulman, F. Y. Y., Avallone, G. et al. Tumors of soft tissue. In: Kiupel, M., ed. Surgical Pathology of Tumors of Domestic Animals, Vol. 3. Chicago: C. L. Davis & S. W. Thompson Foundation (2020).
40. Kuntz, K. et al. Prognostic factors for surgical treatment of soft-tissue sarcomas in dogs: 75 cases (1986–1996). *J Am Vet Med Assoc* 211, 1234–1240 (1997).
41. Patnaik, A. K., Ehler, W. J. & Macewen, E. G. *Canine Cutaneous Mast Cell Tumor: Morphologic Grading and Survival Time in 83 Dogs*. *Vet. Pathol* vol. 21 (1984).
42. Kiupel, M. *et al.* Proposal of a 2-tier histologic grading system for canine cutaneous mast cell tumors to more accurately predict biological behavior. *Vet Pathol* **48**, 147–155 https://doi.org/10.1177/0300985810386469 (2011).

43. Stefanello, D., et al. Comparison of 2- and 3-category histologic grading systems for predicting the presence of metastasis at the time of initial evaluation in dogs with cutaneous mast cell tumors: 386 cases (2009-2014). Journal of the American Veterinary Medical Association, 246(7), 765–769. https://doi.org/10.2460/javma.246.7.765 (2015).
44. Thompson, J. J. *et al.* Canine subcutaneous mast cell tumor: Characterization and prognostic indices. *Vet Pathol* **48**, 156–168 https://doi.org/10.1177/0300985810387446 (2011).
45. Giudice, C. *et al.* Feline injection-site sarcoma: Recurrence, tumour grading and surgical margin status evaluated using the three-dimensional histological technique. *Vet J* **186**, 84–88 https://doi.org/10.1016/j.tvjl.2009.07.019 (2010).
46. Dores, C. B., Milovancev, M. & Russell, D. S. Comparison of histologic margin status in low-grade cutaneous and subcutaneous canine mast cell tumours examined by radial and tangential sections. *Vet Comp Oncol* **16**, 125–130 https://doi.org/10.1111/vco.12321 (2018).
47. Schröer, G. & Trenkler, D. Exact and randomization distributions of Kolmogorov-Smirnov tests for two or three samples. Comput. Stat. Data Anal. 20, 185–202 (1995).
48. Wilson, E. B. Probable inference, the law of succession, and statistical inference. J Am Stat Assoc 22, 209–212 (1927).
49. Brown, L. D., Cai, T. T. & DasGupta, A. Interval estimation for a binomial proportion. Stat. Sci. 16, 101–133 (2001).
50. Ebell, M. H. Evidence-Based Diagnosis. Springer, New York. https://doi.org/10.1007/978-1-4757-3514-7 (2001).
51. Simel, D. L. Sample size estimation for diagnostic test studies. Stat. Med. 10, 325–337 (1991).
52. Stevenson, M. & Sergeant, E. epiR: Tools for the analysis of epidemiological data. R package version 2.0.76. https://CRAN.R-project.org/package=epiR
53. Avallone, G. *et al.* Canine Perivascular Wall Tumors: High Prognostic Impact of Site, Depth, and Completeness of Margins. *Vet Pathol* **51**, 713–721 https://doi.org/10.1177/0300985813503565 (2014).
54. Chiti, L. E. *et al.* Surgical margins in canine cutaneous soft-tissue sarcomas: A dichotomous classification system does not accurately predict the risk of local recurrence. *Animals* **11**, https://doi.org/10.3390/ani11082367 (2021).
55. Chase, D., Bray, J., Ide, A. & Polton, G. Outcome following removal of canine spindle cell tumours in first opinion practice: 104 cases. *JSAP* **50**, 568–574 https://doi.org/10.1111/j.1748-5827.2009.00809.x (2009).

56. Stefanello, D. *et al.* Weishaar's classification system for nodal metastasis in sentinel lymph nodes: Clinical outcome in 94 dogs with mast cell tumor. *J Vet Intern Med* **38**, 1675–1685 https://doi.org/10.1111/jvim.16997 (2024).
57. Baginski, H., Davis, G. & Bastian, R. P. The Prognostic Value of Lymph Node Metastasis with Grade 2 MCTs in Dogs: 55 Cases (2001-2010). *J Am Anim Hosp Assoc* **50**, 89–95 https://doi.org/10.5326/JAAHA-MS-5997 (2014).
58. Lapsley, J. *et al.* Influence of locoregional lymph node aspiration cytology vs sentinel lymph node mapping and biopsy on disease stage assignment in dogs with integumentary mast cell tumors. *Vet Surg* **50**, 133–141 https://doi.org/10.1111/vsu.13537 (2021).
59. Treggiari, E., Valenti, P., Porcellato, I., Maresca, G. & Romanelli, G. Retrospective analysis of outcome and prognostic factors of subcutaneous mast cell tumours in dogs undergoing surgery with or without adjuvant treatment. *Vet Comp Oncol* **21**, 437–446 https://doi.org/10.1111/vco.12902 (2023).
60. Jokiel-Rokita, A. & Pulit, M. Nonparametric estimation of the ROC curve based on smoothed empirical distribution functions. *Stat Comput* **23**, 703–712 (2013).
61. *R Core Team. R: A language and environment for statistical computing. R Foundation for Statistical Computing, Vienna, Austria. https://www.R-project.org/ (2024).*
62. Judy, R. P. *et al.* Quantification of tumor fluorescence during intraoperative optical cancer imaging. *Sci Rep* **5**, https://doi.org/10.1038/srep16208 (2015).
63. Madajewski, B. *et al.* Intraoperative near-infrared imaging of surgical wounds after tumor resections can detect residual disease. *Clin Cancer Res* **18**, 5741–5751 https://doi.org/10.1158/1078-0432.CCR-12-1188 (2012).
64. Favril, S. *et al.* Clinical use of organic near-infrared fluorescent contrast agents in image-guided oncologic procedures and its potential in veterinary oncology. *Vet Rec* vol. 183 354 Preprint at https://doi.org/10.1136/vr.104851 (2018).
65. Holt, D., Singhal, S. & Selmic, L. E. Near-infrared imaging and optical coherence tomography for intraoperative visualization of tumors. *Vet Surg* vol. 49 33–43 Preprint at https://doi.org/10.1111/vsu.13332 (2020).
66. Egloff-Juras, C., Bezdetnaya, L., Dolivet, G. & Lassalle, H. P. NIR fluorescence-guided tumor surgery: New strategies for the use of indocyanine green. *Int J Nanomedicine* vol. 14 7823–7838 Preprint at https://doi.org/10.2147/IJN.S207486 (2019).

5. Indocyanine green fluorescence lymphography: An exploratory study of superficial lymphatic territories in the head and hind limbs of 33 cat cadavers

- This study was published in PlosONE: https://doi.org/10.1371/journal.pone.0327005
- PhD student role: co-first author

Alessandra Ubiali[1], Elisa Maria Gariboldi[1], Luigi Auletta[1], Alessia Di Giancamillo[2], Silvia Clotilde Modina[1], Roberta Ferrari[1], Filippo Tagliasacchi[1], Valeria Martini[1], Damiano Stefanello[1]

[1]Department of Veterinary Medicine and Animal Sciences – University of Milan, Lodi, Italy
[2]Department of Biomedical Sciences – University of Milan, Milano, Italy

In the last decades, lymphography in cadavers has been performed in various animal species as anatomic and translational models for human lymphedema and lymphatic alterations [1-4]. Numerous techniques have been described for assessing superficial lymphatic drainage in human and animal cadavers [1-7]. Among them, near-infrared fluorescence lymphography with indocyanine green (NIRF-ICG) has become the most used technology [7-11].

Data obtained on canine cadavers [7] has been applied in several clinical studies to predict the expected regional draining lymphocentrum (LC) and compare it to the sentinel LC effectively identified [12-16].

Conversely, only few descriptive anatomical studies on the feline lymphatic system are available [17,18]. Furthermore, lymphographic studies in cats are outdated [5,6] or focused only on the mammary gland, either *in vivo* or in cadavers [19-21]. Hence, no lymphographic studies detailing the cutaneous lymphatic territories have been performed in cats. As a result, clinical studies involving lymph node (LN) assessment in cats rely only on what was reported in dogs [22], leading to potential inaccuracies.

Recent advancements in techniques for mapping and removing the sentinel lymph node in dogs have demonstrated that the superficial lymphatic network of the head and hind limb regions is challenging to identify due to its anatomical complexity [12, 23, 7], potentially leading to technique failures. With this in mind, the present study aims to assess the feasibility of NIRF-ICG lymphography in feline

cadavers and to map the superficial lymphatic pathways from selected cutaneous regions of the head and hind limbs, with the goal of detailing potential "lymphosomes." Additionally, the study will explore differences in lymphographic patterns between these two anatomical regions.

5.1. Materials and methods:

This explorative study included cadavers of both client-owned and unowned free-roaming adult cats that died spontaneously or were euthanized for causes unrelated to the study. Written consent was obtained from the owners (owned cats) or the public veterinary officer (unowned free-roaming cats) for the scientific use of cadavers.
All procedures were performed at the Department of Veterinary Medicine and Animal Sciences of the University of Milano.

Case selection

Adult feline cadavers with non-palpable, normal-sized (not clinically enlarged, compared to the contralateral) superficial LNs were included and underwent NIRF-ICG lymphography of selected cutaneous regions belonging to different anatomical districts: head, right hind limb, and left hind limb. The cadavers were defined as “adults” if no deciduous teeth were observed; otherwise, they were defined as “juveniles” and consequently not included. Cadavers were also excluded when they presented evident and severe cadaveric alterations (i.e., extensive areas of hypostasis, cadaveric hemolysis, diffuse tissue autolysis, putrefaction signs like cadaveric emphysema, and tissue colliquation). In addition, each anatomical district was also individually evaluated and was excluded in case of macroscopical alterations such as neoplastic or cutaneous lesions as a consequence of local cadaveric alteration or due to wounds or scars.
The BCS (Body Condition Score) was assigned on a five-point scale and defined as: emaciated, thin, normal, moderately overweight, or obese [24]. For statistical purposes, cadavers were categorized into two classes considering BCS: low BCS (pooling emaciated and thin) and normal-high BCS (pooling normal, moderately overweight and obese) [25]. Moreover, cats were categorized based on craniofacial type into brachycephalic and non-brachycephalic [26,27].

Cadaver preparation for NIRF-ICG lymphography

Cadavers were stored within 1 hour from death at +4°C if lymphography was planned within 24 hours; otherwise, they were stored at -20°C. Based on storage conditions, cadavers were categorized as “refrigerated” if stored at +4°C or “frozen” if stored at -20°C. Frozen cadavers were thawed and

kept at +4°C until completely defrosted, i.e., when flexion and extension of the joints could be performed without effort, before the preparation for lymphography. Regardless of the storage conditions, cadavers were kept for one hour at room temperature before starting the NIRF-ICG lymphography.

Immediately before NIRF-ICG lymphography, the anatomical districts were widely clipped. The head was clipped from the top of the nose to the scapular spine on both sides, and the hind limbs were clipped from digits to the iliac crest and ischiatic tuberosity, medially including the inguinal region. Cadavers were manipulated carefully during the preparation, ensuring that the skin remained macroscopically undamaged during trichotomy and therefore superficial lymphatic vessels were not transected.

Definition of the cutaneous regions within the anatomical districts

Within the anatomical districts, a total of 20 cutaneous regions were predetermined: 6 for the head and 14 for the hind limb **(Tables 1 and 2).** Since the head is an unpaired anatomical district, all median regions were excluded to avoid possible bilateral migrations. For paired bilateral regions, margins were drawn at least 0.5 cm apart from the midline. The borders of each selected cutaneous region were defined based on readily identifiable and unambiguous anatomical landmarks from already described topographic regions [28]. Each selected cutaneous region and the corresponding anatomical landmarks are described in **Tables 1 and 2** and **Fig. 1 and 2.** Each selected cutaneous region was drawn with a skin marker (**Fig. 3**).

Table 1. Selected cutaneous regions in the head anatomical district.

Selected cutaneous region	Anatomical landmarks	Predictability (predictable/unpredictable)	expected LC
Auricular	Semi-circumferential region delimiting the caudal part of the ear cartilage, within 1 cm from the edge. Pinna was not included.	PREDICTABLE	Superficial cervical
Rostral mandibular	Cutaneous portion of the inferior lip from tooth 302 (or 402) to tooth 307 (or 407), ventrally delimited by the ventral ridge of the mandibular bone.	PREDICTABLE	Mandibular
Aboral mandibular	Cutaneous portion of the inferior lip from tooth 307 (or 407) to the labial commissure, ventrally delimited by the ventral ridge of the of mandibular bone.	PREDICTABLE	Mandibular
Rostral maxillary	Cutaneous portion of the superior lip from tooth 102 (or 202) to tooth 107 (or 207), dorsally	PREDICTABLE	Mandibular

	delimited by the alar cartilage and medial canthus of the eye.		
Aboral maxillary	Cutaneous portion of the superior lip from tooth 107 (or 207) to the labial commissure, dorsally delimited by the border between maxillary and zygomatic bones.	PREDICTABLE	Mandibular
Temporal-zygomatic	Triangle of skin delimited by the lateral canthus of the eye, proximal and distal edges of the cranial aspect of ear base.	PREDICTABLE	Parotid

Table 2. Selected cutaneous regions in the hind limb anatomical district.

Selected cutaneous region	Anatomical landmarks	Predictability (predictable/unpredictable)	expected LC
Lateral thigh - cranial	Region delimited by the lateral trochlear ridge of femur, lateral condyle of femur, tuberosity of greater trochanter, and tuber coxae.	**UNPREDICTABLE**	Superficial inguinal Medial Iliac
Lateral thigh - caudal	Region delimited by the lateral condyle of femur, popliteal fossa, ischiatic tuberosity, and tuberosity of greater trochanter.	**UNPREDICTABLE**	Superficial inguinal Medial Iliac Sacral
Medial thigh - cranial	Region delimited by the medial trochlear ridge of femur, medial condyle of femur, laterally delimited femur and fold of flank until the end of abdominal wall proximally.	PREDICTABLE	Superficial inguinal
Medial thigh - caudal	Region delimited by the medial condyle of femur, laterally delimited by femur and caudal aspect of thigh, to the pubis.	PREDICTABLE	Superficial inguinal
Lateral genicular	Region delimited by the lateral trochlear ridge of femur, popliteal fossa, and lateral tibial condyle tuberosity.	PREDICTABLE	Superficial inguinal
Medial genicular	Region delimited by the medial trochlear ridge of femur, popliteal fossa, and medial tibial condyle tuberosity.	PREDICTABLE	Superficial inguinal
Lateral crural	Region delimited by the lateral tibial condyle tuberosity, popliteal fossa, fibula distal tuberosity, and calcaneal tuberosity.	**UNPREDICTABLE**	Superficial inguinal Popliteal
Medial crural	Region delimited by the medial tibial condyle tuberosity, popliteal fossa, tibial distal tuberosity, and calcaneal tuberosity.	PREDICTABLE	Superficial inguinal

Lateral tarsal	Region delimited by the fibular lateral malleolus, calcaneal tuberosity, and base of V metatarsal bone.	**UNPREDICTABLE**	Superficial inguinal Popliteal
Medial tarsal	Region delimited by the tibial medial malleolus, calcaneal tuberosity, base of II metatarsal bone.	PREDICTABLE	Superficial inguinal
Dorsal metatarsal	Dorsal aspect of the region delimited proximally by the base of V and II metatarsal bones, and distally by metatarsophalangeal joints.	PREDICTABLE	Popliteal
Plantar metatarsal	Plantar aspect of the region delimited proximally by the base of V and II metatarsal bones and distally by metatarsophalangeal joints.	PREDICTABLE	Popliteal
Dorsal phalangeal	Dorsal aspect of the region delimited by the metatarsophalangeal joints proximally and base of the claws distally.	PREDICTABLE	Popliteal
Plantar phalangeal	Plantar aspect of the region delimited by the metatarsophalangeal joints proximally and base of claws distally.	PREDICTABLE	Popliteal

Fig 1. Predetermined cutaneous regions of head anatomical district.

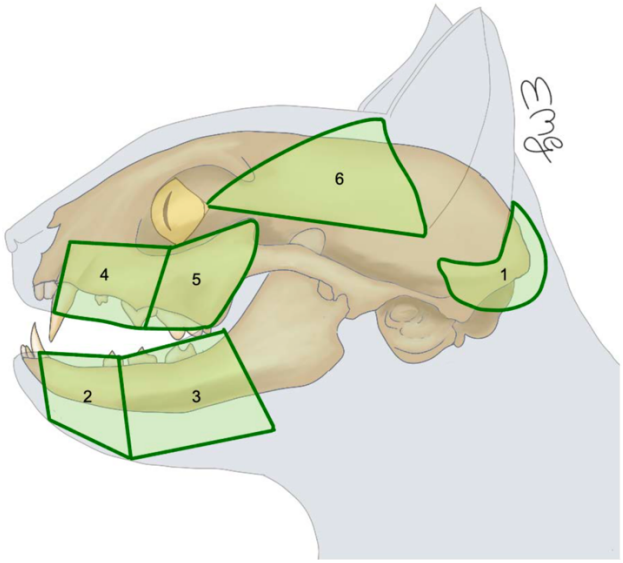

1-Auricular; 2-Rostral-mandibular; 3- Aboral mandibular; 4- Rostral maxillary; 5- Aboral maxillary; 6- Temporal-zygomatic

Fig 2. Predetermined cutaneous regions of hind limb anatomical district.

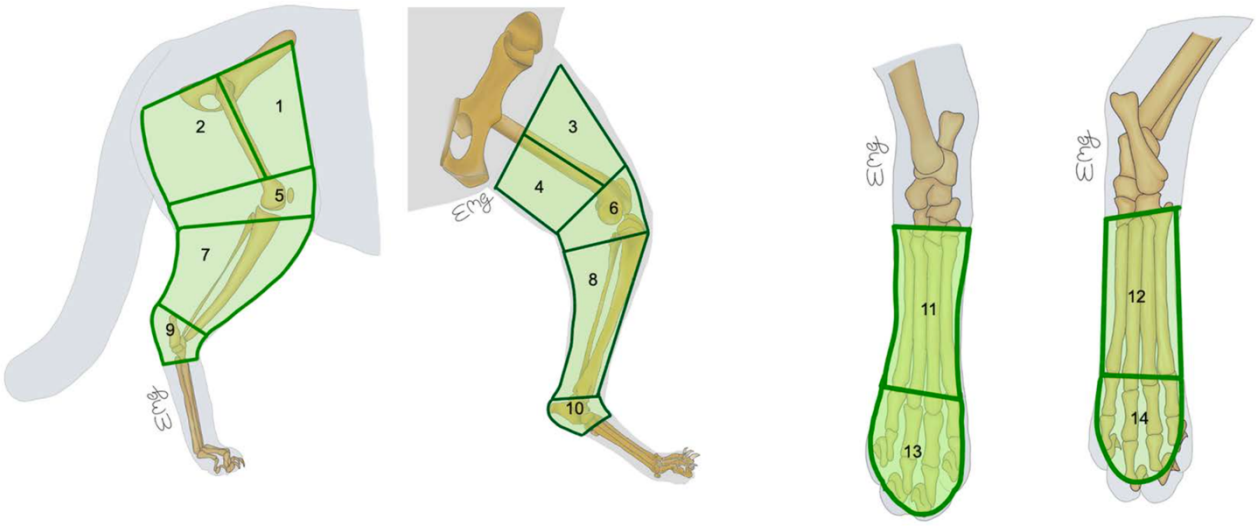

1- Lateral thigh – cranial; 2- Lateral thigh – caudal; 3- Medial thigh – cranial; 4- Medial thigh – caudal; 5- Lateral genicular; 6- Medial genicular; 7- Lateral crural; 8- Medial crural; 9- Lateral tarsal; 10- Medial tarsal; 11- Dorsal metatarsal; 12- Plantar metatarsal; 13- Dorsal phalangeal; 14- Plantar phalangeal.

Fig 3. NIRF-ICG lymphography images of the hind limb.

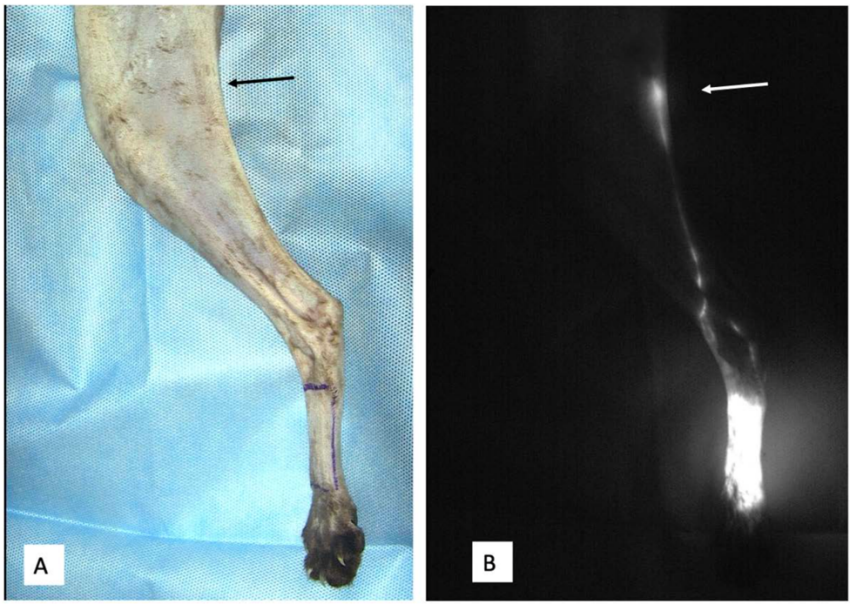

A) The dorsal metatarsal selected cutaneous region is drawn with a skin marker before performing NIRF-ICG lymphography. The anatomical location of the popliteal LC is pointed out by the black arrow; B) NIRF-ICG lymphography images after injection of ICG and massage of the selected cutaneous region showing the lymphatic drainage reaching the popliteal LC (white arrow).

The expected draining LC was recorded for each selected cutaneous region. Since the authors are not aware of any previous study that has identified LC based on specific lymphatic territories in cats, an LC was classified as "predictable" if the defined region was expected to drain to a single LC, or "unpredictable" if the region corresponded to more than one lymphosome based on canine lymphatic territories [7]. Therefore, the draining LC was considered "predictable" for 16 selected anatomical regions (6 from the head and 10 from the hind limb) and "unpredictable'' for 4 (all from the hind limb) **(Tables 1 and 2).**

NIRF-ICG lymphography

After the drawing of one selected cutaneous region, the NIRF-ICG lymphography procedure included intradermal injection of ICG, visualization of the draining lymphatic pathways, and identification and surgical exploration of the draining LC(s) under NIRF camera guidance (**Fig. 3**). In each cadaver, NIRF-ICG lymphography was performed in a maximum of three selected cutaneous regions, one from each anatomical district, i.e., one from the right hind limb, one from the left hind limb, and one from the head. The side of each selected cutaneous region was randomly assigned using an online randomization tool (https://www.random.org/lists/). Considering the two hind limb regions selected per cadaver, to prevent lymphatic drainage from crossing the ventral midline, NIRF-ICG lymphography was performed firstly on the most distal region (either on the left or right side) and then on the opposite leg in the more proximal one.

For each lymphography, each cadaver was placed in lateral recumbency, and intradermal injections in multiple spots of indocyanine green at a distance of 0.5 cm from each other were performed to cover the whole selected cutaneous region. A total volume of 0.4ml of ICG at 1,25mg/ml (0.2 ml of ICG at 2.5 mg/ml diluted in 0.2 ml NaCl 0.9%) was used [7, 10, 29-31], and injection of full volume or volume reduction was recorded. At each injection spot, the needle was pointed towards the center, avoiding going beyond the margins of the selected cutaneous region. At the moment of the injection, room lights were turned off, a timer was started from the last injection of dye, and a NIRF-camera (SPY-Elite Imaging system, Stryker, MIDA Tecnologia medica S.p.A) was positioned 20-30 cm above selected cutaneous region, recording the NIRF-ICG lymphography. Considering that *in vivo* lymphatic circulation works differently than in cadavers, being a dynamic process assisted by anatomical structures and valves, in the present study it was favored by gentle massage and, for the hind limbs, by flexion-extension movements of the limb for 10 minutes. To avoid contaminating the skin around the injected region with ICG, a gauze was used to absorb any residue or reflux from the injection sites, and operators changed their gloves after each injection and any time contamination with ICG was suspected. The LCs detected by NIRF-ICG lymphography were dissected and explored

under the guidance of a NIRF-camera. In the case of intra-abdominal LC, when the detected lymphatic pathway was supposed to run through the inguinal canal, a ventral midline incision was performed, and the abdominal cavity was always surgically explored to detect any intra-abdominal fluorescence.

If no drainage or fluorescent LC was visible after the first 10 minutes, the injections at the same dosage and massage procedures were repeated. Ten minutes after the second injection, if the beginning of drainage was detected, massage of the region was continued for another 10 minutes to a total maximum time of 30 minutes. If that drainage did not progress or no fluorescent drainages or LCs were detected, expected regional LCs were surgically inspected under the guidance of NIRF-camera, and the LNs were removed.

Lymph nodes evaluation

- all extirpated LNs were assessed by NIRF-camera. LNs were defined as "fluorescent" if they were either completely fluorescent or partially fluorescent, if fluorescence of the draining lymphatic vessel arrived at the LN and involved at least one pole of the node. Fluorescence was defined as signal-to-background ratio (SBR) > 1.1 [32]
- Extirpated LNs were measured by caliper on two orthogonal axes (millimeters)
- Further data recorded included: median number of LNs per LC, presence of a single or multiple LNs per LC overall and within the anatomical district

Whenever a fluorescent LN was found, the corresponding LC was designated as draining the assessed selected cutaneous region.

NIRF-ICG lymphography evaluation

- Success: the success of NIRF-ICG lymphography was defined as the detection, after surgical exploration guided by the NIRF-camera, of at least one fluorescent LN in a LC with or without transcutaneous visualization of a fluorescent lymphatic pathway.
- Failure: the NIRF-ICG lymphography was recorded as failed if no fluorescence could be visualized in any LN or LCs, or if only an interrupted lymphatic pathway was detected after a maximum of total 30 minutes of massage.
- Interrupted lymphatic pathways: their definition was used by the authors with a pure descriptive intent and was based only on visible macroscopical evidence, they appeared as fluorescent pathways departing from the injected selected cutaneous region and not arriving at any LC. To confirm the interruption of visible lymphatic pathways, the sites where

drainages stopped and the expected and/or closest regional LCs were always surgically explored under NIRF-camera guidance to confirm the absence of fluorescence.

- Shine-through effect: if the fluorescence of the selected cutaneous region overlapped the fluorescent signal from the LC due to their anatomical proximity, it was defined and recorded as the "shine-through effect" [33]. In that case the LC fluorescence was assessed by post excision fluorescence of at least one the LN belonging to the LC.

Variables collected related to NIRF-ICG lymphography

Variables collected and measured were: 1) the presence or absence of cutaneous pigmentation; 2) volume of ICG injected (full vs half); 3) the number of multiple injection spots needed to fill a selected cutaneous region; 4) the need to perform re-injections; 5) presence or absence of a drainage pathway visible transcutaneously; 6) the lymphatic pathway length (in centimeters), estimated by measuring with a tape the distance between the selected cutaneous regions and the identified LCs; 7) migration time (in minutes).

Data about migration time and lymphatic pathways length in case of "shine-through effect" were not collected. For each NIRF-ICG lymphography, the number, anatomical location, and side (ipsilateral *vs.* contralateral) of identified LC were recorded.

Considering the absence so far of a specific study on cats, correspondence with the predicted LC based on canine study [7] was assessed and defined as: total correspondence, if all predicted LCs were identified by fluorescence; partial correspondence, if fluorescence was identified, in addition to the expected one, in at least one LC at an unpredictable site; non-correspondence, if all LCs identified by fluorescence differed from the predicted ones.

Statistical analysis

All data recorded were imported in a dedicated statistical analysis software (JMP®, v.16.0, SAS Institute, Cary, NC, USA; Prism 8 for MacOS, v. 8.2.0, GraphPad Software Inc., CA, USA). Categorical variables were reported as percentage (%) of the whole sample. Continuous variables were tested for normality with the Shapiro Wilk's *W* test and reported as mean ± standard deviation or median and range, accordingly.

Association between categorical variables was assessed with contingency tables and Fisher's exact test or chi-squared test, while a univariate logistic regression model assessed the association between continuous and categorical variables.

In particular, the association between the following variables were assessed:

- success or failure of NIRF-ICG lymphography and:
    - BCS class
    - storage condition (refrigerated *vs.* frozen)
    - anatomical district (head *vs.* hind limb)
    - selected cutaneous regions
    - presence of cutaneous pigmentation
    - volume of ICG injected (full *vs.* half)
    - number of multiple injection spots
- anatomical districts and technical aspects and results of lymphography, i.e.:
    - need to re-inject ICG
    - volume of ICG injected (full *vs.* half)
    - lymphatic pathway length
    - migration time

The same associations were explored for the selected cutaneous region within the anatomical districts.

- presence of interrupted lymphatic pathways and:
    - anatomical district (head *vs.* hind limb)
    - selected cutaneous regions within the anatomical districts
    - storage conditions (refrigerated *vs.* frozen)
- Storage condition (refrigerated *vs.* frozen) and:
    - Migration time
- Need to re-inject and:
    - volume injected
- Correspondences with lymphosomes in dog [7] and:
    - anatomical district (head *vs.* hind limb)
    - selected cutaneous regions within anatomical districts.

All significant association were further analyzed by Mann-Whitney U test between the anatomical districts or by Kruskal-Wallis test between the selected cutaneous regions. Each region was compared with all the others *post hoc* with Tukey's HSD test. For all tests, significance was set at $P<0.05$.

5.2. Results:

The same two operators performed all procedures in a dedicated room (EMG, AU). A total of 33 feline cadavers were included; 27 (82%) cadavers were frozen, and the remaining 6 (18%) were refrigerated. Out of 99 anatomical districts (3 per cat), 15 (7 heads and 8 hind limbs) were excluded due to macroscopic alterations. A total of 84 NIRF-ICG lymphographies were performed within the remaining 84 anatomical districts, of which 26 heads and 58 hind limbs. Considering the 20 predetermined cutaneous regions, lymphography was performed 5 times in 4 of them (auricular, temporal-zygomatic, medial crural, plantar phalangeal), and 4 times in the remaining 16.

Details regarding overlaying pigmented skin, volume injected, number of multiple injection spots per selected cutaneous region, need to perform re-injection, median lymphatic pathways length and median migration time are summarized in **Tables 3 and 4**. In particular, half volume was injected in the rostral mandibular region four times, in the aboral maxillary and dorsal phalangeal regions two times, and one each in the aboral mandibular, rostral maxillary, lateral tarsal, medial tarsal, and plantar metatarsal regions.

Table 3. Description of median number of multiple injection spots, need to perform re-injection, median lymphatic pathways length, median migration time and volume of ICG injected for each selected cutaneous region.

Selected Cutaneous Region (n=84)	**Median n. of multiple injection spots** Overall, 8 (3-20)	**Need to perform re-injection** (n=48)	**Lymphatic pathways length (cm)** Overall, 4 (0-30)	**Median migration time (min)** Overall, 8 (1-30)	**volume of ICG injected** (full *vs*. half)
Auricular (n=5)	8 (6-10)^{A,B,C,D}	4/5	2 (2-2)^{A,B}	2 (2-2)^{A,B}	5/5 full
Rostral mandibular (n=4)	5 (4-8)^{A}	0/4*	4 (2-6)^{A,B}	2 (1-4)^{A}	4/4 half*
Aboral mandibular (n=4)	5 (4-12)^{A,B}	0/4*	1 (0-2)^{A}	3 (2-10)^{A,B}	3/4 full 1/4 half
Rostral maxillary (n=4)	6 (3-12)^{A,B}	0/4*	4.5 (4-5)^{A,B,C}	4 (1-10)^{A,B,C}	3/4 full 1/4 half
Aboral maxillary (n=4)	5 (4-9)^{A}	2/4	4 (4-14)^{B,C}	15 (8-20)^{D,E}	2/4 half 2/4 full
Temporal-zygomatic (n=5)	8 (6-8)^{A,B}	5/5	3 (1-6)^{A,B}	16 (8-20)^{D,E}	5/5 full
Lateral thigh – cranial (n=4)	14 (6-16)^{E}	3/4	2 (1-2)^{A,B}	15 (10-20)^{D,E}	4/4 full
Lateral thigh – caudal	8 (6-16)^{A,B,C,D,E}	3/4	1 (1-1)^{A,B}	20 (20-20)^{D,E}	4/4 full

(n=4)					
Medial thigh – cranial (n=4)	10 (8-14)^{A,B,C,D,E}	2/4	1 (0-3)^{A}	10 (7-25)^{D,E}	4/4 full
Medial thigh – caudal (n=4)	11 (7-14)^{B,C,D,E}	3/4	1.5 (1-5)^{A,B}	27 (5-30)^{E}	4/4 full
Lateral genicular (n=4)	11 (8-17)^{C,D,E}	4/4	1 (0-7)^{A,B}	9 (5-11)^{A,B,C,D,E}	4/4 full
Medial genicular (n=4)	10 (8-20)^{D,E}	3/4	0.5 (0-1)^{A,B}	Shining effect	4/4 full
Lateral crural (n=4)	12 (12-15)^{E}	1/4	2 (2-2)^{A,B}	2 (2-8)^{A,B,C,D}	4/4 full
Medial crural (n=5)	12 (7-15)^{C,D,E}	4/5	2 (2-2)^{A,B}	10 (10-25)^{A,B,C,D,E}	5/5 full
Lateral tarsal (n=4)	7 (6-10)^{A,B,C,D}	2/4	10 (7-25)^{D,E}	11 (5-20)^{B,C,D}	3/4 full 1/4 half
Medial tarsal (n=4)	7 (4-8)^{A,B}	3/4	7 (7-15)^{C,D}	7 (7-17)^{A,B,C,D}	3/4 full 1/4 half
Dorsal metatarsal (n=4)	7 (6-12)^{A,B,C,D}	2/4	10 (9-10)^{C,D}	7 (1-15)^{A,B,C,D}	4/4 full
Plantar metatarsal (n=4)	9 (6-12)^{A,B,C,D,E}	1/4	14 (11-25)^{E,F}	8 (2-20)^{A,B,C,D}	3/4 full 1/4 half
Dorsal phalangeal (n=4)	8 (3-10)^{A,B}	2/4	15 (11-30)^{F}	14 (2-30)^{C,D,E}	2/4 full 2/4 half
Plantar phalangeal (n=5)	8 (6-10)^{A,B,C}	4/5	14 (11-24)^{E,F}	8 (2-20)^{A,B,C,D}	5/5 full

Legend: LC=lymphocentrum; Statistics: within columns, measures not connected by the same letter are significantly different at $P<0.05$. The * indicates significant difference at chi-square test.

Table 4. Details on lymphographies divided by anatomical districts.

NIRF-ICG Lymphography	**Head** (26 lymphographies)	**Hind Limb** (58 lymphographies)	**Overall** **(head + hind limbs)** (84 lymphographies)
Success	21/26 (81%)	42/58 (72%)	63/84 (75%)
Failure	5/26 (19%)	16/58 (28%)	21/84 (25%)

Interrupted Lymphatic Pathways*	2/26 (8%)	11/58 (19%)	13/84 (16%)
Overlaying pigmented skin	6/26 (23%)	4/58 (7%)	10/84 (12%)
Volume injected (full *vs*. half)	18/26 (69%) full 8/26 (31%) half	53/58 (91%) full 5/58 (9%) half	71/84 (85%) full 13/84 (15%) half
Median n. multiple injection spots	7 (3-12)	8 (3-20)	8 (3-20)
Need to perform re-injection	11/26 (42%)	37/58 (64%)	48/84 (57%)
Median lymphatic pathways length (cm)	4 (1-14)	10 (1-30)	5 (1-30)
Median migration time (min)	4 (1-20)	10 (1-30)	8 (1-30)

* In 9/13 (69%) lymphographies, despite the interrupted drainage, another lymphatic pathway properly reached the draining LC. In the remaining 4/13 (31%), the interrupted lymphatic pathway was the only drainage detected, therefore these lymphographies were counted in the 21 that failed. In the head anatomical district, despite the interrupted drainage, another lymphatic pathway properly reached the draining LC.

The NIRF-ICG lymphography was successful in 63/84 (75%) selected cutaneous regions. Conversely, the NIRF-ICG lymphography failed in the remaining 21/84 (25%) cases related to 11 selected cutaneous regions. Successful NIRF-ICG lymphography was always recorded in the following 9 selected cutaneous regions: rostral and aboral maxillary, rostral and aboral mandibular, dorsal phalangeal, dorsal and plantar metatarsal, lateral tarsal and medial thigh-cranial (**Tables 5 and 6**). Further details regarding NIRF-ICG lymphography for each selected cutaneous region and anatomical district are reported in **Tables 4-6.** An interrupted lymphatic pathway was observed in 13/84 (16%) NIRF-ICG lymphographies. Details on the interrupted lymphatic pathway are reported in **S1 Table and Table 4**.

Table 5. Correspondence between selected cutaneous regions with expected draining LCs in dogs [7]– HEAD.

Selected Cutaneous Region	Success of Lymphography	Detected LCs	Expected LCs in dogs	Correspondence with dogs
Auricular (n= 5)	Successful: 1/5	1/1 Mandibular + Parotid + Superficial Cervical	Superficial cervical	Partial
Rostral mandibular (n=4)	Successful: 4/4	2/4 Mandibular	Mandibular	Total
		2/4 Mandibular + Medial retropharyngeal		Partial
Aboral mandibular (n=4)	Successful: 4/4	3/4 Mandibular	Mandibular	Total
		1/4 Mandibular + Parotid		Partial
Rostral maxillary (n=4)	Successful 4/4	4/4 Mandibular	Mandibular	Total
Aboral maxillary (n=4)	Successful: 4/4	1/4 Mandibular	Mandibular	Total
		1/4 Mandibular + Parotid		Partial
		1/4 Mandibular + Parotid + Medial Retropharyngeal		Partial
		1/4 Superficial cervical		Non-correspondent
Temporal-Zygomatic (n=5)	Successful: 4/5	3/5 parotid	Parotid	Total
		1/5 parotid + mandibular		Partial

Legend: LC= Lymphocentrum; correspondence was defined as: TOTAL= all LC hypothesized based on dogs were identified by fluorescence, PARTIAL=fluorescence identified at least one more LC at an unpredictable site; NON-CORRESPONDENT= all LCs identified by fluorescence were different than the hypothesized ones.

Table 6. Correspondence between selected cutaneous regions with expected draining LCs in dogs [7]– HIND LIMB

Selected Cutaneous Region	Success of Lymphography	Detected LCs	Expected LCs in dogs	Correspondence with dogs
Lateral thigh - cranial (n=4)	Successful: 3/4	2/4 Superficial inguinal	Superficial inguinal	Partial
		1/4 Popliteal	Medial Iliac	Non-correspondent
Lateral thigh - caudal (n=4)	Successful: 2/4	2/4 Popliteal	Superficial inguinal Medial Iliac Sacral	Non-correspondent
Medial thigh - cranial (n=4)	Successful: 4/4	4/4 Superficial inguinal	Superficial inguinal	Total
Medial thigh - caudal (n=4)	Successful: 3/4	1/4 Popliteal + Superficial inguinal	Superficial inguinal	Partial
		1/4 Popliteal		Non-correspondent
		1/4 Popliteal + Medial iliac		Non-correspondent
Lateral Genicular (n=4)	Successful: 3/4	1/4 Popliteal + Superficial inguinal	Superficial inguinal	Partial
		1/4 Popliteal		Non-correspondent
		1/4 Popliteal + Medial iliac		Non-correspondent

Medial Genicular (n=4)	Successful: 2/4	2/4 Popliteal	Superficial inguinal	Non-correspondent
Lateral Crural (n=4)	Successful: 3/4	3/4 Popliteal	Popliteal Superficial inguinal	Partial
Medial Crural (n= 5)	Successful: 1/5	1/5 Popliteal + Superficial inguinal	Superficial inguinal	Partial
Lateral Tarsal (n=4)	Successful: 4/4	3/4 Popliteal	Popliteal Superficial inguinal	Partial
		1/4 Popliteal + Medial iliac		Partial
Medial Tarsal (n=4)	Successful: 2/4	1/4 Popliteal + Medial iliac	Superficial inguinal	Non-correspondent
		1/4 Medial iliac		Non-correspondent
Dorsal Metatarsal (n=4)	Successful: 4/4	4/4 Popliteal	Popliteal	Total
Plantar Metatarsal (n=4)	Successful: 4/4	3/4 Popliteal	Popliteal	Total
		1/4 Popliteal + Superficial inguinal		Partial
Dorsal Phalangeal (n=4)	Successful: 4/4	3/4 Popliteal	Popliteal	Total
		1/4 Popliteal + Medial iliac		Partial
	Successful: 3/5	1/5 Popliteal	Popliteal	Total

Plantar Phalangeal (n= 5)		1/5 Popliteal + Medial iliac		Partial
		1/5 Medial iliac		Non-correspondent

Legend: LC= Lymphocentrum; correspondence was defined as: TOTAL= all LC hypothesized based on dogs were identified by fluorescence, PARTIAL=fluorescence identified at least one more LC at an unpredictable site; NON-CORRESPONDENT= all LCs identified by fluorescence were different than the hypothesized ones.

Data about detected LCs, correspondence with predicted LCs, shine-through effect and detected LNs are reported in **Tables 5-6; S2 Table.**

A total of 114 LNs within the draining LCs were excised; the median number of LN per LC was 1 (1 – 5). Median LNs size was 5 (1 - 22) mm and 5 (1 - 17) mm considering major and minor axis, respectively. The post-excisional NIRF-camera assessment identified 96 (84%) fluorescent LNs and 18 (16%) non-fluorescent LNs.

Association between success or failure of NIRF-ICG lymphography and variables collected - The variables evaluated for association with the success and the failure of NIRF-ICG lymphography are summarized in **S3 Table.** In particular, the failure of NIRF-ICG lymphography was associated with the selected cutaneous regions (P=0.02), with the auricular and medial crural regions displaying the highest failure rate.On the other hand, lymphographies performed with half volume never displayed failures (P=0.02)

Association between anatomical districts/selected cutaneous regions and technical aspects and results of lymphography - Data on the associations between technical aspects, performances, and results of the NIRF-ICG lymphography - both among themselves and with anatomical districts - are summarized in **Table 3** as well as the same associations comparing the selected cutaneous regions within the anatomical districts.

Specifically, the number of lymphographies that needed re-injection did not differ between the head and the hind limb (P=0.09). Considering selected cutaneous regions within the head, the temporal-zygomatic region needed re-injection in 100% of lymphographies, whereas rostral maxillary and rostral and aboral mandibular regions never needed re-injection (P=0.002). On the other hand, no difference in lymphographies that needed re-injection could be detected between the selected cutaneous regions belonging to the hindlimb (P=0.61). When the possible association between the

need to re-inject and the volume injected was evaluated, a significantly lower (P=0.04) number of lymphographies needed re-injection when injecting half volume .

Considering the volume of ICG injected, the use of half the volume of ICG was significantly more frequent in the head compared to the hind limb (P=0.009). Indeed, the rostral mandibular region was injected with half volume in 100% of lymphographies (P=0.01). Conversely, no difference in the use of half or full ICG volume could be detected among the selected cutaneous regions belonging to the hindlimb (P=0.21). Nonetheless, although non-significant, it should be noted that only the lateral and medial tarsal regions (one lymphography each), dorsal phalangeal (two lymphographies) and plantar metatarsal (one lymphography) needed half-volume injection.

The lymphatic pathway length differed significantly between the head and the hind limb (P=0.0006). Indeed, the lymphatic pathway was significantly shorter (P=0.0002) in the head (4; 1 – 20 cm) compared to the hind limb (10; 1 – 30 cm). The selected cutaneous regions belonging to the head differed significantly from each other (P=0.006), with the aboral maxillary region displaying a longer lymphatic pathway compared to the other regions. Indeed, in one lymphography of the aboral maxillary region, the identified LC was the superficial cervical node. The selected cutaneous regions belonging to the hind limb differed significantly from each other (P=0.003), with the dorsal and plantar phalangeal and plantar metatarsal regions displaying the longer lymphatic pathway compared to the other regions . In one lymphography of the dorsal and two lymphographies of the plantar phalangeal region, one of the identified LC was the medial iliac. Conversely, in one lymphography of the plantar metatarsal region, one of the identified LC was the superficial inguinal.

As for the migration time, it differed significantly between the head and the hind limb (P=0.024). In particular, migration time was significantly shorter (P=0.026) in the head (4; 1 – 20 min) compared to the hind limb (10; 1 – 30 min). The selected cutaneous regions belonging to the head differed significantly from each other (P=0.001), with a longer migration time in the aboral maxillary and the temporal-zygomatic regions. Particularly, in the aforementioned lymphography of the aboral maxillary region, migration time might have been affected by the longer lymphatic pathway length. The selected cutaneous regions belonging to the hind limb did not differ between each other for migration time (P=0.69) . Finally, considering storage conditions, migration time was significantly lower (P=0.04) in refrigerated (2; 1 – 20 min) cats compared to frozen (10; 1 – 30 min) ones.

Association between presence of interrupted lymphatic pathways and variables collected - The identification of an interrupted lymphatic pathway was not associated with the anatomical district (P=0.33), nor to the selected cutaneous regions whether belonging to the head (P=0.43) or to the hind limb (P=0.68). It was also not associated to the storage condition (P=0.80).

Association between correspondence with lymphosomes in dogs [7] and variables collected - When correspondence with lymphosomes in dogs [7] was explored, it differed significantly between the anatomical districts (P=0.049), with the head displaying a lower number of non-correspondences. No differences could be detected in correspondence with lymphosomes in dogs [7] between the selected cutaneous regions belonging to the head (P=0.40), while within the hind limb, the medial tarsal, medial genicular, and lateral thigh-caudal regions displayed only non-correspondence, whereas the lateral tarsal, lateral and medial crural regions showed only partial correspondence (P=0.0004).

5.3. Discussion:

The results of this exploratory study demonstrated the feasibility of NIRF-ICG lymphography for superficial lymphatic pathways definition in the head and hind limb anatomical districts of feline cadavers. We obtained a 75% overall success rate (81% for the head and 72% for the hind limb). Beyond feasibility, this study differs from previous ones due to the higher number of repetitions, the larger sample size, and the broader range of variables explored, allowing for consideration of technical aspects that may influence lymphography performance [2-7]. While lymphography in cats has been reported to be successful with other tracers, such as isosulfan blue or India ink [5,6,19], to the authors' knowledge, only Ratzlaff's study investigated the superficial lymphatic system, but in living cats, euthanizing them after injection of dye. Although there are limitations compared to studies on live animals, the approach reported in the present paper offered interesting results without compromising animal welfare and respecting the ethical principles of research.

The limited number of studies on the superficial lymphatic system of cats makes it challenging to compare our results with previously published data, given the differing inclusion criteria and the numerous variables explored in our study. Considering our results, no association was found between the success of NIRF-ICG lymphography and the variables considered, neither related to the cadaver itself (BCS, storage conditions, anatomical districts, selected cutaneous regions, cutaneous pigmentation) nor the technique applied (number of multiple injection spots, need to perform re-injection, injected volume). Unfortunately, these variables were not explored in previous studies, thus preventing comparison. Similarly, no information about failure has been reported in literature so far [2-7, 19], but in the present study failure of NIRF-ICG lymphography resulted significantly associated to selected cutaneous regions. In particular, the auricular and medial crural regions showed the highest failure rate, with 4/5 failures. On one hand, the high failure rate recorded for the auricular region could be due to the difficulty in massaging the regions and the inability to perform any flexion-

extension movement. Additionally, the auricular region may have less elastic skin and underlying tissues than other anatomical areas, with a lower ability to deform or move freely. This could prevent the correct massaging and uniform diffusion of the dye. On the other hand, no factors have been identified for the medial crural region that would support a scientifically sound hypothesis. Difficulties in massaging and moving the area further may contribute to tracer failure, but further studies on a higher number of samples may help to find an explanation to this result.

Moreover, the failure rate of NIRF-ICG lymphography was lower when half volume of dye was injected, although the concentration of ICG injected remained the same. A low number of half-volume injections were performed, possibly biasing statistical analyses. Still, this result may suggest that a cutaneous NIRF-ICG lymphography in feline cadavers would be successful regardless of the volume injected, at least for the volumes and ICG concentration used in this study.

Besides the success and failure rates, the performance characteristics of the NIRF-ICG lymphography and variables potentially influencing them were deeply explored in the present study. Among them, the storage conditions were associated with migration time, which was shorter in refrigerated cadavers compared to frozen ones, even if this result should be contextualized in light of a small number of refrigerated cadavers included in this study. However, the migration time recorded in feline cadavers, either refrigerated or frozen, was higher than that reported in studies on live healthy cats and dogs [34, 35]. This could be explained by the hypothesis that microscopic cadaveric alterations have influenced the integrity of superficial lymphatic vessels, slowing down ICG migration. Indeed, in canine cadavers, storage conditions have been reported to affect the integrity of lymphatic vessels [36]. Furthermore, migration time and the lymphatic pathways length, were associated with the anatomical districts and selected cutaneous regions. The fact that migration time was shorter in the head rather than in the hind limb might be explained by anatomical characteristics: in fact, selected cutaneous regions of the hind limb are often more distant from their detected LC compared to the regions of the head. Anyway, the difference in migration time between selected cutaneous regions of the head may also depend on difficulty in massaging and migration due to reduced presence of underlying soft tissues (temporal-zygomatic regions) and to the migration from one aboral mandibular region to a superficial cervical LC that may have influenced the migration time. Considering the lymphatic pathways length recorded, the most interesting finding concerned some regions of the distal portion of hind limb. As discussed later, a selected cutaneous region might physiologically drain toward one or more LCs, even at a long distance. Hence, the distance recorded in the present study varied highly even within each selected cutaneous region, most likely due to individual differences. In particular, the plantar phalangeal region in two lymphographies, and the dorsal phalangeal, lateral, and medial tarsal regions in one lymphography each displayed ICG

migration to the medial iliac LC (alone or in association with the popliteal LC) always bypassing the superficial inguinal LC, determining a significantly longer lymphatic pathway.

Concerning technique characteristics, more than half (57%) of NIRF-ICG lymphographies needed re-injections, suggesting that NIRF-ICG lymphography on feline cadavers may be less immediate than *in vivo* [34]. In particular, the temporal-zygomatic region needed re-injection in 100% of its NIRF-ICG lymphographies, hampering, together with the aforementioned longer migration time, the hypothesis of a more difficult migration of the tracer for this specific cutaneous region. The need to re-inject has been previously reported in a canine cadaveric study, with up to four re-injections [10]. Overall, ICG migration may need more time and even re-injection of the dye to happen in cadavers.

In some instances, a reduction of the injected volume was needed. Half volume was used when the predetermined region was completely filled before the total volume was injected. Since some small regions received the full volume while others received half, clinical and anatomical factors such as the level of dehydration, the relative thickness of the cutis and subcutis, and the tight adherence to underlying tissues (as seen in the head region, where most half-volume injections were recorded) may have influenced the need to reduce the volume. In fact, while certain small regions tolerated the full volume, others required only half.

The association of half volume and a lower number of re-injections identified in the present study confirms the aforementioned hypothesis that the amount of ICG injected might not be determining the success of NIRF-ICG lymphographies.

The phenomenon of interrupted lymphatic pathways has not been previously described in lymphographic studies [2,7] or studies on the feasibility of NIRF-ICG lymphography in human cadavers [8, 37, 38]. In the present study, interrupted lymphatic pathways were mostly detected in the hind limb district (84%), but this was also the anatomical district including a higher number of selected cutaneous regions and lymphographies. Anyway, interrupted lymphatic pathways were not associated to any of the variables explored, and it could be supposed that the interruption of migration may be linked to peculiar anatomical characteristics or post-mortem alterations.

In the present study, in 56% of overall successful NIRF-ICG lymphographies, the selected cutaneous regions displayed a detected LC partially or totally non-correspondent, thus confirming the prediction of the draining LC in cats based on canine studies could be misleading. Correspondence was associated with the anatomical district, with the head showing the highest number of correspondences, with mandibular LC representing the more frequently detected, and the only one for the rostral maxillary region. This result contrasts with what is reported in the literature regarding the complexity of the superficial lymphatic system in this anatomical district [12, 39, 40]. However, the decision in

this study to exclude the median regions may have significantly influenced the outcome, and thus, this result should be interpreted with caution.

Among the interesting findings regarding the identified LCs, the auricular, aboral mandibular, aboral maxillary regions migrated to the parotid LC. This is in partial contrast with what has been reported in cadaveric studies of dogs and cats, in which the parotid LC was considered to drain only the temporal-zygomatic, ocular and auricular area [7, 5, 41]. In the present study, three NIRF-ICG lymphographies (2 rostral mandibular, and 1 aboral maxillary) showed migration to medial retropharyngeal LC in addition to the expected one. Since it is considered the collector of all LCs of the head [41, 42] and it was never the sole draining LC in the present study, the medial retropharyngeal LC might be considered as a 2nd-tier LC [43]. Lastly, one aboral maxillary NIRF-ICG lymphography displayed migration only to the superficial cervical LC. This migration seemed quite peculiar and has not been previously reported either in cats or in dogs [5, 7].

Concerning the hind limb, in the present study, total correspondence was reported in 36% of successful NIRF-ICG lymphographies with only the medial thigh-cranial and dorsal metatarsal regions displaying 100% migrations to the same expected LC (superficial inguinal and popliteal, respectively). Six NIRF-ICG lymphographies from different selected cutaneous regions, also belonging to the lower hind limb, distal to the knee, showed the medial iliac as unexpected draining LC. This is in contrast to what is reported in the dog [7], with the medial iliac LC draining mainly the cranial part of the lateral thigh, whereas it is in partial agreement with Ratzlaff [5], who reported the presence of a drainage pathway running from the lateral distal hind limb, bypassing the popliteal LC and directly getting to the iliac LCs. A possible explanation might be the lack of separation between the superficial and deep lymphatic system in the distal part of the hind limb, as reported in the rabbit [3]. In this case, the dye might have reached the deep lymphatic system, leading to different lymphatic pathways.

In the present study, medial and lateral genicular, medial thigh-caudal, lateral thigh-cranial and caudal regions displayed migration only to the popliteal LC, in contrast to what was reported in the dog [7]. This is intriguing, since these regions are in proximity or even proximally to the popliteal LC and for which the expected draining LCs were the superficial inguinal, medial iliac, or sacral. A similar finding was reported by Ratzlaff [5], but in that study, it was limited to the lateral compartment of the thigh.

The present study might be considered based on a clinical setting rather than a purely descriptive anatomical study. Anatomical landmarks were chosen to be easily assessable during clinical practice, mostly by palpation, while in previous studies [3-5, 7] cutaneous regions were not univocally defined by landmarks, and they were deduced according to the draining LC. Furthermore, in the present

study, NIRF-ICG lymphography was chosen since ICG can be injected intradermally, mimicking mapping procedures of sentinel LCs in vivo [22, 29, 35, 44, 45]. As mentioned before, both Ratzlaff [5] and Suami [7] injected multiple regions per lymphographic study, while in the present study, a single selected cutaneous region from the head and the two hind limbs was assessed in each cadaver. This allowed us to avoid the overlapping of lymphatic drainages coming from different selected cutaneous regions, leading to a univocal definition of LC drainage. Further differences included in the study design are related to the species involved, but also to the inclusion of a larger number of cadavers (33 cats in the present study vs 4 dogs in Suami [7]) and at least four repetitions of NIRF-ICG lymphographies for each selected cutaneous region. The univocal definition of the selected cutaneous regions by anatomical landmarks as well as increasing the number of NIRF-ICG lymphographies per selected cutaneous regions, were performed to improve repeatability and reliability and reduce the influence of individual cadaver variability.

Considering the limitations of this study, a relatively low number of refrigerated cadavers compared to the frozen ones has been studied, masking other possible associations. Even if this study included a higher number of lymphographies (84 NIRF-ICG lymphographies) than any previous study, only four to five lymphographies were repeated per region. A higher number of repetitions might confirm the identified draining patterns or even unveil new ones. Additionally, due to the high variability in the LCs detected by NIRF-ICG lymphography within the same selected cutaneous regions (such as the aboral maxillary, medial thigh-caudal, lateral genicular, and plantar phalangeal regions), there appears to be significant individual variation among cat cadavers included in this study. This variability prevented us from definitively describing predictable lymphatic draining patterns for all regions. The association of anatomical districts, and selected cutaneous regions within them, with several of the technical aspects investigated suggests that anatomical characteristics of the regions themselves may influence the NIRF-ICG lymphography results. Again, further studies with a larger number of repetitions for each selected cutaneous region may shed light on possible unidentified associations with these factors.

In conclusion, based on the results of the present study, NIRF-ICG lymphography is feasible on selected cutaneous regions belonging to the head and hind limb of feline cadavers. These results suggest that superficial lymphatic drainage of the head and hind limb anatomical districts of cats may be complex to predict and seem different from what is reported in dogs. The use of repeatable anatomical landmarks can provide valuable assistance in determining lymphatic drainage from predetermined skin areas. However, the unpredictability of lymphatic drainage, combined with the high individual variability observed in this study, hampers the importance of using technologies such as NIRF-ICG for LC lymphography for the detection of SLCs in a clinical setting for staging and/or

therapeutical purpose. Future studies might aim at mapping the whole superficial cutaneous lymphatic system, including unpaired median regions.

5.4. References:

1. Suami H, Taylor GI, O'Neill J, Pan WR. Refinements of the radiographic cadaver injection technique for investigating minute lymphatic vessels. Plast Reconstr Surg. 2007;120:61-67.
2. Suami H, Scaglioni MF. Lymphatic Territories (Lymphosomes) in the Rat: An Anatomical Study for Future Lymphatic Research. Plast Reconstr Surg. 2017;140:945-951. doi: 10.1097/PRS.0000000000003776.
3. Soto-Miranda MA, Suami H, Chang DW: Mapping superficial lymphatic territories in the rabbit. Anat Rec. 2013;296:965–970.
4. Ito R, Suami H: Lymphatic territories (lymphosomes) in swine, an animal model for future lymphatic research. Plast Reconstr Surg. 2015;136:297–304.
5. Ratzlaff MH. The superficial lymphatic system of the cat. Lymphology. 1970;3:151-159.
6. Wong JH, Cagle LA, Morton DL. Lymphatic drainage of skin to a sentinel lymph node in a feline model. Ann Surg. 1991;214:637-641. doi: 10.1097/00000658-199111000-00015.
7. Suami H, Yamashita S, Soto-Miranda MA, Chang DW. Lymphatic territories (lymphosomes) in a canine: an animal model for investigation of postoperative lymphatic alterations. PLoS One. 2013 24;8:e69222. doi: 10.1371/journal.pone.0069222.
8. Shinaoka A, Koshimune S, Yamada K, Kumagishi K, Suami H, Kimata Y, et al. A Fresh Cadaver Study on Indocyanine Green Fluorescence Lymphography: A New Whole-Body Imaging Technique for Investigating the Superficial Lymphatics. Plast Reconstr Surg. 2018;141:1161-1164. doi: 10.1097/PRS.0000000000004315.
9. Shinaoka A, Koshimune S, Yamada K, Kumagishi K, Suami H, Kimata Y, et al. Correlations between Tracer Injection Sites and Lymphatic Pathways in the Leg: A Near-Infrared Fluorescence Lymphography Study. Plast Reconstr Surg. 2019;144:634-642. doi: 10.1097/PRS.0000000000005982.
10. Sánchez-Margallo FM, Veloso Brun M, Sánchez-Margallo JA. Identification of intra-abdominal lymphatics in canine carcasses by laparoscopic fluorescence lymphography with intradermal and intrapopliteal ICG administration. PLoS One. 2020;15:e0241992. doi: 10.1371/journal.pone.0241992.

11. Suami H, Scaglioni MF, Dixon KA, Tailor RC. Interaction between vascularized lymph node transfer and recipient lymphatics after lymph node dissection-a pilot study in a canine model. J Surg Res. 2016;204:418-427. doi: 10.1016/j.jss.2016.05.029.
12. Chiti LE, Stefanello D, Manfredi M, Zani DD, De Zani D, Boracchi P, et al. To map or not to map the cN0 neck: Impact of sentinel lymph node biopsy in canine head and neck tumours. Vet Comp Oncol. 2021;19:661-670. doi: 10.1111/vco.12697.
13. Ferrari R, Chiti LE, Manfredi M, Ravasio G, De Zani D, Zani DD, et al. Biopsy of sentinel lymph nodes after injection of methylene blue and lymphoscintigraphic guidance in 30 dogs with mast cell tumors. Vet Surg. 2020;49:1099–1108. doi: 10.1111/vsu.13483.
14. Gariboldi EM, Stefanello D, Nolff MC, De Zani D, Zani DD, Grieco V, et al. Sentinel Lymph Node Biopsy Is Feasible in Dogs with Scars from Prior Local Excision of Solid Malignancies. Animals (Basel). 2022;12:2195-2208. doi: 10.3390/ani12172195.
15. Gariboldi EM, Ubiali A, Chiti LE, Ferrari R, De Zani D, Zani DD, et al. Evaluation of Surgical Aid of Methylene Blue in Addition to Intraoperative Gamma Probe for Sentinel Lymph Node Extirpation in 116 Canine Mast Cell Tumors (2017-2022). Animals (Basel). 2023;13:1854-1868. doi: 10.3390/ani13111854.
16. Stefanello D, Gariboldi EM, Boracchi P, Ferrari R, Ubiali A, De Zani D, et al. Weishaar's classification system for nodal metastasis in sentinel lymph nodes: Clinical outcome in 94 dogs with mast cell tumor. J Vet Intern Med. 2024;38:1675-1685. doi: 10.1111/jvim.16997.
17. Tobón Restrepo M, Espada Y, Aguilar A, Moll X, Novellas R. Anatomic, computed tomographic, and ultrasonographic assessment of the lymph nodes in presumed healthy adult cats: The head, neck, thorax, and forelimb. J Anat. 2021;239:264-281. doi: 10.1111/joa.13429.
18. Tobón Restrepo M, Novellas R, Aguilar A, Moll X, Espada Y. Anatomic, computed tomographic, and ultrasonographic assessment of the lymph nodes in presumed healthy adult cats: the abdomen, pelvis, and hindlimb. Acta Vet Scand. 2022;64:18-43. doi: 10.1186/s13028-022-00638-x.
19. Raharison F, Sautet J. The topography of the lymph vessels of mammary glands in female cats. Anat Histol Embryol. 2007;36:442-452. doi: 10.1111/j.1439-0264.2007.00783.x.
20. Papadopoulou PL, Patsikas MN, Charitanti A, Kazakos GM, Papazoglou LG, Karayannopoulou M, et al. The lymph drainage pattern of the mammary glands in the cat: a lymphographic and computerized tomography lymphographic study. Anat Histol Embryol. 2009;38:292-299. doi: 10.1111/j.1439-0264.2009.00942.x.
21. Patsikas MN, Papadopoulou PL, Charitanti A, Kazakos GM, Soultani CB, Tziris NE, et al. Computed tomography and radiographic indirect lymphography for visualization of

mammary lymphatic vessels and the sentinel lymph node in normal cats. Vet Radiol Ultrasound. 2010;51:299-304. doi: 10.1111/j.1740-8261.2009.01657.x.

22. Chiti LE, Gariboldi EM, Stefanello D, De Zani D, Grieco V, Nolff MC. Sentinel Lymph Node Mapping and Biopsy in Cats with Solid Malignancies: An Explorative Study. Animals (Basel). 2022;12:3116-3128. doi: 10.3390/ani12223116.
23. Annoni M, Borgonovo S, Aralla M. Sentinel lymph node mapping in canine mast cell tumours using a preoperative radiographic indirect lymphography: Technique description and results in 138 cases. Vet Comp Oncol. 2023;21:469-481. doi: 10.1111/vco.12906.
24. Thuesen IS, Agerholm JS, Mejer H, Nielsen SS, Sandøe P. How serious are health-related welfare problems in unowned unsocialised domestic cats? A study from Denmark based on 598 necropsies. Animals. 2022;12:662-677.
25. Nielsen SS, Thuesen IS, Mejer H, Agerholm JS, Nielsen ST, Jokelainen P, et al. Assessing welfare risks in unowned unsocialised domestic cats in Denmark based on associations with low body condition score. Acta Vet Scand. 2023;65:1-12. doi: 10.1186/s13028-023-00665-2.
26. Mestrinho LA, Louro JM, Gordo IS, Niza MMRE, Requicha JF, Force JG, et al. Oral and dental anomalies in purebred, brachycephalic Persian and Exotic cats. J Am Vet Med Assoc. 2018;253:66-72. doi: 10.2460/javma.253.1.66.
27. Sieslack J, Farke D, Failing K, Kramer M, Schmidt MJ. Correlation of brachycephaly grade with level of exophthalmos, reduced airway passages and degree of dental malalignment' in Persian cats. PLoS One. 2021;16:e0254420. doi: 10.1371/journal.pone.0254420.
28. Done SH, Goody PC, Evans SA, Stickland NC. Color atlas of veterinary anatomy: volume 3, the dog and cat. 2nd ed. Mosby Elsevier; 2009.
29. Arz R, Seehusen F, Meier VS, Nolff MC. Indocyanine-based near-infrared lymphography for real-time detection of lymphatics in a cat with multiple mast cell tumours. JFMS Open Rep. 2022;8:20551169221074961. doi: 10.1177/20551169221074961.
30. Wan J, Oblak ML, Ram A, Singh A, Nykamp S. Determining agreement between preoperative computed tomography lymphography and indocyanine green near infrared fluorescence intraoperative imaging for sentinel lymph node mapping in dogs with oral tumours. Vet Comp Oncol. 2021;19:295-303. doi:10.1111/vco.12675
31. Beer P, Rohrer-Bley C, Nolff MC. Near-infrared fluorescent image-guided lymph node dissection compared with locoregional lymphadenectomies in dogs with mast cell tumours. J Small Anim Pract. 2022;63:670-678. doi:10.1111/jsap.13529

32. Verbeek FP, Troyan SL, Mieog JS, Liefers GJ, Moffitt LA, Rosenberg M, et al. Near-infrared fluorescence sentinel lymph node mapping in breast cancer: a multicenter experience. Breast Cancer Res Treat. 2014;143:333-342. doi: 10.1007/s10549-013-2802-9.
33. den Toom IJ, Boeve K, Lobeek D, Bloemena E, Donswijk ML, de Keizer B, et al. Elective Neck Dissection or Sentinel Lymph Node Biopsy in Early Stage Oral Cavity Cancer Patients: The Dutch Experience. Cancers (Basel). 2020;12:1783-1795. doi: 10.3390/cancers12071783.
34. Lu HY, McKenna C, Ram A, Oblak ML. Effect of volume and methylene blue on fluorescence intensity and transit of indocyanine green for sentinel lymph node mapping in a simulated feline tumor model. Am J Vet Res. 2023;84:ajvr.23.07.0168. doi: 10.2460/ajvr.23.07.0168.
35. Favril S, Stock E, Hernot S, Hesta M, Polis I, Vanderperren K, et al. Sentinel lymph node mapping by near-infrared fluorescence imaging and contrast-enhanced ultrasound in healthy dogs. Vet Comp Oncol. 2019;17:89-98. doi: 10.1111/vco.12449.
36. Baraibar MA, Schoning P. Effects of freezing and frozen storage on histological characteristics of canine tissues. J Forensic Sci. 1985;30:439-447.
37. Shinaoka A, Koshimune S, Suami H, Yamada K, Kumagishi K, Boyages J, et al. Lower-Limb Lymphatic Drainage Pathways and Lymph Nodes: A CT Lymphangiography Cadaver Study. Radiology. 2020;294:223-229. doi: 10.1148/radiol.2019191169.
38. Suami H. Anatomical Theories of the Pathophysiology of Cancer-Related Lymphoedema. Cancers (Basel). 2020;12:1338-1351. doi: 10.3390/cancers12051338.
39. Tanis PJ, Nieweg OE, van den Brekel MW, Balm AJ. Dilemma of clinically node-negative head and neck melanoma: outcome of "watch and wait" policy, elective lymph node dissection, and sentinel node biopsy-a systematic review. Head Neck. 2008;30:380-389. doi: 10.1002/hed.20749.
40. de Wilt JH, Thompson JF, Uren RF, Ka VS, Scolyer RA, McCarthy WH, et al. Correlation between preoperative lymphoscintigraphy and metastatic nodal disease sites in 362 patients with cutaneous melanomas of the head and neck. Ann Surg. 2004;239:544-552. doi: 10.1097/01.sla.0000118570.26997.a1.
41. Baum, H. The Lymphatic System of the Dog. University of Saskatchewan: Saskatoon, SK, Canada. 2021. Available from: https://openpress.usask.ca/k9lymphaticsystem/.
42. Belz GT, Heath TJ. Lymph pathways of the medial retropharyngeal lymph node in dogs. J Anat. 1995;186:517-526.
43. Frumovitz M, Plante M, Lee PS, Sandadi S, Lilja JF, Escobar PF, et al. Near-infrared fluorescence for detection of sentinel lymph nodes in women with cervical and uterine cancers

(FILM): a randomised, phase 3, multicentre, non-inferiority trial. Lancet Oncol. 2018;19:1394-1403. doi: 10.1016/S1470-2045(18)30448-0.

44. Kitai T, Inomoto T, Miwa M, Shikayama T. Fluorescence navigation with indocyanine green for detecting sentinel lymph nodes in breast cancer. Breast Cancer. 2005;12:211-215. doi: 10.2325/jbcs.12.211.
45. Tagaya N, Yamazaki R, Nakagawa A, Abe A, Hamada K, Kubota K, et al. 2008. Intraoperative identification of sentinel lymph nodes by near-infrared fluorescence imaging in patients with breast cancer. Am J Surg. 195:850-853. doi: 10.1016/j.amjsurg.2007.02.032.

6. General discussion and future directions:

This PhD project was structured three years ago to implement and explore the use of near-infrared fluorescence with indocyanine green in several areas of surgical oncology in dogs and cats. The objectives set have been achieved and reported in this PhD thesis.
As there are three projects in three distinct fields of application of indocyanine green the following discussions are organized around the arms of the project: the use of NIRF-ICG for sentinel lymph node (SLN) mapping, tumor fluorescence-guided surgery (TFGS), and lymphography in cadaveric models.

Use of NIRF-ICG in Sentinel Lymph Node Mapping:

Concurrently with the recent increase in studies on SLN mapping and extirpation, a significant advancement in the application of NIRF-ICG imaging in canine and feline oncology has been reported in the literature (Chiti et al., 2025, 2022). This progress has also been supported by some of my own research, published prior to the beginning of my PhD program (Chiti et al., 2022; Gariboldi et al., 2023, 2022).
As extensively discussed in the introduction, despite the numerous SLN mapping techniques published, there was a lack of studies comparing the performance of two comparable methods. In the present project, NIRF-ICG was demonstrated to have comparable performance to lymphoscintigraphy in SLN detection. These findings support the integration of NIRF-ICG into routine clinical practice as a reliable and effective tool for lymphatic mapping in small animal oncology.
The study by Gariboldi et al. (2025) as a part of this PhD Thesis confirmed that these two SLN mapping techniques (NIRF-ICG and lymphoscintigraphy) are effectively equivalent in terms of accuracy and reliability for the identification and extirpation of SLNs. This represents a significant achievement, especially considering that the limited availability of nuclear medicine units in Italy, Europe, and globally has so far avoided the widespread adoption of lymphoscintigraphy in routine clinical practice.
Our findings offer a new perspective for clinical veterinary oncology, suggesting that a broader population of canine cancer patients could now benefit from SLN mapping using a technique that is both accessible and aligned with human oncology standards. The integration of NIRF-ICG into clinical workflows may thus enable the widespread use of SLN biopsy in veterinary settings, bridging the gap between veterinary and human surgical oncology.

Furthermore, the use of guided techniques such as lymphoscintigraphy and NIRF, has allowed us to refine and consolidate the concept of the sentinel lymphocentrum (SLC), a concept that has often been overlooked or poorly defined in the veterinary literature.

The concept of ‘’sentinel lymphocentrum” intended as the final outcome of the mapping process, has previously appeared in the literature, including in prior work from our group (Ferrari et al., 2021; Gariboldi et al., 2023; Stefanello et al., 2024). However, only in the past three years, data collection has become increasingly detailed, including within the scope of this PhD project, and focused on characterizing the lymphocentrum as a defined anatomical and functional unit that may contain one or more SLNs (Gariboldi et al., 2023; Gariboldi et al., 2025). This clearer delineation may serve as the basis for future investigations, such as exploring the anatomical and functional interconnections between distinct lymphocentrum or single SLN within the same SLC and the impact of oncologic outcome (Stefanello et al., 2024). Based on the knowledge and expertise gained through this research project, we believe that NIRF imaging and lymphoscintigraphy are the only techniques capable of providing objective and reproducible results since they use a single tracer for each phases of detection (ICG and technetium).

Despite this progress, significant gaps in knowledge remain. It is still unclear whether the involvement of multiple lymphocentrums truly reflects the presence of lymphatic interconnections between them or rather indicates that only one is the actual sentinel lymphocentrum, while the others represent second-echelon drainage sites. Similarly, in cases where multiple SLNs are detected, either within a single SLC or in different SLCs, it is not yet well understood whether among them a second-echelon lymph node is present. A ‘**’second-echelon lymph node**” is a lymph node that receives lymphatic drainage from a SLN representing the next anatomical station in the lymphatic flow following the SLN and may be involved in secondary tumor spread. Considering this evolving framework, the concept of second-echelon lymph node gains increasing relevance in human medicine (Bassi et al., 2006.; Rathod et al., 2020). While this is the subject of active investigation in several human cancers, it may represent a new frontier for oncologic research in veterinary medicine. Techniques such as NIRF-ICG and/or lymphoscintigraphy could be employed to study the frequency of second-echelon lymph nodes, location, and metastatic involvement, as well as the prognostic impact of their removal. A recent study from our group demonstrated that an increased number of tumor-associated SLNs and SLCs was correlated with a higher incidence of nodal metastasis in mast cell tumors (MCTs) (Ferrari et al., 2021). These findings highlight the need for further investigations on the oncological relevance of second-echelon lymph node removal.

This topic is also addressed in our study (currently under review) on sentinel lymphatic mapping in dogs with enlarged regional lymph nodes (eRLNs). Indeed, unlike most previous studies, including

several from our own research group (Ferrari et al., 2020; Stefanello et al., 2024), which focused primarily on non-palpable/normal-sized lymph nodes, the present project also wanted to address the clinical challenge posed by eRLNs. Until now, SLN mapping in case of eRLN has often been omitted in literature. Our findings suggest that SLN mapping remains feasible and informative even in the presence of eRLNs. The use of NIRF-ICG and/or lymphoscintigraphy enabled the detection of neo-sentinel nodes, potentially revealing occult metastases that might otherwise go unnoticed. This represents an important step toward addressing the clinically relevant question of how lymphatic mapping behaves in the presence of enlarged lymph nodes. Moreover, further research studies are needed to evaluate whether guided SLN excision in presence of eRLN contributes to improved oncologic outcomes.

Additionally, different nodal tracer uptake patterns were observed in our results. The high pressure in the metastatic lymph node may cause a re-routing of the tracer to a neo-sentinel lymph node. In this context of re-routing of the tracer, the metastatic node can have an incomplete or absent tracer uptake. The re-routing of tracer could happen also in case of normal sized lymph nodes. The preliminary findings of this project constitute an initial step in exploring a topic that is already under investigation in human medicine (Goyal et al., 2005): how the nodal distribution of tracer uptake within each nodes relates to histological metastatic status. It should be object of future study the characterization of the neo-sentinel lymph node and the second echelon lymph node within the mapping phases.

Furthermore, it would be of interest to further investigate the concept of real-time quantification of tracer intensity (fluorescence and/or radioactivity), in order to assess, intraoperatively, whether a lymph node may be at risk of metastasis. This could support more informed surgical decision-making on whether to excise the node or not. Such an approach would be particularly valuable in anatomically complex regions, such as the neck, where dogs and cats often present with multiple closely associated lymph nodes.

Use of NIRF-ICG for Tumor Fluorescence-Guided Surgery

The second aim of the present project was to investigate the clinical application of Tumor Fluorescence-Guided Surgery (TFGS) using NIRF imaging with free ICG in dogs affected by soft tissue sarcomas (STS) and mast cell tumors (MCT). This topic had never been addressed before, as previously published experiences were primarily translational medicine studies applied to spontaneous oncologic diseases, most of which included multiple histotypes (Favril et al., 2020; Holt et al., 2015, 2014). Only recently have some studies focused exclusively on soft tissue sarcomas (Holt et al., 2015), while no study to date has compared the feasibility of SLN mapping in two distinct and

common histotypes in the canine species. The results of our study confirmed the feasibility of the technique in both tumor types, although with markedly higher performance in sarcomas. These findings reinforce the potential of intraoperative, real-time fluorescence quantification to guide surgical decisions and improve tumor resection outcomes in clinical practice.

Given the differing performance between STS and MCT observed in this study, future investigations should focus on refining TFGS protocols based on tumor type, likely based on differences in tumor biology that affect ICG uptake and retention. Tumor specific protocols are needed, including optimized timing of administration, adjusted dosing strategies, and tumor-specific tumor-to-background ratio (TBR). A dedicated pharmacodynamic study could be an instrumental in establishing these parameters for MCTs in future research.

However, the distribution of free ICG in tissues after intravenous administration may depend on several variables that are not yet well explored in veterinary medicine. These include clinical and pathological factors such as blood albumin levels, other blood proteins, tumor histotypes, timing of administration, and ICG dosage (Egloff-Juras et al., 2019). In this context, the next steps should aim to investigate how these variables affect the performance of the technique. Future studies should evaluate the tissue-level distribution of ICG and the fluorescence intensity measured by NIRF imaging across different tissues (including neoplastic tissue, peritumoral areas, and healthy tissue). It would be valuable to assess fluorescence microscopy in various tissues and examine the microscopic distribution of ICG within tumors and the surrounding neoplastic microenvironment. This microenvironment is a complex and dynamic network of non-cancerous cells, signaling molecules, blood vessels, immune cells, and extracellular matrix that interact with the tumor. The study of the ICG distribution and fluorescence quantification in the macroenvironmental could address to important question on tissues that play a fundamental role in cancer grow and control. Such ex vivo analysis could offer important insights into the accuracy and reliability of NIRF imaging and support its broader application in veterinary oncology.

The use of NIRF-ICG in the decision-making process during tumor excision has the potential to significantly enhance surgical precision. By clearly delineating tumor margins and identifying residual neoplastic tissue in real time, this technique can support more accurate and complete resections. Furthermore, in the future, fluorescence-guided surgery could also enable the targeted application of local adjuvant treatments, such as intraoperative electrochemotherapy, directly to the tumor bed. The real-time guidance provided by fluorescence could help optimize the placement and effectiveness of these treatments, paving the way for a more personalized and effective surgical oncology approach.

Ultimately, the integration of NIRF-ICG techniques into veterinary surgical oncology could start the way for standardized protocols during TFGS (timing of administration, doses of ICG and cut-off of TBR), contributing to improved diagnostic precision and therapeutic outcomes.

NIRF-ICG Lymphography in Feline Cadavers

Cadaveric lymphographic studies have long served as a foundational tool for the development of future diagnostic and therapeutic applications, as widely demonstrated in the scientific literature (Ito and Suami, 2015; Sánchez-Margallo et al., 2020; Suami et al., 2013, 2012). Both historical and recent investigations have explored lymphatic anatomy in various animal species, including humans, using a range of tracers, among them, ICG (Ito and Suami, 2015; Soto-Miranda et al., 2013; Suami et al., 2012; Suami and Shinaoka, 2019).

The introduction of NIRF imaging, which enables transcutaneous visualization of lymphatic vessels without the need for anatomical dissection, opens new avenues for studying the lymphatic system in dogs and cats. However, feasibility studies in veterinary medicine are still lacking. Aiming to fill this gap, the present project demonstrated the feasibility of NIRF-ICG lymphography in feline cadavers (Ubiali et al., 2025). These preliminary findings underscore the relevance of NIRF-ICG in anatomical and lymphographic research and support its potential within the framework of translational medicine. The technique was successfully applied to selected superficial regions of the head and hind limbs. However, a comprehensive anatomical mapping of the feline superficial lymphatic system is still needed. In fact, significant inter-individual variability and unpredictable drainage patterns in cats represent major limitations for its current clinical application. Despite these challenges, the use of consistent anatomical landmarks has shown promise in improving mapping reliability (Ubiali et al., 2025).

Moreover, future studies on canine cadavers should consider the anatomical differences among various morphotypes (brachymorphic, mesomorphic, and dolichomorphic), as these may influence lymphatic architecture and tracer distribution. Such findings could inform the development of species- and breed-specific approaches.

The successful application of NIRF-ICG technology in cadaveric lymphography opens the door to further research on this imaging modality and supports efforts toward its clinical standardization.

In conclusion, the studies presented in this PhD thesis provide strong support for the clinical integration of NIRF-ICG imaging in fluorescence-guided surgical oncology. Although several challenges and open questions remain, the findings represent a crucial first step toward addressing key clinical needs. Moreover, many other potential applications of this technique still need to be thoroughly explored in the literature (e.g. guided plastic reconstruction, bowel perfusion, liver surgery). These data lay the basis for future research aimed at enhancing surgical outcomes and promoting the application of this innovative technique in different fields of both canine and feline oncology.

6.1. References:

Bassi, K.K., Seenu, V., Ballehaninna, U.K., Parshad, R., Chumber, S., Dhar, A., Gupta, S.D., Kumar, R., Srivastava, A., 2006. Second echelon node predicts metastatic involvement of additional axillary nodes following sentinel node biopsy in early breast cancer. Indian Journal of Cancer 43, 103–109. https://doi.org/10.4103/0019-509X.27931

Chiti, L.E., Beer, P., Ohlerth, S.M., Hartnack, S., Nolff, M.C., 2025. SHINE – Validation of Near Infrared Fluorescence Lymphography Against Lymphoscintigraphy for Sentinel Lymph Node Biopsy in Dogs With Mast Cell Tumours. Veterinary and Comparative Oncology. https://doi.org/10.1111/vco.13058

Chiti, L.E., Gariboldi, E.M., Stefanello, D., De Zani, D., Grieco, V., Nolff, M.C., 2022. Sentinel Lymph Node Mapping and Biopsy in Cats with Solid Malignancies: An Explorative Study. Animals 12, 3116. https://doi.org/10.3390/ani12223116

Egloff-Juras, C., Bezdetnaya, L., Dolivet, G., Lassalle, H.P., 2019. NIR fluorescence-guided tumor surgery: New strategies for the use of indocyanine green. International Journal of Nanomedicine. https://doi.org/10.2147/IJN.S207486

Favril, S., Abma, E., Stock, E., Devriendt, N., Van Goethem, B., Blasi, F., Brioschi, C., Polis, I., De Cock, H., Miragoli, L., Oliva, P., Valbusa, G., Vanderperren, K., De Rooster, H., 2020. Fluorescence-guided surgery using indocyanine green in dogs with superficial solid tumours. Veterinary Record 187, 273. https://doi.org/10.1136/vr.105554

Ferrari, R., Boracchi, P., Chiti, L.E., Manfredi, M., Giudice, C., De Zani, D., Spediacci, C., Recordati, C., Grieco, V., Gariboldi, E.M., Stefanello, D., 2021. Assessing the risk of nodal metastases in canine integumentary mast cell tumors: Is sentinel lymph node biopsy always necessary? Animals 11. 2373. https://doi.org/10.3390/ani11082373

Ferrari, R., Chiti, L.E., Manfredi, M., Ravasio, G., De Zani, D., Zani, D.D., Giudice, C., Gambini, M., Stefanello, D., 2020. Biopsy of sentinel lymph nodes after injection of methylene blue and lymphoscintigraphic guidance in 30 dogs with mast cell tumors. Veterinary Surgery 49, 1099–1108. https://doi.org/10.1111/vsu.13483

Gariboldi, E.M., Stefanello, D., Nolff, M.C., De Zani, Donatella, Zani, Davide, Grieco, V., Giudice, C., Recordati, C., Ferrari, F., Ferrari, R., Chiti, L.E., 2022. Sentinel Lymph Node Biopsy Is Feasible in Dogs with Scars from Prior Local Excision of Solid Malignancies. Animals 12, 2195. https://doi.org/10.3390/ani12172195

Gariboldi, E.M., Ubiali, A., Chiti, L.E., Ferrari, R., De Zani, D., Zani, D.D., Grieco, V., Giudice, C., Recordati, C., Stefanello, D., Auletta, L., 2023. Evaluation of Surgical Aid of Methylene Blue in Addition to Intraoperative Gamma Probe for Sentinel Lymph Node Extirpation in 116 Canine Mast Cell Tumors (2017–2022). Animals 13, 1854. https://doi.org/10.3390/ani13111854

Gariboldi EM, Ubiali A, Boracchi P, Luconi E, Ferrari R, Auletta L, De Zani D, Zani DD, Roccabianca P, Grieco V, Giudice C, Recordati C, Stefanello D, (2025) Intrapatient application of lymphoscintigraphy and near-infrared fluorescence in canine and feline sentinel lymph node mappingg and removal. BMC Veterinary Research. https://doi.org/10.1186/s12917-025-05013-2

Goyal, A., Douglas-Jones, A.G., Newcombe, R.G., Mansel, R.E., 2005. Effect of lymphatic tumor burden on sentinel lymph node biopsy in breast cancer. Breast Journal 11, 188–194. https://doi.org/10.1111/j.1075-122X.2005.21591.x

Holt, D., Okusanya, O., Judy, R., Venegas, O., Jiang, J., DeJesus, E., Eruslanov, E., Quatromoni, J., Bhojnagarwala, P., Deshpande, C., Albelda, S., Nie, S., Singhal, S., 2014. Intraoperative near-infrared imaging can distinguish cancer from normal tissue but not inflammation. PLoS One 9. https://doi.org/10.1371/journal.pone.0103342

Holt, D., Parthasarathy, A.B., Okusanya, O., Keating, J., Venegas, O., Deshpande, C., Karakousis, G., Madajewski, B., Durham, A., Nie, S., Yodh, A.G., Singhal, S., 2015. Intraoperative near-infrared fluorescence imaging and spectroscopy identifies residual tumor cells in wounds. ournal of Biomedical Optics 20, 076002. https://doi.org/10.1117/1.jbo.20.7.076002

Ito, R., Suami, H., 2015. Lymphatic territories (Lymphosomes) in Swine: An animal model for future lymphatic research, in: Plastic and Reconstructive Surgery. Lippincott Williams and Wilkins, pp. 297–304. https://doi.org/10.1097/PRS.0000000000001460

Rathod, R., Bakshi, J., Panda, N.K., Verma, R., Bhattacharya, A., Bal, A., 2020. Can sentinel lymph node biopsy predict various levels of echelon nodes in oral cancers? International Archives of Otorhinolaryngology 24, E51–E57. https://doi.org/10.1055/s-0039-1695762

Sánchez-Margallo, F.M., Brun, M.V., Sánchez-Margallo, J.A., 2020. Identification of intra-abdominal lymphatics in canine carcasses by laparoscopic fluorescence lymphography with intradermal and intrapopliteal ICG administration. PLOS ONE 15, e0241992. https://doi.org/10.1371/journal.pone.0241992

Soto-Miranda, M.A., Suami, H., Chang, D.W., 2013. Mapping superficial lymphatic territories in the rabbit. Anatomical Record 296, 965–970. https://doi.org/10.1002/ar.22699

Stefanello, D., Gariboldi, E.M., Boracchi, P., Ferrari, R., Ubiali, A., De Zani, D., Zani, D.D., Grieco, V., Giudice, C., Recordati, C., Caniatti, M., Auletta, L., Chiti, L.E., 2024. Weishaar's classification system for nodal metastasis in sentinel lymph nodes: Clinical outcome in 94 dogs with mast cell tumor. Journal of Veterinary Internal Medicine 38, 1675–1685. https://doi.org/10.1111/jvim.16997

Suami, H., Shin, D., Chang, D.W., 2012. Mapping of lymphosomes in the canine forelimb: Comparative anatomy between canines and humans. Plast Reconstr Surg 129, 612–620. https://doi.org/10.1097/PRS.0b013e3182402c6d

Suami, H., Shinaoka, A., 2019. The methodology of lymphatic anatomy studies in a cadaver model: an overview. Plast Aesthet Res. https://doi.org/10.20517/2347-9264.2019.46

Suami, H., Yamashita, S., Soto-Miranda, M.A., Chang, D.W., 2013. Lymphatic Territories (Lymphosomes) in a Canine: An Animal Model for Investigation of Postoperative Lymphatic Alterations. PLoS One 8. e69222. https://doi.org/10.1371/journal.pone.0069222

Ubiali, A., Gariboldi, E.M., Auletta, L., Di Giancamillo, A., Modina, S.C.B., Ferrari, R., Tagliasacchi, F., Martini, V., Stefanello, D., 2025. Indocyanine green fluorescence lymphography: An exploratory study of superficial lymphatic territories in the head and hind limbs of 33 cat cadavers. PLoS One 20. e0327005 https://doi.org/10.1371/journal.pone.0327005

7. Scientific production unrelated to the project (October 2022-September 2025):

During the years leading up to the completion of the present PhD project, I was actively involved in other ongoing research projects as well as in the clinical activities of the Veterinary Teaching Hospital (VTH) of the University of Milan, as part of my training as a clinical researcher. In particular, I participated in the daily clinical work of the VTH to collect cases not only for the current project but also for other active research initiatives. Working closely with my tutor and the research group strongly oriented in oncologic surgery, I had the opportunity to engage directly in clinical and surgical decision-making processes, which proved essential for planning and developing clinically relevant research projects. Although not all these activities were directly related to the main focus of my PhD, they significantly contributed to the development of both practical and interpersonal skills that were crucial to the successful completion of this work. Moreover, my training as a researcher and the consolidation of key competencies (such as data analysis, interpretation of results, manuscript writing, and managing peer-review revisions) were strongly enhanced through my involvement in the preparation and submission of other scientific papers. These experiences provided me with a comprehensive and structured research training. A brief overview of these additional studies and activities is provided in the following section:

- **Gariboldi E.M.;** Stefanello D.; Nolff M.C.; De Zani D.; Zani D.; Giudice C.; Recordati C.; Ferrari F.; Ferrari R.; Chiti L.E. (2022) Sentinel lymph node biopsy is feasible in dogs with scars from prior local excision of solid malignancies. *Animals*, 12, 2195. https://doi.org/10.3390/ani12172195
  PhD student role: First author

- Chiti LE, **Gariboldi E.M.;** Stefanello D., De Zani D.; Grieco V.; Nolff M.C. (2022) Sentinel lymph node mapping and biopsy in cats with solid malignancies: an explorative study. *Animals*, 12(22): 3116. https://doi.org/10.3390/ani12223116
  PhD student role: co-author

- Chiti L.E.; **Gariboldi E.M;** Ferrari R.; Luconi E.; Boracchi P.; De Zani D.; Zani D.; Manfredi M.; Spediacci C.; Grieco V.; Giudice C.; Recordati C.; Ferrari F.; Stefanello D. (2023) Surgical complications following sentinel lymph node biopsy guided by γ-probe and

methylene blue in 113 tumor-bearing dogs. *Veterinary and Comparative Oncology*.. 21(1): 62-72. https://doi.org/10.1111/vco.12861
PhD student role: co-author

- **Gariboldi, E.M.**, Ubiali, A., Chiti, L.E., Ferrari, R., De Zani, D., Zani, D.D., Grieco, V., Giudice, C., Recordati, C., Stefanello, D., Auletta, L., (2023). Evaluation of Surgical Aid of Methylene Blue in Addition to Intraoperative Gamma Probe for Sentinel Lymph Node Extirpation in 116 Canine Mast Cell Tumors (2017–2022). *Animals* 13, 1854. https://doi.org/10.3390/ani13111854
  PhD student role: First author

- Dall'Ara P.; Filipe J.; Pilastro C.; Turin L.; Lauzi S.; **Gariboldi E.M**.; Stefanello D. (2023) Can chemotherapy negatively affect the specific antibody response toward core vaccines in canine cancer patients?. *Veterinary Sciences*, 10, 303. https://doi.org/10.3390/vetsci10040303
  PhD student role: co-author

- Cino, M., **Gariboldi, E.M.**, Stefanello, D., Spindler, K. P., Ferraris, E. I., Morello, E. M., Bertola, L., Maniscalco, L., & Martano, M. (2023). Ki67 Index in Patnaik Grade 2/Kiupel Low-Grade Canine Cutaneous Mast Cell Tumors with Early Lymph Node Metastasis: A Descriptive Study. *Veterinary Sciences*, *10*(7), 436. https://doi.org/10.3390/vetsci10070436
  PhD student role: co-first author

- Stefanello D.; **Gariboldi E.M**; Boracchi P.; Ferrari R.; Ubiali A.; De Zani D.; Zani D.; Grieco V.; Giudice C.; Recordati C.; Caniatti M.; Auletta L.; Chiti L. (2024) Weishaar's classification system for nodal metastasis in sentinel lymph nodes: update on clinical outcome in 94 dogs with mast cell tumor, *Journal of Veterinary Internal Medicine*, 38(3), 1675–1685. https://doi.org/10.1111/jvim.16997
  PhD student role: co-first author

- Mattioli, G., Cino, M., Stefanello, D., Drudi, D., Morello, E. M., Pisani, G., Chiti, L. E., Pierini, A., **Gariboldi, E. M.**, De Zani, D., Massari, F., Giacobino, D., & Martano, M. (2025). Peripheral sentinel lymphadenectomy in 163 dogs: Postoperative surgical complications and comparison between intraoperative dissection techniques. *Veterinary Surgery: VS*, *54*(4), 766–776. https://doi.org/10.1111/vsu.14246

PhD student role: co-author

- Dell'Aere, S., Balbi, V., Stefanello, D., Avallone, G., Ghisleni, G., Perfetto, S., Ferrari, R., Auletta, L., **Gariboldi, E. M**., Ubiali, A., Romanello, C., Verdi, A., & Roccabianca, P. (2025). CD117 (KIT) in canine soft tissue sarcoma: an immunohistochemical and c-kit gene mutation assessment. *Frontiers in Veterinary Science*, *12*, 1572923. https://doi.org/10.3389/fvets.2025.1572923
  PhD student role: co-author